



# **Effects of Sound Barriers on Dispersion from Roadways**

**DRAFT**

**Final Report**

June 17, 2013

**Prepared for:**

South Coast Air Quality Management District

21865 Copley Drive

Diamond Bar, CA 91765-4178

(909) 396-3520

Attn: Ian MacMillan

By

Nico Schulte and Akula Venkatram

Mechanical Engineering

Bourns College of Engineering

## **Abstract**

Exposure to roadway emissions is linked to increased risk of developing asthma and other respiratory symptoms. One proposed solution is to build physical barriers next to large roads to reduce near-road concentrations of road-related emissions. Several field studies, laboratory experiments, and computational fluid dynamics simulations have been conducted to examine the impact of barriers. The objective of the research summarized in this report is to use the results from these studies to develop a semi-empirical model that can be used to design roadside barriers to reduce exposure to pollutants from vehicles. In developing this model, we have focused on a tracer study (Finn et al., 2010) and a wind-tunnel experiment (Heist et al., 2009) that were specifically designed to estimate the impact of barriers on near surface dispersion under a variety of atmospheric conditions. We have developed three semi-empirical models that incorporate the dominant physical effects of barriers. The first model treats the effect of the barrier as an upwind shift of the source, where the upwind shift depends on the height of the barrier and atmospheric stability. The second model assumes that the primary role of the barrier is to mix pollutants behind the barrier. The concentration is well mixed behind the barrier, and follows an exponential distribution above it. The third model is an adaptation of that proposed by Puttock and Hunt (Puttock et al, 1979) for predicting dispersion behind obstacles. All three models perform well in describing data from the Idaho Falls field study (Finn et al., 2010) and a wind tunnel study (Heist et al, 2009). The model that mixes pollutants behind the barrier performs the best in describing ground-level concentrations, while the PH model best describes concentrations above the barrier.

Although CFD models are not yet capable of simulating the effects of atmospheric stability and cannot be readily calibrated with data from field experiments, we assumed that they can provide information on the relationships among the governing processes. We used two CFD models to examine the relationship between concentrations and barrier height: OpenFOAM, which is a free CFD code and the Quick Urban Industrial Complex (QUIC) modeling system. QUIC CFD did not provide realistic results and was abandoned. We found that model predictions from the source shift model qualitatively match OpenFOAM simulation results. The mixed wake model predicts a larger effect of barrier height on concentrations than OpenFOAM does. The Puttock-Hunt model matched some of the OpenFOAM predictions, but the model predicts a much larger effect of barrier height for tall barriers than OpenFOAM does.

We have conducted sensitivity studies with the three models to examine the impact of barrier height on ground-level concentrations at different distances from the barrier under varying atmospheric stabilities. Although there are differences among the sensitivities predicted by the three models, the results lead to some general conclusions. As expected, changes in barrier height have the greatest influence on concentrations at receptors near the roadside barrier. Atmospheric stability influences how far downwind the concentrations are affected by the change in barrier height. During unstable or neutral conditions, the barrier height effect decreases with distance and becomes small at 600 m from the barrier. On the other hand, during stable condition, the impact is evident as far as 600 m from the barrier. This suggests that increasing the barrier height is likely to have the greatest impact when it is most needed: during stable conditions when ground-level concentrations are the highest.

The models described in this report can provide useful guidance on the design of roadside barriers to mitigate exposure to roadway emissions. However, we need more observations to evaluate some of the assumptions made in formulating these models.

# 1. Contents

Abstract.....	2
2. Introduction and Objectives of Research.....	6
3. Literature Review.....	7
3.1. Summary of Findings.....	7
3.2. Raleigh Field Study (Bowker et al. 2007).....	12
3.3. Putten Study (Hooghwerff et al. 2010; McCrae 2010).....	15
3.4. Southern California Study (Ning et al. 2010).....	17
3.5. Wind Tunnel Study (Heist et al. 2009).....	18
3.6. Computational Fluid Dynamics (CFD) Study (Hagler et al. 2011).....	20
3.7. Tracer Study (Finn et al. 2010).....	23
3.8. Conclusions of Literature Review.....	29
4. Model Development and Evaluation.....	29
4.1. Description of concentrations measured during NRTS08 and in the wind tunnel.....	30
4.2. Models for Dispersion behind Barriers.....	34
Meandering.....	36
4.3. Source-shift Model.....	36
Comparison with NRTS08.....	38
Comparison with wind tunnel.....	46
4.4. Mixed-wake Model.....	48
Comparison with NRTS08.....	50
Comparison with wind tunnel.....	58
4.5. Puttock-Hunt.....	60
Extension for Finite Source Length and Wind Direction.....	63
Comparison with NRTS08.....	64
Comparison with wind tunnel.....	66

5.	Conclusions of the Model Comparison with Observations .....	68
6.	CFD Simulations to Examine the Effect of Barrier Height .....	69
6.1.	QUIC .....	70
6.2.	OpenFOAM CFD Model .....	73
7.	Barrier height Sensitivity .....	76
7.1.	Impact of Meteorology on Barrier height Sensitivity .....	80
8.	Conclusions.....	90
8.1.	Hypothetical Scenario where a Barrier is used to Reduce Near-Road Concentrations of Roadway Emissions .....	93
9.	Recommendations.....	94
10.	References.....	95

## 2. Introduction and Objectives of Research

The impact of roadway emissions on air quality has been studied since the 1970s. This issue has become prominent in light of a number of recent epidemiological studies reporting associations between living within a few hundred meters of high-traffic roadways and adverse health effects such as asthma and other respiratory impacts, birth and developmental effects, premature mortality, cardiovascular effects, and cancer (e.g. Harrison et al. 1999; Brauer 2002; Hoek et al. 2002; Finkelstein et al. 2004).

Air quality monitoring studies conducted near major roadways indicate that these health effects are associated with elevated concentrations, compared with overall urban background levels, of motor-vehicle-emitted compounds, which include carbon monoxide (CO); nitrogen oxides (NO<sub>x</sub>); coarse (PM<sub>10-2.5</sub>), fine (PM<sub>2.5</sub>), and ultrafine (PM<sub>0.1</sub>) particle mass; particle number; black carbon (BC), polycyclic aromatic hydrocarbons (PAHs), and benzene (Kim et al. 2002; Hitchins et al. 2000; Zhu et al. 2002a; Zhu et al. 2002b; Kittelson et al. 2004).

Several approaches have been suggested to mitigate the near road impact of vehicle emissions. They include

1. More stringent vehicle emission standards;
2. Noise barriers with a variety of shapes and coatings;
3. Roadside vegetation;
4. Road canopies in combination with methods to treat the pollutants trapped in the canopies (McCrae 2010);
5. Catalytic coatings on barriers to convert NO<sub>2</sub> to nitrate (McCrae 2010);
6. Dynamic traffic management based on forecasts of conditions that might lead to poor air quality (McCrae 2010).

Road canopies can confine pollutants within the road, but the trapped pollutants have to be treated or released at heights that reduce ground-level concentrations. The construction of canopies, stacks, and the removal of pollutants using methods such as electrostatic precipitation of particles are expensive and less than reliable. Catalytic coating on barriers to absorb or convert pollutants such as NO<sub>2</sub> has not been effective because the contact time between the pollutants and the coated surface is not large enough. Dynamic traffic management, which is reducing traffic flows when the meteorology is conducive to high air pollution levels, is difficult to

implement even if adverse meteorological conditions could be forecast accurately. The most practical and potentially successful short-term mitigation strategy is based on physical barriers and roadside vegetation. Elevated or depressed roadways can also reduce near-road air pollution. This report focuses on mitigation strategies based on barriers.

The primary objective of the research program described in this report is to develop and evaluate dispersion models that can be used to evaluate how near-road barriers might reduce the exposure of people living next to large roads. The second objective of this study is to conduct sensitivity studies with the dispersion models to examine the effects of 1) barrier dimensions, 2) wind speed and direction, 3) atmospheric stability, and 4) road dimensions on nearby concentrations in the presence of barriers. The third objective is to use the results from the sensitivity studies to recommend optimum barrier designs.

We first provide a review of the literature on studies conducted to date on the impact of physical barriers on near road dispersion of roadway emissions. We then describe three models of roadside barriers and evaluate the models with data from wind tunnel and field studies. Finally we use these models to examine the sensitivity of near road concentrations to changes in barrier height.

### **3. Literature Review**

#### **3.1. Summary of Findings**

Physical barriers affect concentrations associated with vehicle emissions by modifying the flow field and turbulence in the vicinity of the barrier. For perpendicular winds the pollutant plumes from vehicles are carried over the barrier by the mean flow that is deflected upwards by the barrier, as indicated in Figure 1 (Bowker et al. 2007). A recirculating region forms behind the barrier, in which the near surface flow is opposite to that in the mean flow aloft. Above the cavity, the flow is deflected downwards, and turbulence levels are enhanced in a vertically expanding wake whose effects extend to a distance of about 10-20 times the height of the barrier.

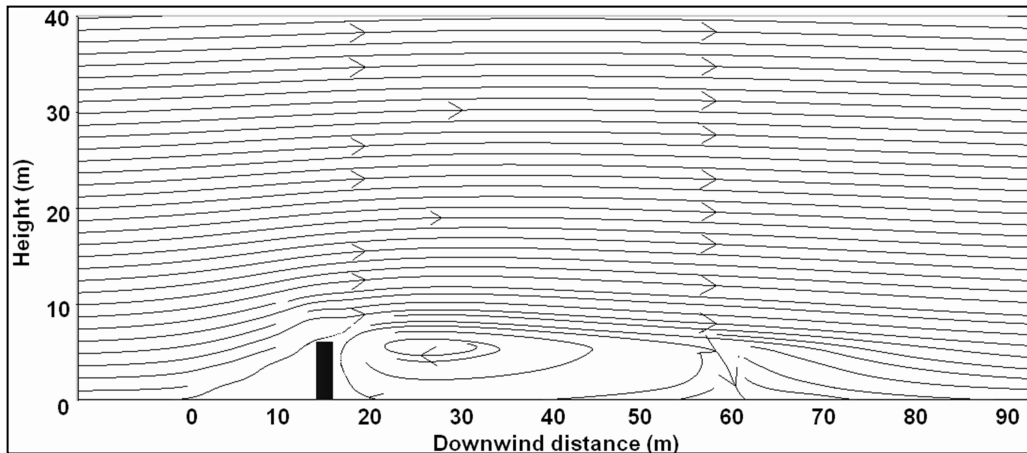


Figure 1: Flow induced by physical barrier. (Bowker et al. 2007)

Physical barriers effectively raise the height of emissions from near ground-level to the approximate height of the barrier. A fraction of these elevated emissions is entrained into the recirculating cavity and then reemitted into the wake region of the flow. The material entrained into the cavity represents a ground-level source with an initial vertical spread proportional to the barrier height. In general, the combination of all these barrier induced effects leads to a reduction in concentrations relative to those without the barrier.

Most barrier studies have focused on “standard” barriers, which are simple walls. Exceptions to this include a study conducted in Putten, the Netherlands (Hooghwerff et al. 2010), and the EU-LIFE Sound and Particle Absorbing System (SPAS, Magistrat Klagenfurt 2011) project. The Putten study examined variations in the shape of the barrier top, porous barriers, catalytic coatings (to reduce  $\text{NO}_2$ ), and barriers with vegetation. The SPAS project investigated barriers with built-in particulate filters (Rodler et al. 2009; Iser et al. 2009). The SPAS study found that filters installed in noise barriers can sometimes reduce  $\text{PM}_{10}$  concentrations, but this effect depends on wind direction (Rodler et al. 2009). Figure 2 shows an example of the filters used in the study installed on a noise barrier. The study found that pressure due to wind is not sufficient to overcome the filter resistance (Iser et al. 2009). Passing trucks generated sufficient pressure to overcome the filter resistance and cause some removal of PM, but passenger cars did not generate the required pressure increase.



**Figure 2: Filter panel installed on a noise barrier for the SPAS study. (Magistrat Klagenfurt 2011)**

Major experimental studies on the effects of barriers on dispersion include a wind tunnel study (Heist et al. 2009), a tracer study in Idaho Falls (Finn et al. 2010), and three field studies, one in Raleigh North Carolina (Bowker et al. 2007; Baldauf et al. 2008) one in Southern California (Ning et al. 2010), and one in Putten, The Netherlands (Hooghwerff et al. 2010). The wind tunnel study also investigated elevated and depressed roadways. The Raleigh study investigated the effects of barriers and barriers combined with vegetation.

Most of these studies focused on dispersion of inert gases, while the Raleigh, NC, Southern California, and Putten field studies also investigated the dispersion of particulate matter (PM). In the Raleigh study, total particle number and 20 nm and 75 nm concentrations were measured. The Southern California study measured particle number and mass distributions between 6-523 nm.

The Idaho Falls study (Finn et al., 2010) evaluated the effect of atmospheric stability on the reduction of concentrations behind barriers. The wind tunnel study (Heist et al., 2009) investigated the effect of boundary layer roughness on dispersion behind the barrier. It also examined the impact of roadside barriers along several road configurations, including elevated and depressed roadways. A recent study (Hagler et al. 2011) used computational fluid dynamics (CFD) to examine the air quality impact of barriers with varying heights.

Table 1 summarizes the important features and the type of measurements made in each study.

**Table 1: Summary of studies on near-road barriers**

<b>Study</b>	<b>Important features</b>	<b>Measurements</b>	<b>References</b>
Raleigh	Real-world conditions; Barrier combined with vegetation; Effects of wind direction; Edge effects	CO, CO <sub>2</sub> , NO <sub>x</sub> , NO <sub>2</sub> , PM <sub>10</sub> , PM <sub>2.5</sub> , PM number and size distributions, Air toxics	(Baldauf et al. 2008; Bowker et al. 2007)
Southern California	Real-world conditions	Black Carbon, CO, NO <sub>2</sub> , PM distribution	(Ning et al. 2010)
Putten	Variation in barrier height, material, and shape; Vegetated barriers	NO <sub>x</sub> , NO <sub>2</sub> , PM <sub>10</sub>	(McCrae 2010; Hooghwerff et al. 2010)
Project SPAS	Built in PM filters	PM <sub>10</sub>	(Rodler et al. 2009; Iser et al. 2009)
Idaho Falls	Variation in atmospheric conditions; Edge effects	SF <sub>6</sub>	(Finn et al. 2010)
Wind Tunnel	Elevated and depressed roadway; Sloped roadway walls; Upwind and downwind barriers; Variation in Barrier height and boundary layer roughness	Neutrally buoyant Ethane	(Heist et al. 2009)
CFD	Variation in barrier height and wind direction; Minor emission source directly downwind of the barrier	Inert gaseous tracer	(Hagler et al. 2011)

In all these studies, the concentration immediately behind the barrier was 15-50% lower than the concentration with no barrier when the wind direction was close to perpendicular to the barrier, although the Idaho Falls study found some concentration deficits greater than 50%. The effect of the barrier persisted up to about 50 times the barrier height in all studies, after which the concentration approached the value that would occur without the barrier. The data on whether concentrations are reduced for all downwind distances is not as clear. The Idaho Falls, CFD, and wind tunnel studies found reduced concentrations at all downwind distances for all atmospheric stabilities. The field studies in Raleigh and Southern California found some instances where larger concentrations occurred downwind of a barrier than in the no-barrier case. This effect was most evident in the Southern California study, where reduced concentrations were found immediately behind the barrier followed by a surge of concentrations about 80-100 m downwind. This is shown in Figure 8 for particle number and mass concentrations. A similar result was found for gaseous pollutants.

One possible explanation for this is that traffic activity on small roads near the freeways contributed to these high concentrations. The Raleigh study also observed some high concentrations at larger distances, and the conclusion was that traffic on small roads downwind of the barrier was responsible for these anomalous concentrations.

The wind tunnel and CFD studies found that elevated or depressed roadways and barriers placed upwind or downwind of the road caused reduced downwind concentrations compared to flat roads with no barriers. The Raleigh study found that vegetation further decreased concentration compared to just barriers. The noise barrier reduced 20 nm PM number concentrations up to about 100 m from the road. The presence of both a barrier and vegetation caused greater reductions in both 20 nm and 75 nm particle number concentrations. This study also measured barrier edge effects and found that concentrations did not decrease significantly compared with the open field until about 40 m from the barrier edge.

The Putten study found that the variations in the shape of the barrier top, porous barriers, catalytic coatings, and vegetated barriers did not reduce the concentration more than a simple 4 m tall wall. There has been criticism of the study and this result is questionable (McCrae 2010). Further research on “optimized” barriers is needed.

We next provide details of field and numerical studies that are most relevant to the objectives of this research program.

### 3.2. Raleigh Field Study (Bowker et al. 2007)

In this field study, concentrations of  $\text{NO}_x$ , particulate matter, and air toxics were measured near interstate I-440. An aerial view of the experimental setup is shown in Figure 3. There is a clearing next to the interstate and a 1 km long noise barrier begins near the edge of the clearing. Vegetation stands behind a section of the barrier next to the clearing. Concentrations were measured using fixed sampling instruments and a mobile laboratory measured PM size distributions at several locations. This mobile laboratory allowed measurements without a barrier, with a barrier, and with a barrier and vegetation.

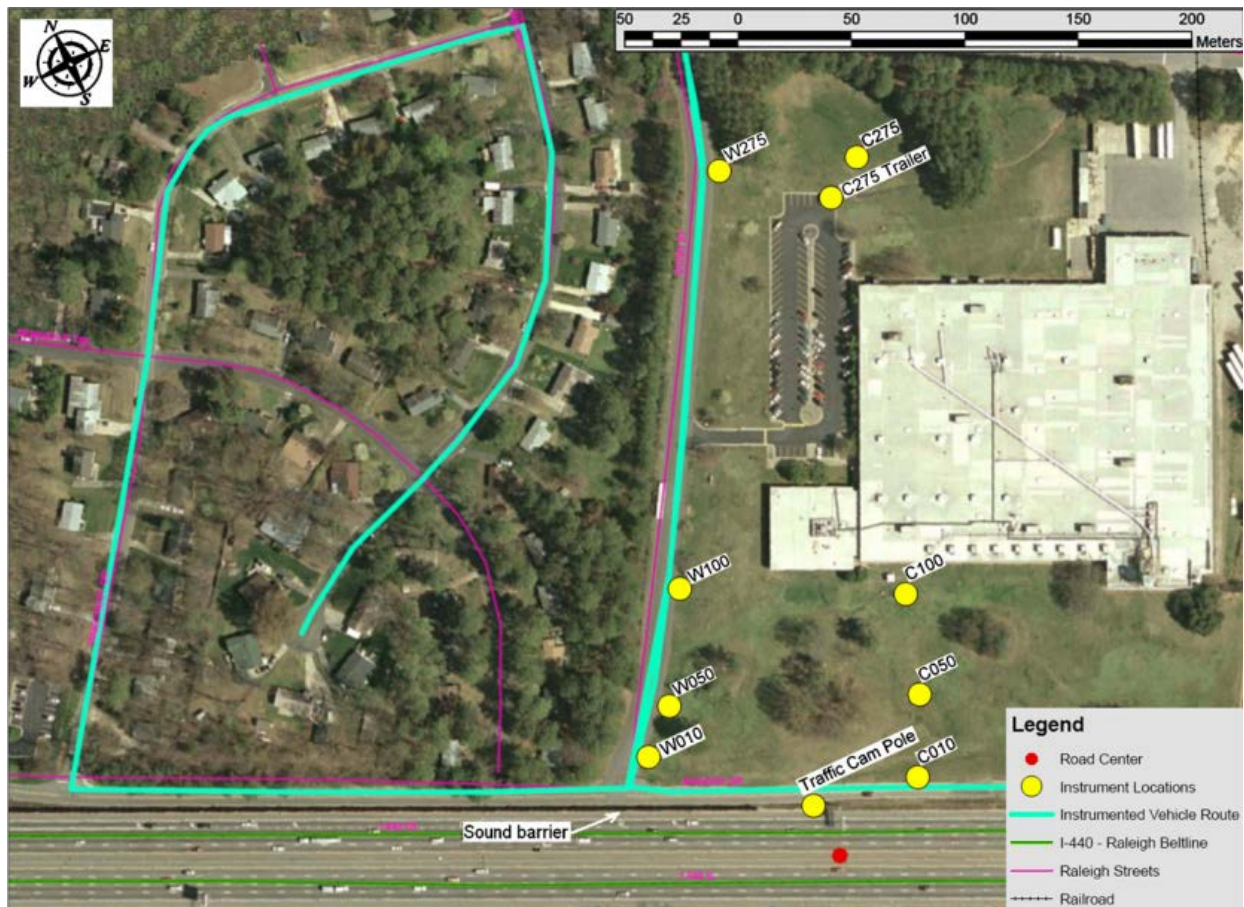
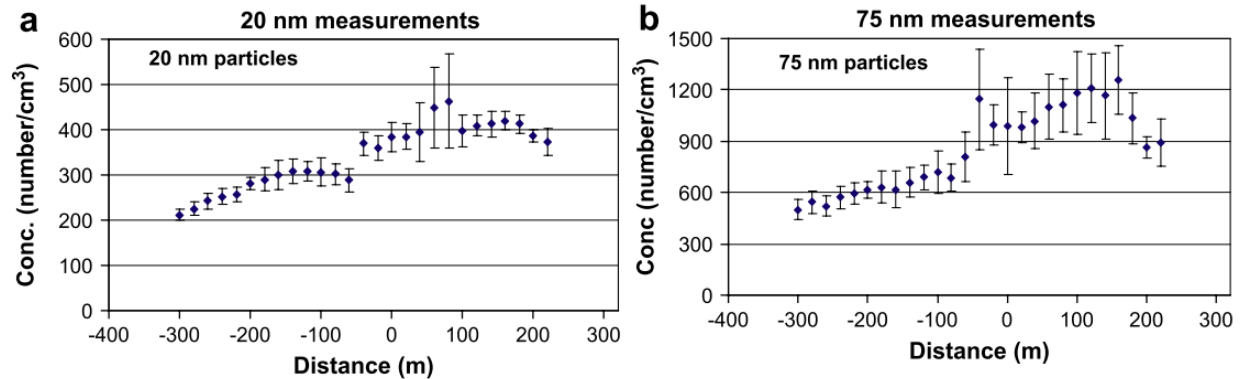


Figure 3: Aerial map of the near-road field study site along I-440 in Raleigh, North Carolina showing locations of mobile measurements (teal) using a GPS sensor. (Bowker et al. 2007)

Based on measurements at the fixed measuring sites, concentrations downwind of the barrier decreased by 15-50% relative to the section with no barrier when the wind blew from the road. However, concentrations were higher on the upwind side of the barrier compared to the open field. The barrier reduced PM concentrations by up to 50%, with an average reduction of

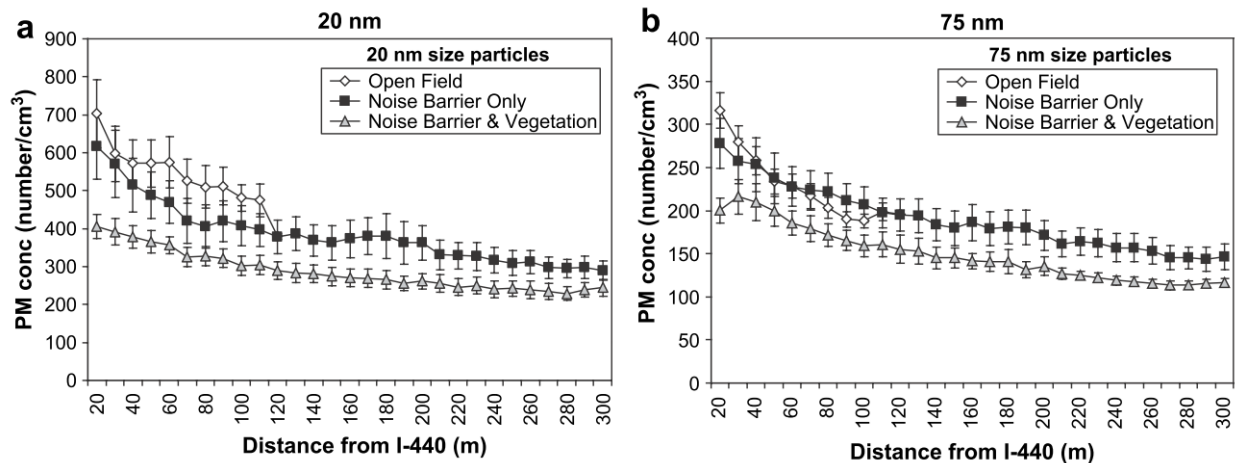
20%. In some cases higher, PM concentrations were measured behind the barrier even when the wind blew from the road, but this could be due to unmonitored traffic activity behind the barrier.

Figure 4 shows concentrations measured parallel to the barrier. Concentrations were measured along the barrier past the end and into the open field. These measurements showed that some pollutants were swept around the end of the barrier and that concentrations were not decreased significantly until about 40 m past the end of the barrier.



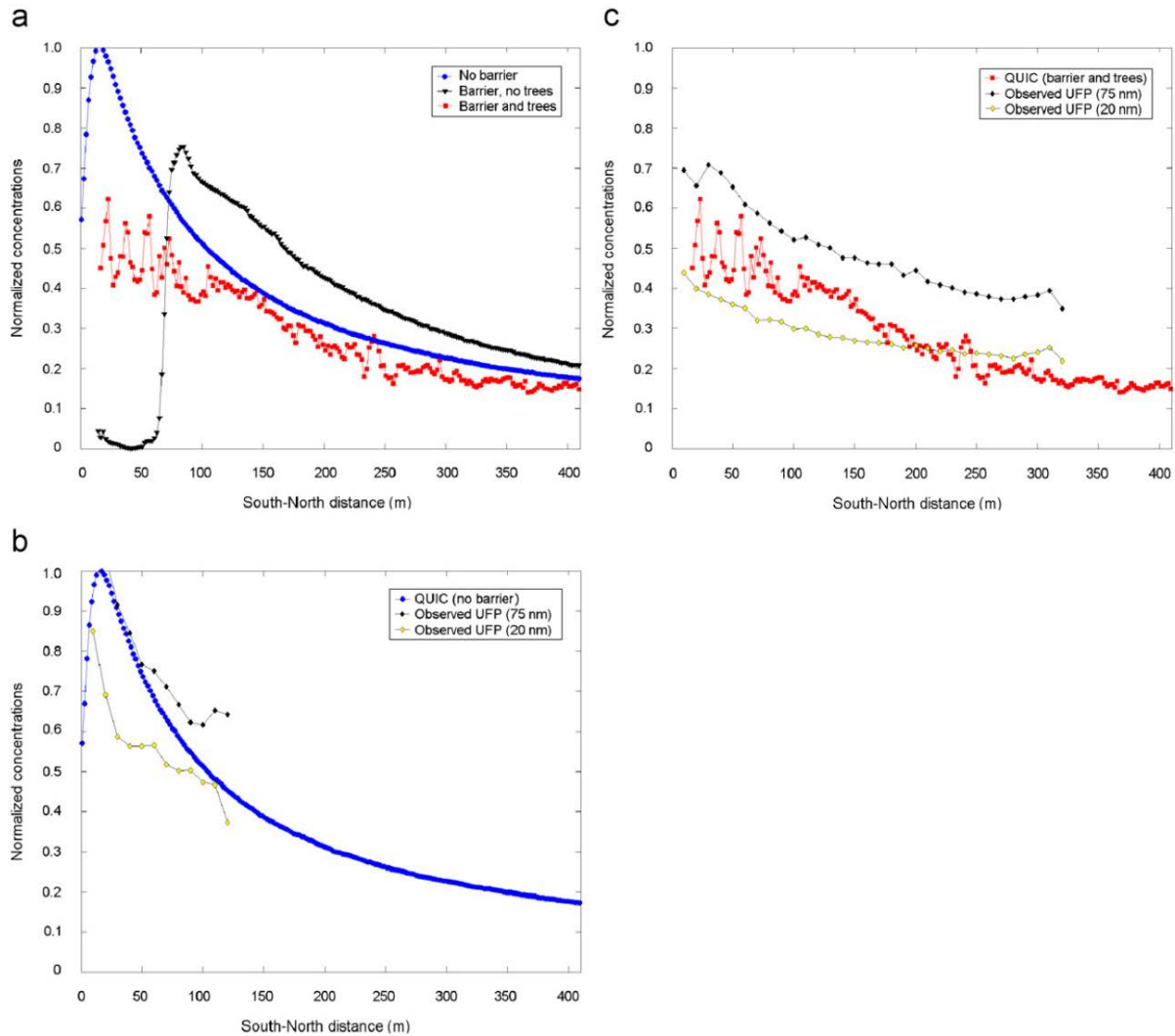
**Figure 4: Comparison of 20 nm and 75 nm particle number concentrations measured with the DMA-CPC units parallel to the highway 15 m from the nearest travel lane. Each data point represents the average and 95% confidence interval of approximately 40 measurements taken at that location with winds directionally from the road. The origin indicates the beginning of the noise barrier with negative x-value measurements taken behind the barrier. (a) 20 nm measurements and (b) 75 nm measurements. (Baldauf et al. 2008)**

Figure 5 shows concentration measurements at varying distances from the road. The study found that concentrations of smaller diameter particles were decreased more than concentrations of large particles. Concentrations of 20 nm particles reached open field concentrations at 120 m downwind of the road while concentrations of 75 nm particles reached open field concentrations at 50 m downwind of the road. Concentrations were decreased further for the section of barrier that had mature vegetation (trees taller than 10 m with leaves) next to it. Concentrations were decreased up to about 150-200 m downwind of the barrier, after which the concentrations were about the same as in the open field.



**Figure 5: Mobile monitoring measurements of (a) 20 nm and (b) 75 nm size particles using the DMA–CPC units at varying distances from the road for open terrain, behind a noise barrier only, and behind a noise barrier with vegetation. Bars represent 95% confidence intervals for each distance. (Baldauf et al. 2008)**

The Raleigh data has been compared with estimated concentrations of the Quick Urban and Industrial Complex (QUIC) model (Bowker et al. 2007). QUIC takes account of the presence of obstacles by using empirical formulations to model the wind flow around these obstacles. The study compared time averaged measured concentrations of 20 nm and 75 nm particles with QUIC modeled concentrations. QUIC models were run including only the barrier and the barrier with vegetation. Figure 6 shows a comparison of the QUIC results with measured PM concentrations. All concentrations were normalized by the median concentration in the open area along the access road directly adjacent to the highway. QUIC estimates were in qualitative agreement with the spatial patterns of observed concentrations, but the magnitude of measurements and predictions were different. More evaluation of QUIC is necessary before it can be used for regulatory planning.



**Figure 6: Normalized concentrations as a function of downwind distance (at 3 m) for: (a) the three different QUIC simulations (base, sound barrier only, and field site); (b) the mobile measurements in the open area and the QUIC model for the base case; and, (c) comparison between mobile measurements and the QUIC model for the field site in the region downwind of the sound barrier in the residential neighborhood. For all cases, the sound barrier is located at X =12 m. (Bowker et al. 2007)**

### **3.3. Putten Study (Hooghwerff et al. 2010; McCrae 2010)**

The study conducted in Putten, the Netherlands, between 2007 and 2009 measured PM, NO<sub>x</sub>, and NO<sub>2</sub> concentrations behind 9 different barriers next to a major freeway. Measurements were taken for 3 months for each barrier. A 4 m tall barrier was chosen as a reference and evaluated against a 7 m tall barrier and seven other 4 m tall barriers with different shapes and

coatings designed to remove pollutants (Figure 7). These barrier types included those with TiO<sub>2</sub> coatings, vegetated barriers, porous barriers, and barriers with a T-shaped top.



**Figure 7: Photos of the optimized barriers. (Hoogwerff et al. 2010)**

The study found reduced concentrations immediately behind all of the barriers. The reduction was about 20% for NO<sub>x</sub> for the reference barrier and about 50% for the 7 m barrier. The “optimized” barriers also reduced concentrations, but the reduction was slightly less than for the reference barrier. The measurements also indicated a seasonal effect, where the reduction of NO<sub>2</sub> was larger during winter months than during summer months.

The reductions in concentrations by the altered barriers were not statistically different from that of the reference simple barrier due to large uncertainties in the results. The length of the barriers may have been too short, and edge effects could have played a significant role. Because of these problems, it was not possible to draw definite conclusions on optimizing barrier configurations to reduce near-road concentrations.

### 3.4. Southern California Study (Ning et al. 2010)

The Southern California study measured particulate and gas concentrations near the I-710 and I-5 freeways. Measurements were made at two sites near each freeway, one in the presence of a noise barrier and the other without. A mobile platform sampled PM size distributions as well as black carbon, CO, and NO<sub>2</sub>, concentrations.

The results of this study are notable because, unlike in other studies, mass and number concentrations of particulate matter increased with distance from the barrier, reaching peaks at distances of 80-100 m, and then decreasing. These peaks were about twice those observed at the same distance in the absence of the barrier. Figure 8 shows the downwind particulate mass and number concentrations. The figure shows reduced concentrations immediately behind the barrier followed by a surge of concentrations about 80-100 m downwind. The occurrence of this peak concentration is attributed to the effective elevation of the emissions by the barrier. This spatial pattern is not consistent with a tracer experiment, described later (Finn et al., 2010), in which concentrations always decreased with distance from the barrier. However, the tracer experiment was performed with a single barrier, whose effects might be different from those of two barriers on highways.

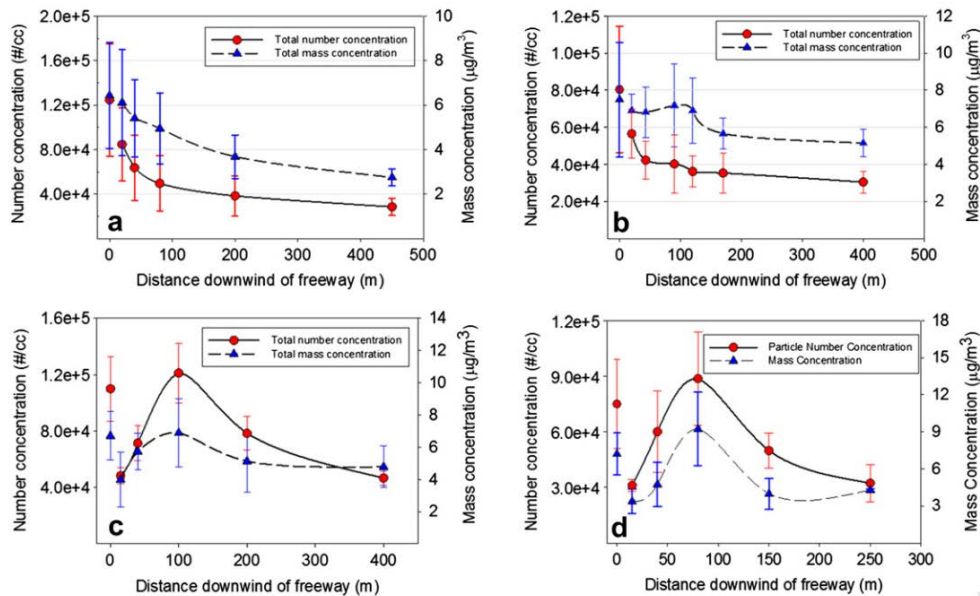
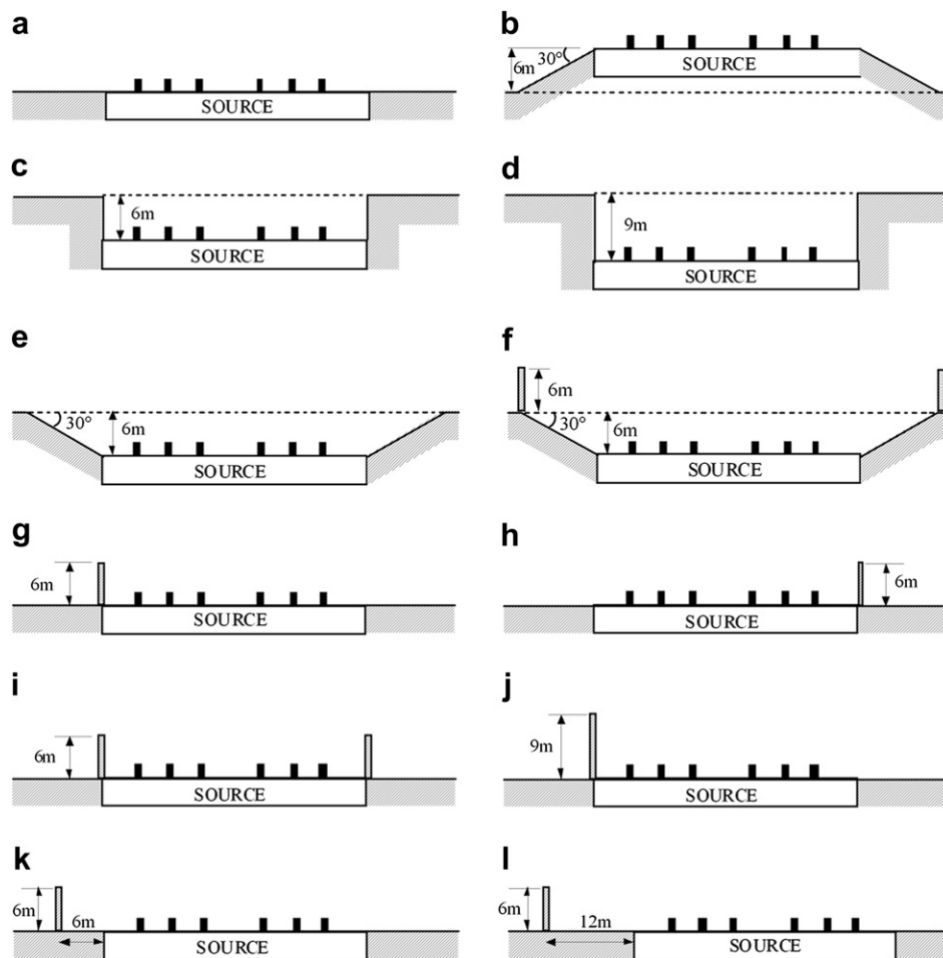


Figure 8: Particle number and mass concentrations at different distance downwind of the freeway (a) I-710 no noise barrier (b) I-5 no noise barrier; (c) I-710 with noise barrier; (d) I-5 with noise barrier. Note: The total particle number and mass concentrations at  $X = 0$  are derived from SMPS (10-225 nm) data at stationary sampling station; the concentrations at  $X > 0$  are derived from FMPS (6-523 nm) data. (Ning et al. 2010)

### 3.5. Wind Tunnel Study (Heist et al. 2009)

The wind tunnel study measured dispersion of roadway emissions in a 1:150 scale model of a 6 lane divided highway. Figure 9 shows the 12 configurations used in the study. They were one with flat terrain with no barrier, six with flat terrain and upwind or downwind barriers, one with an elevated roadway, three with depressed roadways, and one with a depressed roadway with both upwind and downwind barriers. Barriers with real heights corresponding to 6 m and 9 m were placed both upwind and downwind of the barrier as shown in Figure 9.



**Figure 9:** Elevation view showing cross sections through the various roadway configurations studied (cases A through L corresponding to figure lettering). Flow is from left to right. Dashed line in (b) through (f) represents at-grade elevation. (Heist et al. 2009)

Barriers or depressed roadways with vertical walls created recirculation zones. When both upwind and downwind barriers were present, the downwind barrier recirculation zone

length was reduced from 5 to 3 times the barrier height. Turbulent kinetic energy (TKE) calculated based on velocity measurements showed that the greatest increases in TKE were caused by the shear at the top of the barriers.

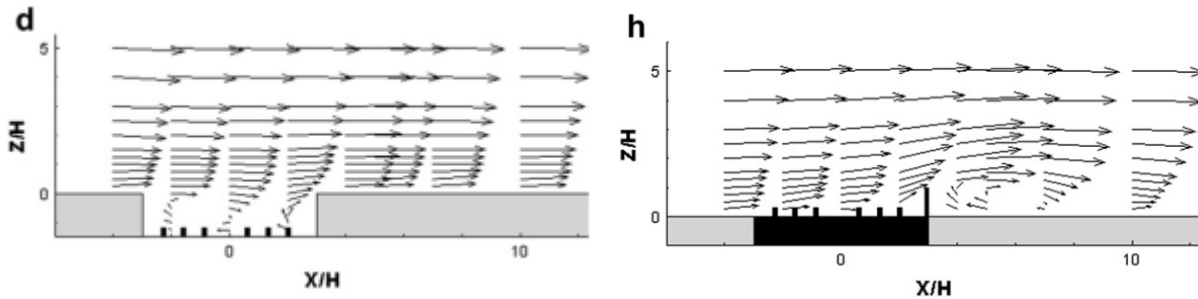


**Figure 10: Average velocity vectors measured with laser Doppler velocimetry for cases d and h of the wind tunnel study. Recirculation zones are present behind the barrier and above the depressed roadway. (Heist et al. 2009)**

All of the configurations reduced downwind concentrations relative to the flat terrain case. The elevated roadway showed the least difference relative to the flat terrain case. Vertical concentration profiles indicated that the barriers and elevated roadway shifted peak concentrations vertically upward, as found in the CFD study (Figure 13). The lowest downwind concentration occurred for the case when the depressed roadway was combined with upwind and downwind barriers. The effect of barrier placement upwind or downwind and distance from road, was much smaller than the effects of the presence of barrier and the elevation of the road.

The study found that the ground-level concentrations beyond a distance of about 10 times the height of the barrier could be modeled as a ground-level source with two modifications: 1) the source is shifted upwind, and 2) and the effective rate of vertical plume spread, the entrainment velocity,  $w_e$ , relative to the friction velocity,  $u_*$ , is increased in the presence of a barrier. The upwind shift in source location depends on road geometry, with larger shifts necessary when multiple physical effects are combined. Figure 11 shows that the concentrations associated with three roadway configurations can be described by shifting the flat terrain curve upwind by prescribed distances. They also found that the entrainment velocity depends on the surface friction velocity and the road geometry, with larger entrainment velocities occurring for cases with barriers rather than flat terrain and for rougher boundary layers with greater surface friction velocities. This is shown in Figure 12.

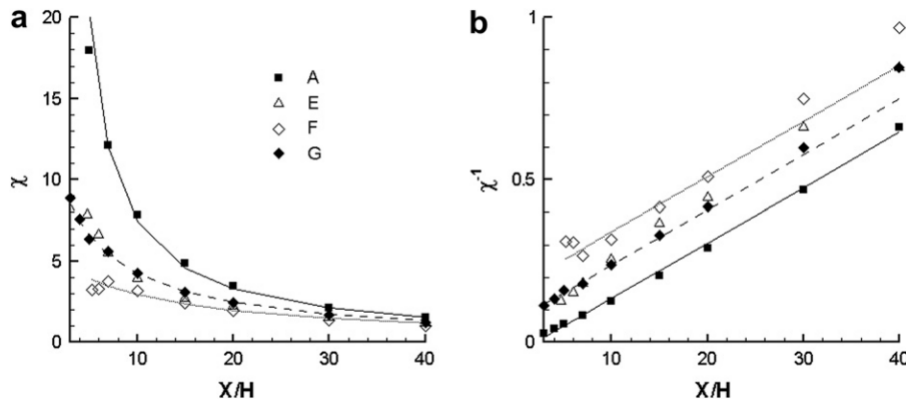


Figure 11: (a) Ground-level concentration as a function of downwind distance. (b) Inverse ground-level concentration as a function of downwind distance. Solid line is a straight-line fit to flat terrain data. Other lines show the effect of shifting source location for flat case a distance of 6H (dashed) and 11H (dotted) upwind. (A = flat terrain; E = depressed roadway, sloped walls; F = depressed roadway, sloped wall, and noise barriers; G = noise barrier at  $x/H = 3$ ). (Heist et al. 2009)

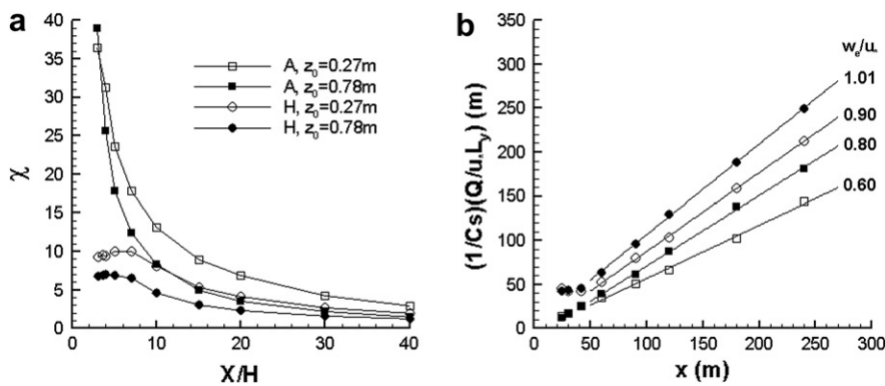
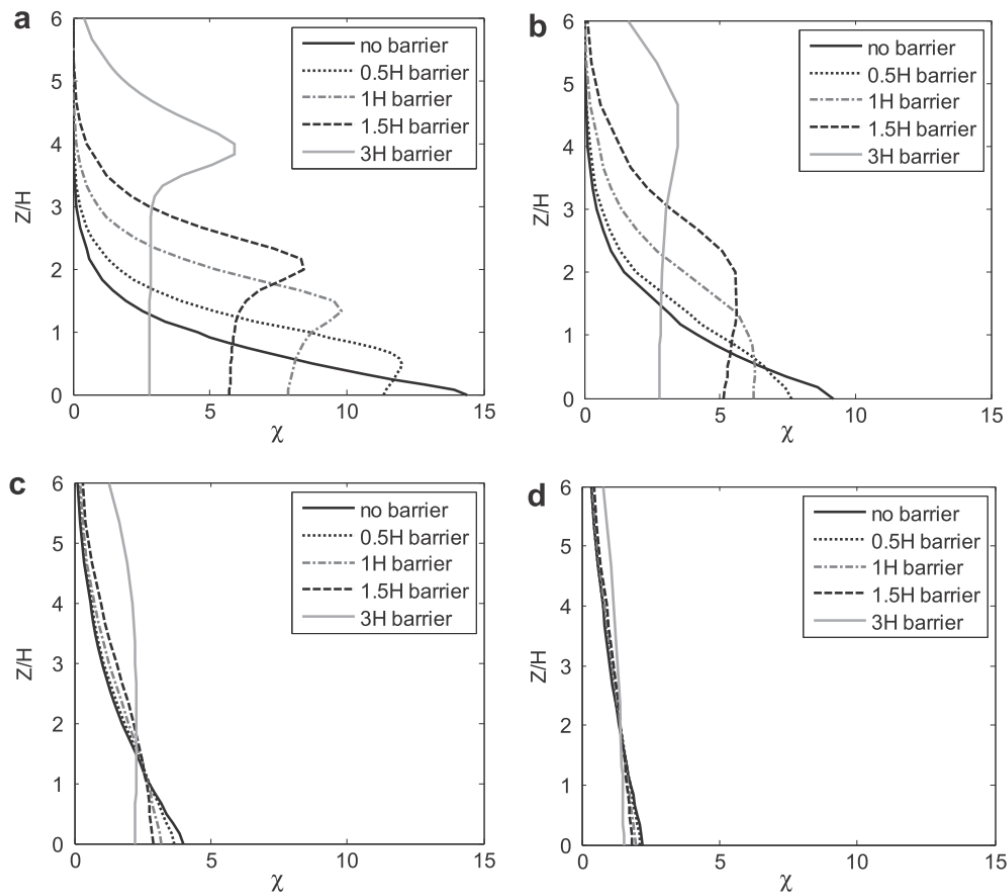


Figure 12: (a) Ground-level concentration versus downwind distance for two boundary layer wind profiles with different roughness lengths and for two different roadway configurations (Cases A and H). (b) Inverse ground-level concentration for the same cases, scaled to yield  $w\epsilon/u^*$  as slope of best-fit line (axes units are full-scale meters). (A = flat terrain; H = noise barrier at  $x/H = 3$ ). (Heist et al. 2009)

### 3.6. Computational Fluid Dynamics (CFD) Study (Hagler et al. 2011)

The CFD study simulated dispersion from a six lane divided highway with a 750 m long barrier next to the road. Barrier heights ranged from 3-18 m and the incident wind directions were 90, 75, and 45 degrees. The study investigated the performance of 3 different k-epsilon models: standard k- $\epsilon$ , Re-Normalization Group k- $\epsilon$ , and Realizable k- $\epsilon$ , and 3 different Schmidt numbers: 0.7, 1.0, and 1.3. They found that the realizable k-epsilon model with a Schmidt number of 1.0 agrees best with the wind tunnel study (Heist et al. 2009).

The study found that the barrier decreased downwind ground level concentrations. For a 3m barrier, a 20% reduction was found immediately downwind of the barrier while for the very tall (18m) barrier the concentrations were reduced by about 70% (based on Figure 4 in Hagler’s paper) (Hagler et al. 2011). No evidence was found for increased concentrations at large distances from the road. The barriers caused the vertical location of maximum concentration to move upward, as shown in Figure 13. The concentrations were found to be greater than those for the no-barrier case at heights above about half the barrier height. The horizontal extent of the barrier effect is about 30 times the barrier height. The study also found on-road concentrations increased by 1.1-2.3 times depending on barrier height.



**Figure 13: Vertical distribution of normalized concentrations ( $\chi$ ) at 20 m/3.3H (a), 50 m/8.3H (b), 150 m/25H (c), and 300 m/50H (d) from the edge of the roadway under perpendicular winds, for barriers of 3 to 18 m compared with a no-barrier scenario. The barrier is located 9.5 m from the road edge. (Hagler et al. 2011)**

Under oblique winds the maximum concentration was found at the far barrier edge (the edge farthest along the wind direction). The concentration at this edge is increased while the concentration is reduced at the other edge of the barrier (Figure 14).

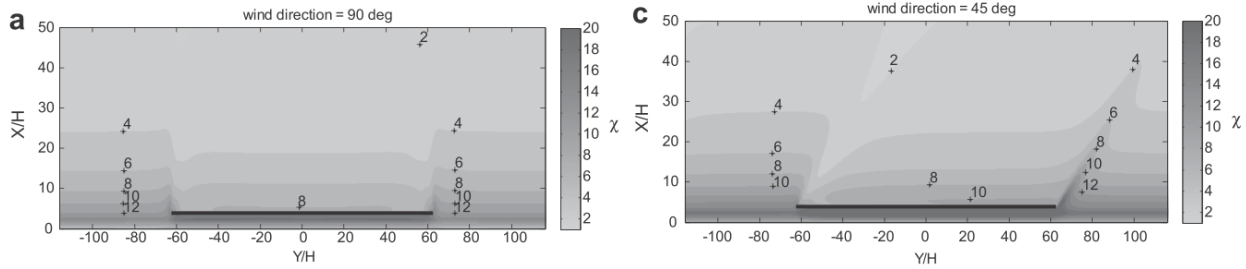


**Figure 14: Top view of modeled air pollutant concentrations at 2 m above the ground surface, for cases with a barrier of height 6 m and incident wind directions of  $90^\circ$  (a) and  $45^\circ$  (c). The barrier is located between  $-62.5$  and  $+62.5$   $Y/H$  (750 m in length). (Hagler et al. 2011)**

The CFD study also found that an emission source with a strength about 5% of the roadway emission strength placed just downwind of the barrier created concentrations that were larger than the concentrations found in the same situation with no barrier present. Figure 15 shows this effect for minor emission sources of 5% and 10% the strength of the main roadway. This effect persists for downwind distances less than about 2 times the barrier height (within the near wake of the barrier). This result is not consistent with our understanding of dispersion from a ground-level source, which suggests that concentrations associated with the service road should be lower in the presence of a barrier because of the initial dispersion induced by the wake of the barrier. This points to the uncertainty associated with CFD modeling.

Hagler et al. (2011) conclude that roadside barriers can be used to mitigate near-road air pollution, although local meteorology, the barrier structure, and the degree of lee-side emission sources are critical factors determining the outcome.

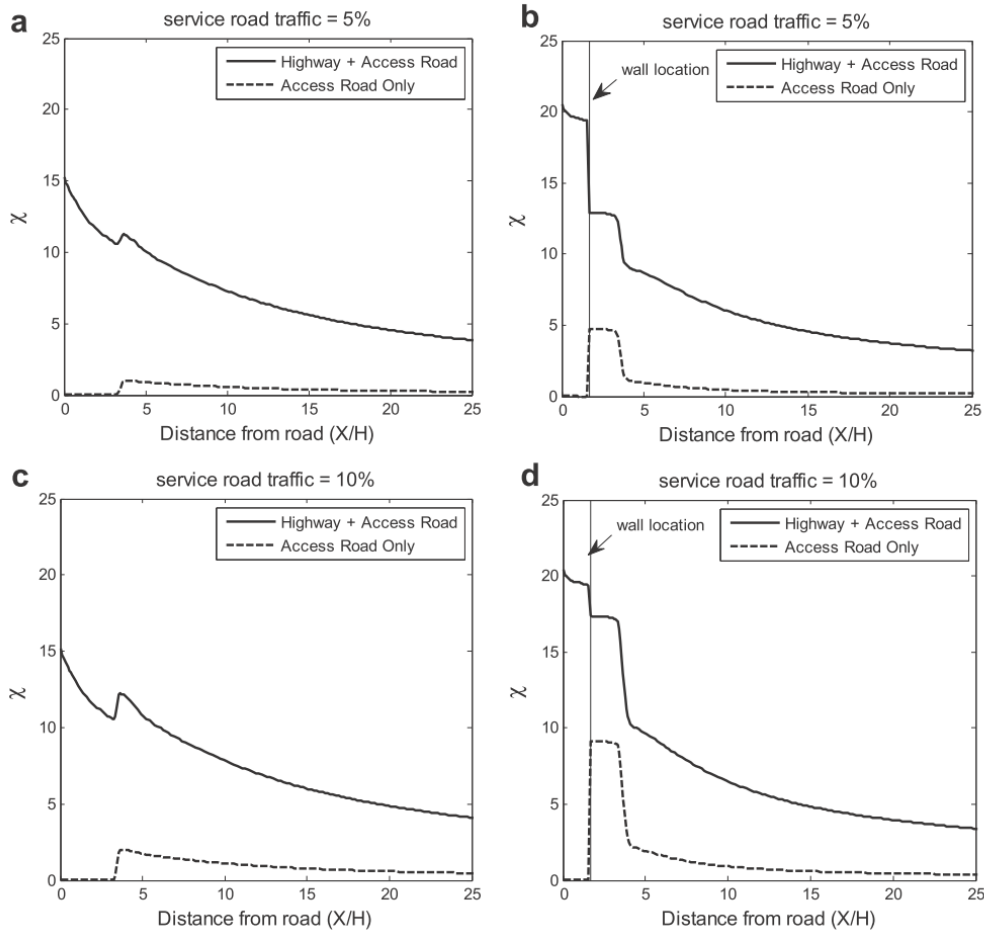


**Figure 15: Modeled total  $\chi$  and access road-attributed  $\chi$  at  $1/3H$  (2 m) above ground as a function of distance from the road up to  $25H$  (150 m). The access road is located parallel to the highway, with traffic levels at 5% (a, b) and 10% (c, d) of the highway traffic volume. Two scenarios are shown - a no barrier case (a, c) and a case with a barrier of height  $H$  (6 m) located between the highway and service road (b, d). This figure has the road edge set to  $0H$  and the wall positioned at  $1.6H$ . (Hagler et al. 2011)**

### 3.7. Tracer Study (Finn et al. 2010)

The field study was conducted near NOAA's Grid 3 diffusion grid at the Department of Energy's Idaho National Laboratory (INL), which is located across a broad, relatively flat plain on the western edge of the Snake River Plain in southeast Idaho. A 90 m long by 6 m high straw bale stack represented a roadway barrier for the primary experiment (Figure 16). The primary and reference control experiments both had a 54 m long  $SF_6$  tracer line source release positioned 1 m above ground level (AGL) representing pollution sources from a roadway. In the primary experiment, the line source was positioned 6 m upwind of the 6 m high barrier with a gridded

array of 58 bag samplers downwind of the line source and barrier for measuring mean 15-min concentrations. The control experiments (conducted at an adjacent location and simultaneous to the primary) include identical source and concentration sampling but without the barrier in the array. An array of six 3-d sonic anemometers was deployed for making wind and turbulence measurements, 5 on the primary experiment and 1 on the control experiment.

Five tests were conducted during the study, each spanning a 3-h period broken into 15-min tracer sampling intervals. One test was conducted in unstable conditions, one in neutral conditions, and three in stable conditions.



**Figure 16: Mock straw bale sound barrier, 6 m high and 90 m long. (Finn et al. 2010)**

This study found several important results. The barrier always decreased concentrations downwind of the barrier compared to those in the open field, but increased concentrations upwind of the barrier. Increasing atmospheric stability increased downwind concentrations. The barrier enhanced both lateral as well as vertical dispersion (Finn et al. 2010).

The average centerline concentration measurements for four trials from the tracer study are shown in Figure 17. This figure demonstrates that reduced concentrations relative to the flat terrain case are found at all downwind distances along the centerline downwind of the barrier.

Concentration reductions were found up to about 20 times the barrier height downwind for neutral and unstable conditions (cases a and b), and further downwind for stable conditions (c and d). Concentrations were typically less than about 50% of the non-barrier concentrations in the wake zone of the barrier, although in some cases concentrations were as low as 20% of the non-barrier concentrations. This is similar to the concentration reduction found by the wind tunnel study by (Heist et al. 2009).

Figure 18 shows contour plots of the ratio of barrier to non-barrier concentrations. This figure demonstrates that a concentration deficit exists near the center of the barrier, with increased concentrations along the barrier edges. The large concentration ratio at the edges is due to the increased lateral plume spread and also possibly due to barrier edge effects. The magnitude of the concentration at the barrier edges is only a few tens of ppb, compared with thousands of ppb at the center, so the large ratios do not represent significant concentrations.

Increases in concentrations were found upwind of the barrier in some trials, especially in case **d**, which was conducted in the most stable conditions of the study. Low wind speeds and high atmospheric stability in general tended to trap tracer upwind of the barrier to create high upwind concentrations.

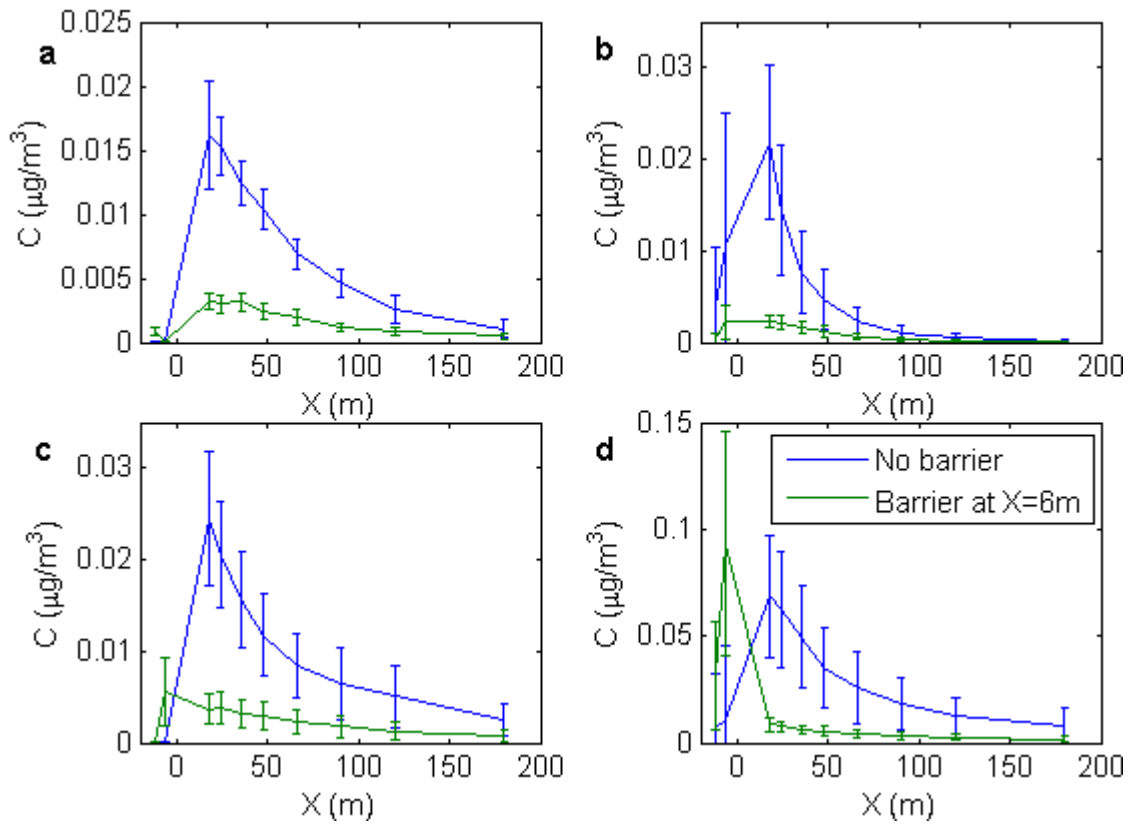


Figure 17: Average centerline concentration measurements from the Idaho Falls tracer study on (a) day 1 (neutral); (b) day 2 (unstable); (c) day 3 (stable); (d) day 5 (stable). The blue line represents the open field site and the green line represents the barrier site. Error bars represent one standard deviation.

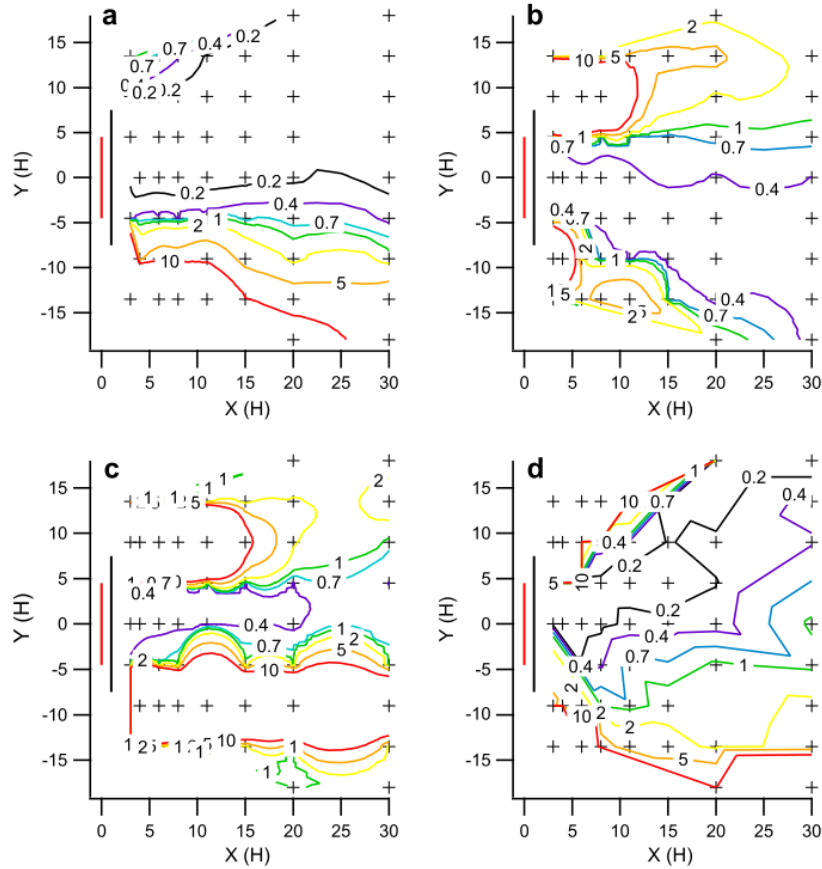


Figure 18: Contour maps of the ratio between barrier and non-barrier tracer concentrations at corresponding grid locations for the selected (a) unstable, (b) neutral, (c) weakly stable, and (d) stable cases. Tracer release line (bright red) and barrier (bold black) are shown for reference. (Finn et al. 2010)

The barrier tended to enhance lateral dispersion and plume spread. Figure 19 shows concentration maps for the non-barrier and barrier grids for different atmospheric stability conditions. The figure shows that on the non-barrier grid the plume tended to be narrow with well-defined boundaries while on the barrier grid, the plume had a greater lateral extent with less well-defined boundaries.

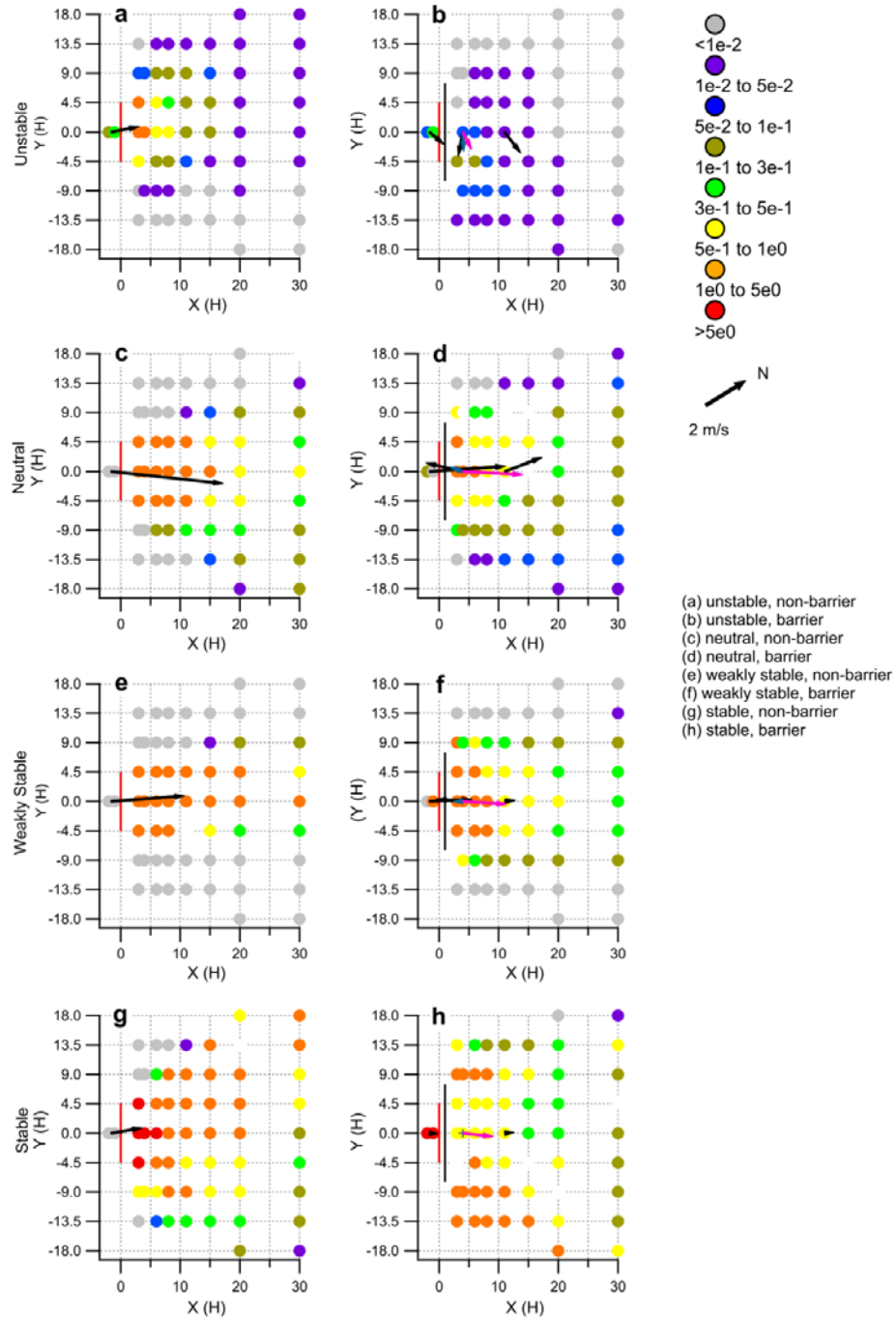


Figure 19: Corresponding non-barrier (left column) and barrier (right column) normalized tracer concentration/wind vector maps for representative (a, b) unstable, (c, d) neutral, (e, f) weakly stable, and (g, h) stable cases. Tracer release line is shown in bright red; the barrier in bold black. Wind vectors are color coded by height  $z$ : black = 3 m; light blue = 6 m; and red = 9 m. (Finn et al. 2010)

### **3.8. Conclusions of Literature Review**

Data from field and laboratory studies indicate that physical barriers are effective in reducing the near road impact of vehicle emissions. The most effective barriers seem to be simple physical walls. Modifying barrier shapes or coating the barriers with pollutant absorbing materials has little impact on concentration reductions. Filters installed on the barriers may be effective at reducing  $PM_{10}$  concentrations if moving vehicles can induce flow through the wall. Vegetative barriers can reduce concentrations by increasing vertical dispersion just as solid wall do. They can also filter particles from the air flowing through the vegetation; this need not be an additional mechanism for reducing concentrations because flow through the vegetation will reduce the vertical dispersion effect.

The modeling studies conducted to date have provided incomplete explanations of the effects of barriers especially at downwind distances of a few barrier heights, where recirculating flow is induced by the barrier. At larger distances, the variation of concentration with distance can be described with a model for flat terrain in which the source is shifted upwind and the rate of the plume growth, the entrainment velocity, is enhanced (Heist et al. 2009). The relationships between the extent of the upwind shift and the degree of enhancement of the entrainment velocity are poorly understood.

Computational fluid dynamics models (Hagler et al. 2011) have provided useful understanding of the effects of barriers, but some of the results are not consistent with observations. In principle, CFD models can be used to estimate the impact of barriers on dispersion. However, they have difficulty in simulating the effects of atmospheric stability, which can modify the effects of barriers on dispersion. Also, they cannot be readily calibrated with field data. Thus, at this stage semi-empirical dispersion models represent the best tools for modeling the effects of barriers. We refer to these models as semi-empirical because they rely on observations for parameterizing some of the governing processes. Their structure is deliberately simple to allow calibration with observations. These models are described next.

## **4. Model Development and Evaluation**

There are several models that describe concentrations associated with emissions near bluff bodies (Huber et al. 1982) and buildings (Huber 1984; Huber 1988; Huber et al. 1982; Wilson et al. 1982; Schulman et al. 2000), which in principle can be applied to estimate the

impact of barriers on dispersion. However, these models are specialized for narrow buildings and thus cannot be readily adapted to describe flow and dispersion behind long barriers next to roads.

As described earlier, the lack of adequate models and associated field data motivated the USEPA to conduct the Near Roadway Tracer Study (NRTS08) in Idaho Falls, ID in 2008 (Finn et al. 2010) and a wind tunnel study of near road dispersion in 2007 (Heist et al. 2009). A CFD study was also conducted to examine the effect of barrier height, wind direction, and secondary emission sources downwind of the barrier (Hagler et al. 2011). These studies have provided qualitative understanding of the processes that govern dispersion in the presence of a barrier. This understanding has not yet been translated into a practical dispersion model that can be used to estimate concentrations of roadway emissions in the presence of a barrier. The models described in this report represent progress in developing such a model. They are based primarily on the data from the NRTS08 field study conducted in Idaho Falls (Finn et al., 2010).

#### **4.1. Description of concentrations measured during NRTS08 and in the wind tunnel**

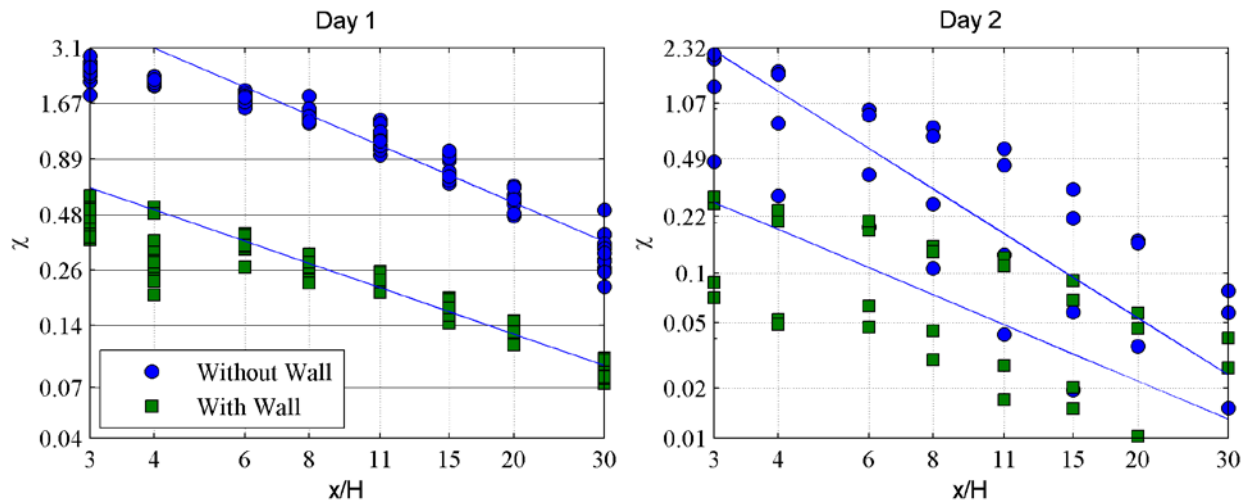
Figure 20 shows plots of the non-dimensionalized crosswind maximum concentration,  $\chi$ , at each downwind distance measured during days 1, 2, 3, and 5 of NRTS08 with and without a barrier. The non-dimensionalized concentration is calculated as:

$$\chi = \frac{CHLU}{Q} \quad (1)$$

where  $C$  is the measured concentration,  $H$  is the barrier height, which is equal to 6 meters when non-dimensionalizing both the barrier and no-barrier concentration,  $L$  is the source length,  $U$  is the wind speed measured by a sonic upwind of the source, and  $Q$  is the emission rate. Best fit lines to the log transformed data are also included. The figure shows a large reduction in concentrations at the sampler height of 1.5 meters above ground level at downwind distances up to  $30H$  from the source. The ratio of behind-barrier to no barrier crosswind maximum concentration is about 0.2 during days 1, 3, and 5 at all downwind distances. The concentration ratio increases much more rapidly with downwind distance during day 2, reaching 1 at about  $11H$  downwind of the source. The smallest observed concentrations occur during day 2.

We evaluated the idea proposed by Heist et al. (2010) that near ground-level concentrations in the presence of the barrier could be described by moving the measured no-

barrier concentrations upwind. We can only do this for day 2 because during days 1, 3, and 5 the measured no-barrier concentrations at 30H are of the same order of magnitude as the measured behind-barrier concentrations at 3H, so an upwind shift would leave no data to compare with. Figure 21 shows the result of shifting the day 2 no-barrier concentrations upwind by 11H, a distance which was chosen to best match the shifted concentration with the concentration measured in the presence of a barrier. The best fit line is also shown shifted upwind. The mean of the shifted concentration is within the range of variation of the with-barrier concentration at all downwind distances. So the source-shift idea appears to provide an adequate description of the ground-level concentrations downwind of the barrier for this particular case. However, the high concentrations close to the barrier top, seen in the wind tunnel, cannot be described by the source-shift model; the top of the barrier behaves like an elevated source, which the source-shift model does not describe.



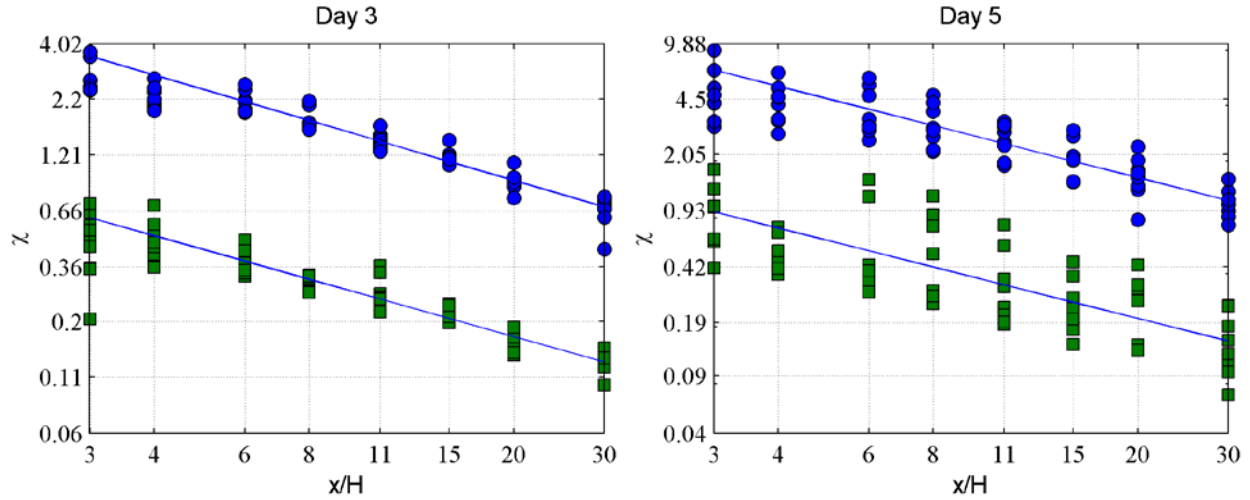


Figure 20: Non-dimensionalized crosswind maximum concentration both with and without a barrier during 4 days of NRTS08 representing the following atmospheric stabilities: Day 1 – Neutral, Day 2 – Unstable, Day 3 – Weakly Stable, Day 5 – Strongly Stable. Best fit lines to the log transformed data are included. The concentration ratio during days 1, 3, and 5, is constant at about 0.2 for all downwind distances while it increases from 0.2 to 1 at a downwind distance of about 11H during day 2.

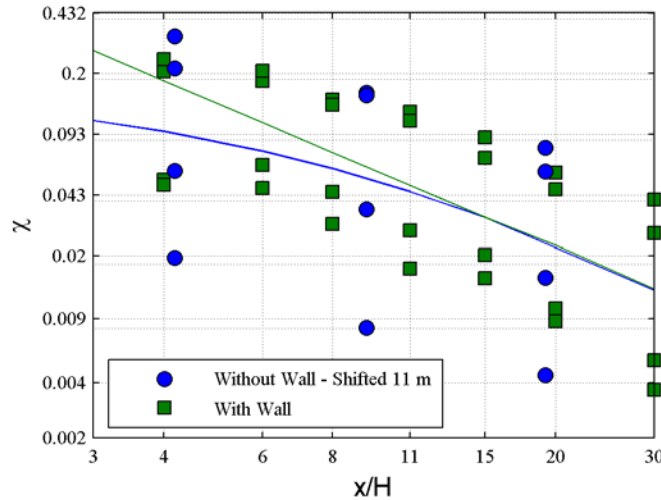
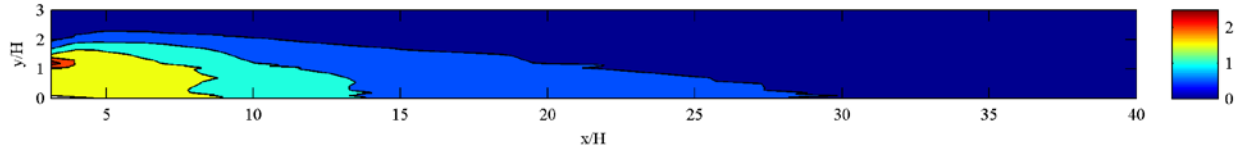


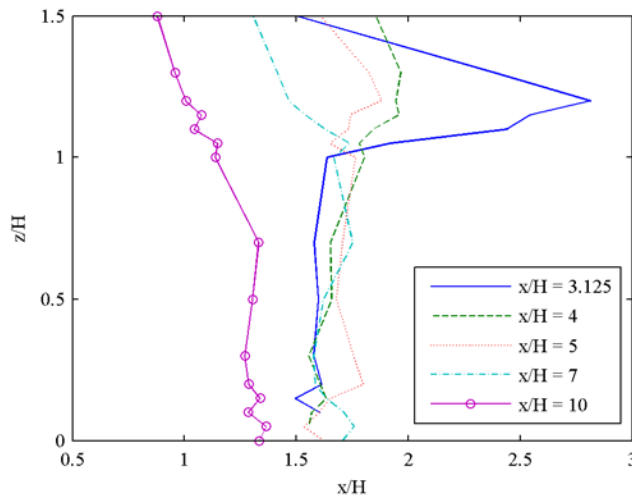
Figure 21: No-Barrier data shifted by 11H compared with the with-barrier data. The best fit line of the no-barrier data shifted 11H is also shown.

Figure 22 shows contours of concentration measured in the wind tunnel with one barrier at the downwind edge of the simulated road. The concentration has a maximum at the top of the barrier as expected because the tracer must travel over the barrier. Additionally, there is a well-mixed region below a height of 1H and extending downwind from the barrier to about 8H where

the concentration is uniform at a value of about 1.6. This is more clearly seen in Figure 23, where vertical concentration profiles for locations within or close to the near wake of the barrier are shown. The concentration does not vary much with height or downwind distance below the height of the barrier and up to a downwind distance of at least  $7H$ . The vertical profile at  $x/H = 10$  shows a slightly smaller concentration, but this also does not vary much with height below the barrier height.



**Figure 22: Non-dimensionalized concentration contours for a wind tunnel case where a barrier is located at the downwind edge of the road ( $x/H = 3$ ). The contours are similar to those for an elevated release, with a maximum at a height of  $1H$ . There is a well-mixed-wake region below  $1H$  and extending downwind to  $8H$ .**



**Figure 23: Vertical profiles of concentration within or close to the near wake of the barrier. Profiles are shown at  $x/H = 3.125, 4, 5, 7,$  and  $10$ . The contours show that the concentration is uniform within a region up to a height of  $1H$  and extending downwind to at least  $7H$ .**

The ground level concentration from an elevated release has a maximum at some downwind distance where the plume initially touches the ground. We expect similar behavior downwind of the barrier, but this does not happen: the ground level concentration measured downwind of the barrier is largest very close to the barrier. This is because the recirculating flow, seen in Figure

10, mixes the concentrations both in the horizontal and vertical directions. These features of the observed concentration patterns are the basis of the three models proposed next.

#### 4.2. Models for Dispersion behind Barriers

We propose three models: the source-shift model, the mixed-wake model, and the Puttock-Hunt model. These models account for the dominant physical effects of barriers on downwind concentrations: vertical lofting of the pollutant above the barrier, increased turbulent mixing downwind of the barrier, and recirculation of pollutants within a cavity which extends a few barrier heights downwind of the barrier. Vertical lofting creates elevated concentrations near the top of the barrier, increased turbulent mixing reduces near ground level concentrations downwind of the barrier, and concentrations within the cavity downwind of the barrier are uniform due to the recirculating flow that exists there.

The source-shift and mixed-wake models are based on the Gaussian plume formulation. For a point source the concentration is described by equation 2:

$$C(x, y, z) = \frac{Q}{U} F_y(x, y) F_z(x, z) \quad (2)$$

where  $x$ ,  $y$ , and  $z$  are the downwind distance from the source, crosswind distance, and height of the receptor,  $U$  is the wind speed,  $Q$  is the emission rate, and  $F_y$  and  $F_z$  are the horizontal and vertical concentration distribution functions. For the Gaussian plume formulation,  $F_y$  and  $F_z$  are given by equation 3a and 3b:

$$F_y = \frac{1}{\sqrt{2\pi}\sigma_y(x)} \exp\left(-\frac{y^2}{2\sigma_y(x)^2}\right) \quad (3a)$$

$$F_z = \frac{1}{\sqrt{2\pi}\sigma_z(x)} \left[ \exp\left(-\frac{(z-h)^2}{2\sigma_z(x)^2}\right) + \exp\left(-\frac{(z+h)^2}{2\sigma_z(x)^2}\right) \right] \quad (3b)$$

where  $\sigma_y$  and  $\sigma_z$  are the horizontal and vertical plume spreads.

We treat the modeled roadways as line sources. The concentration due to a line source is calculated by integrating equation 2 along the source as follows:

$$C_L(x, y, z) = \int_0^1 \frac{q}{U} F_y \left( x - ((x_2 - x_1)s + x_1), y - ((y_2 - y_1)s + y_1) \right) F_z \left( x - ((x_2 - x_1)s + x_1), z \right) ds \quad (4)$$

where  $q$  is the emission rate per unit source length and  $(x_1, y_1)$  and  $(x_2, y_2)$  are the endpoints of the source. We perform this integration numerically using Romberg integration.

The plume spreads are calculated using new plume spread formulations (Venkatram et al. 2013) derived from the concentrations measured at the open terrain site during the Idaho Falls study (Finn et al., 2010). They are given by equations 5 and 6:

$$\sigma_z = 0.57 \frac{u_*}{U(\bar{z})} x \frac{1}{1 + 3 \frac{u_*}{U(\bar{z})} \left( \frac{x}{L} \right)^{2/3}}, L > 0 \quad (5a)$$

$$\sigma_z = 0.57 \frac{u_*}{U(\bar{z})} x \left( 1 + 2 \frac{u_*}{U(\bar{z})} \frac{x}{|L|} \right), L < 0 \quad (5b)$$

$$\sigma_y = 1.6 \frac{\sigma_v}{u_*} \sigma_z \left( 1 + 1.5 \frac{\sigma_z}{L} \right), L > 0 \quad (6a)$$

$$\sigma_y = 1.6 \frac{\sigma_v}{u_*} \sigma_z \left( 1 + 0.5 \frac{\sigma_z}{|L|} \right)^{-1/3}, L < 0 \quad (6b)$$

where  $U(\bar{z})$  is the wind speed at the effective plume centerline height,  $\bar{z}$ ,  $u_*$  is the surface friction velocity,  $\sigma_v$  is the standard deviation of horizontal velocity fluctuations, and  $L$  is the Monin-Obukhov length. The effective plume centerline height is defined by:

$$\bar{z} = \frac{\int_0^\infty z C^y(x, z) dz}{\int_0^\infty C^y(x, z) dz} \quad (7)$$

where  $C^y(x, z)$  is the crosswind integrated concentration. Using the concentration profiles from equation 3, the expression for  $\bar{z}$  when the source height is zero is  $\bar{z} = \sqrt{2/\pi} \sigma_z$ . The plume spreads and wind speed (at  $\bar{z}$ ) are interdependent and must be evaluated simultaneously within this formulation.

## Meandering

In addition to the coherent plume formulation described above, we include a meandering plume formulation in the same manner as is done in AERMOD (Cimorelli et al. 2005). Meandering is used in dispersion models to describe the concentration distribution which exists during low wind speed conditions. The final model concentration is calculated by interpolating between the random plume concentration (the meandering component),  $C_r$ , and the coherent plume concentration,  $C_c$ , as follows:  $C = C_c(1 - f) + C_r f$ , where  $f$  is defined by equation 8:

$$f = \frac{2\sigma_v^2}{U^2} \quad (8)$$

The random plume concentration is calculated using equation 4, where the horizontal concentration distribution is calculated using equation 9:

$$F_{yr} = \frac{1}{2\pi x_r} \quad (9)$$

where  $x_r$  is the radial distance from source to receptor. The distribution described by equation 9 is the same in all horizontal directions, which accounts for random variation in wind direction which occurs during low wind speeds. The vertical concentration distribution used in the random plume concentration is calculated with equation 3b with  $x$  replaced by  $x_r$ .

The source-shift and mixed-wake models are developed within the Gaussian plume framework described above.

### 4.3. Source-shift Model

The source-shift model is a Gaussian plume line source dispersion model (equations 2 and 3) where the source is moved upwind to account for the barrier's effect on concentrations. This model was previously proposed by Heist et al. (2009), who also modify the turbulence downwind of the barrier by making the vertical entrainment velocity a function of the surface friction velocity and the roadway geometry. In our formulation, we do not modify the turbulence, and only use the meteorology determined from the upstream boundary layer. We include a meandering formulation, which we find improves the correlation between the model and observations and makes the turbulence modification unnecessary.

Figure 24 shows a schematic of the concepts behind the source shift. The physical source is indicated in black, and the shifted source is indicated in red. If there were no barrier we would predict concentrations using the Gaussian plume formulation, where the downwind distance  $x$  is calculate from the physical source location to the receptor. To account for the barrier we place the source at some point upwind of the physical source (indicated in red) and predict concentrations using the Gaussian plume formulation where  $x$  is now the distance from the shifted source location to the receptor. In the absence of a barrier the vertical concentration profile at some location downwind would be similar to the profile indicated as “No Barrier” in Figure 24. The vertical concentration profile the source shift model predicts is indicated as “With Barrier” in Figure 24. The vertical plume spread predicted by the source shift model at this location is larger than that of the Gaussian plume model without a source shift. So the concentration predicted by the source shift-model is smaller than that predicted by the Gaussian plume formulation near the surface, and larger far from the surface.

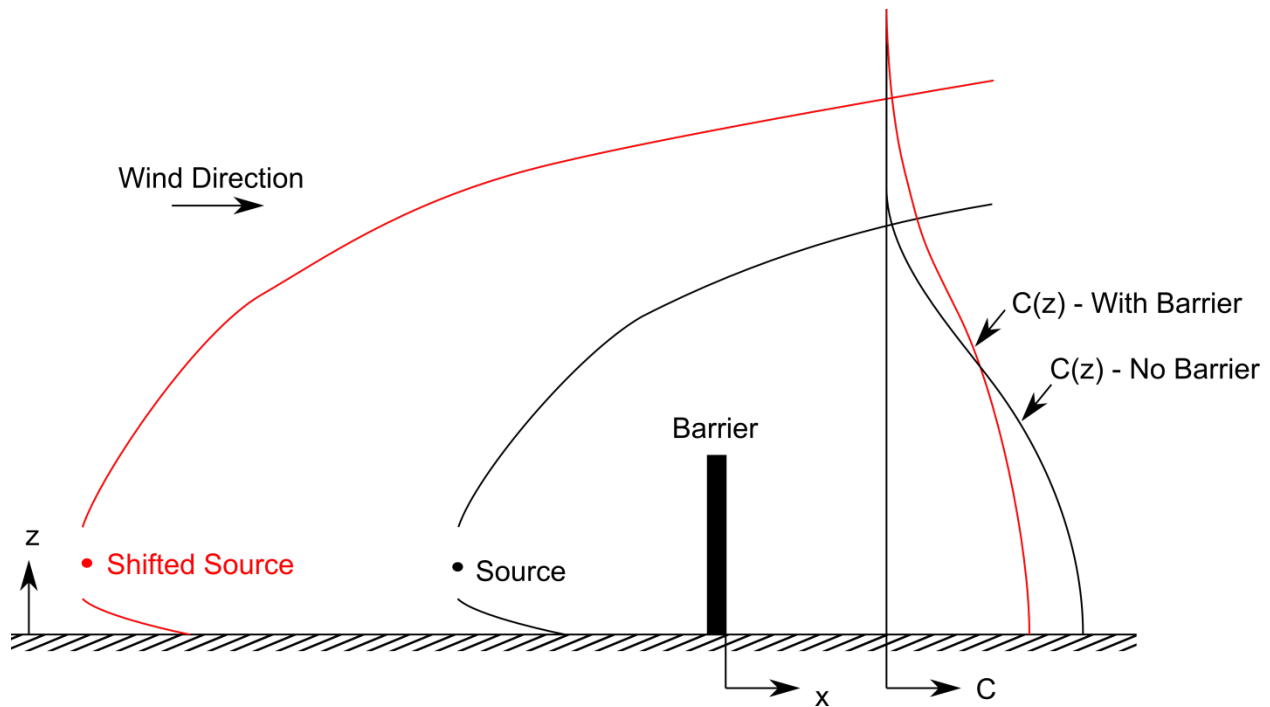


**Figure 24: Schematic of the source-shift model. The physical source is indicated in black. The vertical concentration profile at some receptor location will be similar to the black “No Barrier” profile if the downwind distance, used in calculating the vertical plume spread, is the distance from the physical source to the receptor. If we shift the source upwind then the downwind distance, which is now calculated from the shifted source to the receptor, is larger so the vertical plume spread is larger and the resulting concentration profile is similar to the red “With Barrier” profile.**

The plume spread formulation used in the source-shift model is the same as that used to predict concentrations over flat terrain with no barrier (equation 5). The concentration is given by equation 4, where the downwind distance  $x$  is replaced by the distance from the shifted source to the receptor,  $x_s = x + d$ , where  $d$  is the distance the source is moved upwind.

The upwind shift increases the plume spread at a specified distance and thus reduces ground level concentrations. The source-shift model does not account for vertical lofting of pollutants above the barrier, so the concentration predictions of this model are reliable only for near ground level receptors. The model also does not account for recirculation within the cavity downwind of the barrier, and thus will not produce accurate concentrations for receptors located within the cavity.

To complete the model we must formulate a method to calculate the source shift distance  $d$ . If we assume that the concentration is well mixed downwind of the barrier and below the barrier height (as measurements indicate), then the vertical plume spread at the location of the barrier should be proportional to the barrier height. Based on this assumption we can write the shift distance as:

$$\sigma_z \left( \frac{d + x_b}{f_1 \cos(\theta)} \right) = \sqrt{\frac{2}{\pi}} H \quad (10)$$

where  $H$  is the barrier height,  $x_b$  is the distance from the physical source to the barrier,  $\theta$  is the angle between the mean wind direction and the normal to the barrier, and  $f_1$  is an empirical constant, which we include to calibrate the model. By calculating  $d$  with equation 10 we are setting the plume spread at the barrier equal to  $\sqrt{2/\pi} H$ , which ensures that the concentration at the barrier corresponds to that when the tracer is well mixed through the height  $H$ .

Equation 10 is only valid if the source is near the barrier. The plume from a distant source has a vertical plume spread larger than  $\sqrt{2/\pi} H$  at the barrier, so that  $d$  would have to be negative to satisfy equation 10, so  $d$  is limited to be positive or zero.

### **Comparison with NRTS08**

In this section we evaluate the performance of the source-shift model in explaining near ground level concentrations measured during NRTS08. The model performance is expressed quantitatively by the geometric mean and standard deviation of the residuals between the log-

transformed observations and predictions, by the fraction of data points that are within a factor of two of the observations, and by the correlation coefficient between the data. The geometric mean,  $m_g$ , and standard deviation,  $s_g$ , are defined as:

$$\ln m_g = \sum_i \varepsilon_i / N \quad (11)$$

$$\ln s_g = \left[ \sum_i (\varepsilon_i - \ln m_g)^2 / (N - 1) \right]^{1/2} \quad (12)$$

where  $\varepsilon$  is the residual and  $N$  is the number of data points. A perfect correspondence between observations and predictions will produce  $m_g$  and  $s_g$  equal to 1. If  $m_g$  is less than 1 the observations are on average smaller than the model predictions.

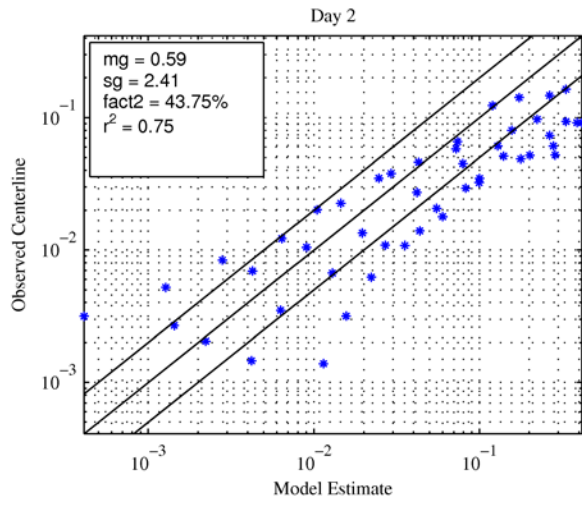
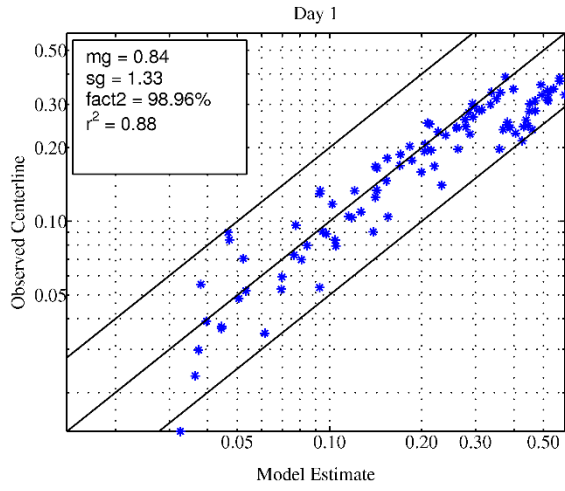
We compare the source-shift and mixed-wake models with the NRTS08 centerline and crosswind maximum concentrations. The comparison between crosswind maximum concentrations should reduce the effect of variations in wind direction on the comparison, and allow us to determine if the underlying model concepts are useful. The comparison between centerline concentrations gives us a better picture of the model performance at predicting concentrations within the recirculation zone downwind of the barrier. Concentrations near the barrier edges are larger than the centerline because the barrier was not long enough to prevent tracer from leaking around the edges. So the crosswind maximum observations do not capture the true behavior of concentration within the recirculation zone.

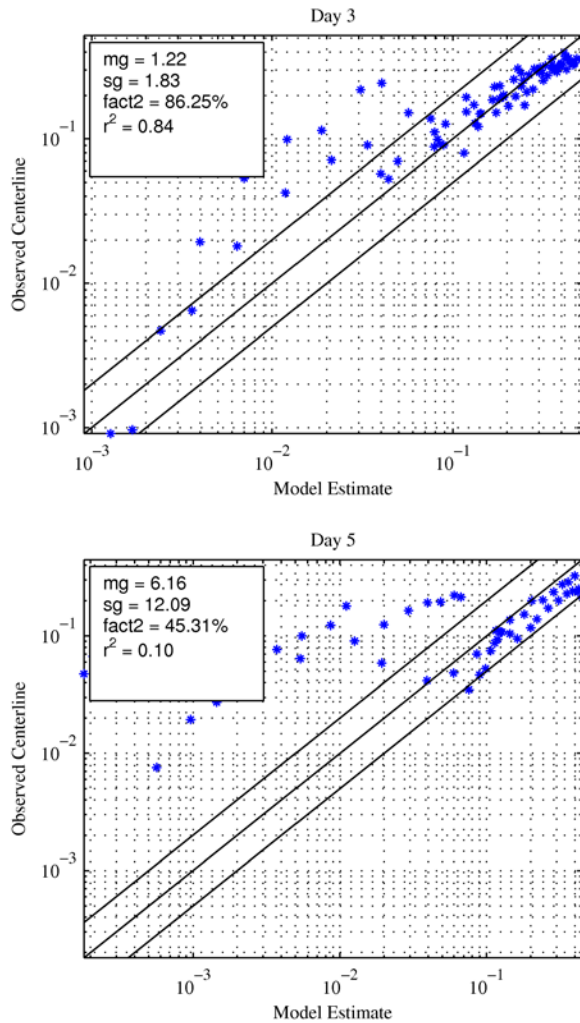
The meteorology required for the models was taken from the sonic anemometer placed 9.6 m upwind of the source during NRTS08.

The scatterplots in Figure 25 show the performance of the source-shift model at explaining NRTS08 centerline concentrations. The model was run with  $f_l = 0.5$ . During the neutral conditions of day 1 almost all model predictions are within a factor of two of observations. The model performs best during neutral conditions and worst during the very stable conditions of day 5. During day 1, 2, and 3 the model overestimates concentrations mainly due to one group of data points which were measured at receptors located within a distance of about 5H from the barrier. These receptors are within the barrier's near wake, where the tracer is uniformly mixed and the concentration is uniform. This can also be seen in Figure 27, which plots the mean

centerline concentration vs. distance from the source. There is a region (most visible during day 1) where the concentration does not change with downwind distance and the model overestimates concentrations.

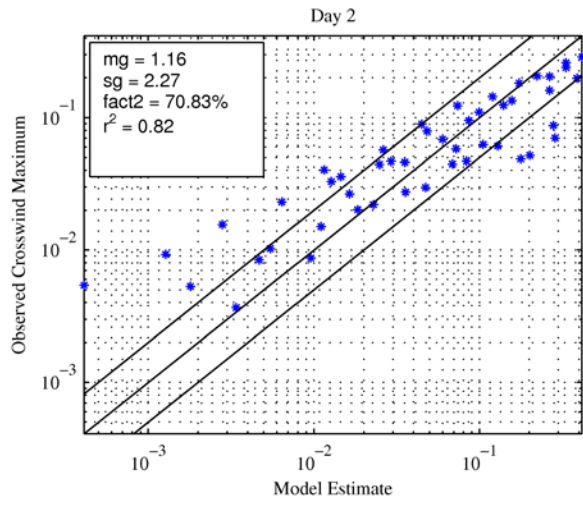
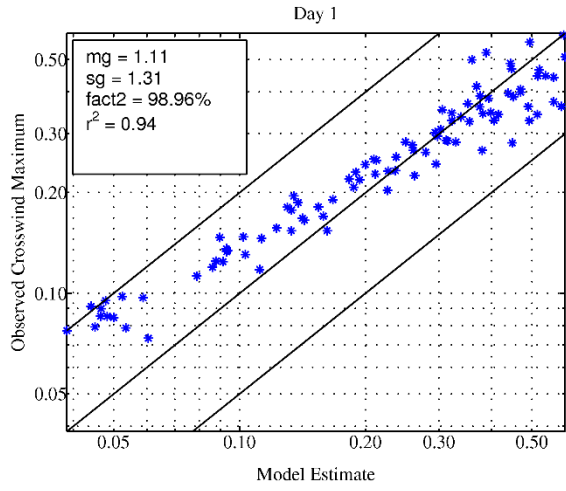
The comparison during day 5 may be misleading, because during very stable atmospheric conditions, the tracer moved around the edges of the barrier rather than over the top of the barrier, altering the concentration distribution from the ideal case of an infinitely long barrier. The data points where the model underestimates concentrations correspond to receptors far from the barrier, where tracer that traveled around the barrier edges has mixed back into the center, causing large observed concentrations. There are a few data points where the model underestimates during day 3, but these are probably not due to tracer moving around the barrier edges.

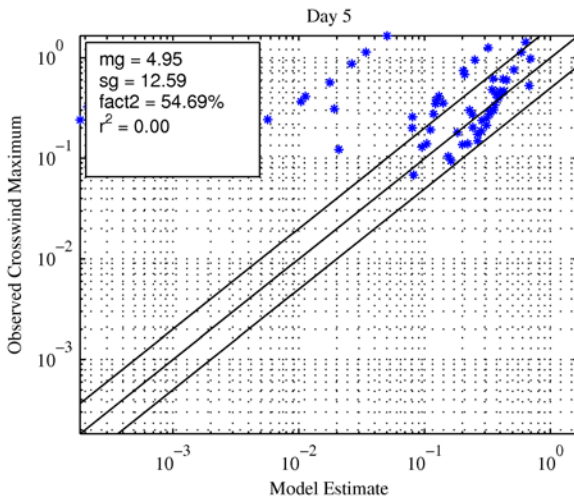
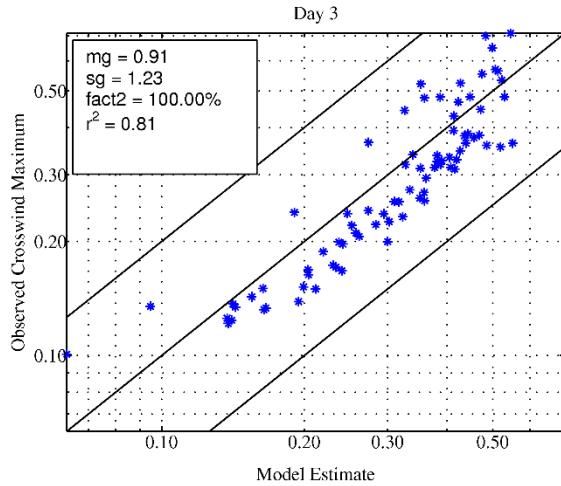




**Figure 25:** Scatterplots comparing the source-shift with centerline concentrations observed during NRTS08. The model was run with  $f_t=0.5$ . The model overestimates concentrations for receptors located within a distance of about 5H of the barrier. The model underestimates the concentration for several receptors during day 5 where the tracer moved around the barrier edges rather than over the top because the atmosphere was very stable during this day.

Figure 26 shows a comparison of the source-shift model with the crosswind maximum concentrations. Again we see that the model performs best during neutral atmospheric stability and worst during very stable conditions. The model also performs well during the slightly stable conditions of day 3, although it overestimates by a small amount. The model tends to underestimate concentrations far from the barrier during days 1 and 2, which may be caused by the meandering algorithm; the model may be predicting too large of an effect due to meandering during these stabilities.

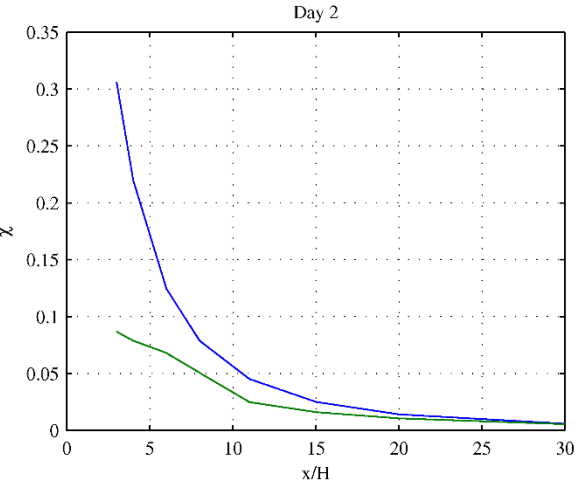
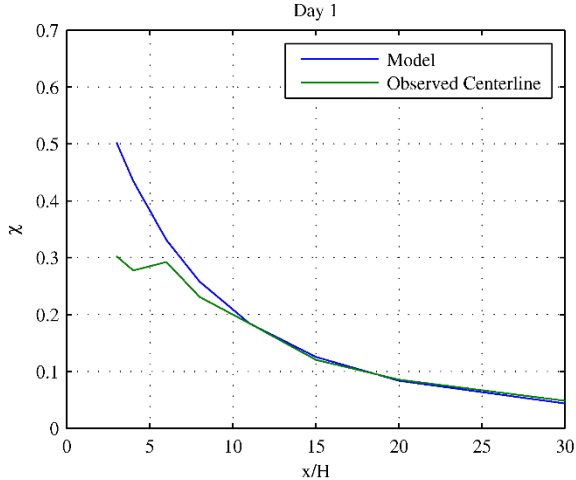




**Figure 26: Scatterplots comparing the source-shift with crosswind maximum concentrations observed during NRTS08. The model was run with  $f_t=0.5$ . The model performs best during neutral conditions and worst during very stable conditions. The model slightly overestimates during day 3, and tends to underestimate concentrations far from the barrier.**

Figure 27 compares the spatial variation of the mean centerline concentration predicted by the source-shift with that of the corresponding NRTS08 observations. The model describes the variation of mean centerline concentration very well for neutral and slightly stable conditions, and overestimates and underestimates the mean concentration for unstable and very stable conditions, respectively. The model overestimates concentrations within a region extending to a distance of about  $5H$  from the barrier, which corresponds with the barrier's near wake, where the tracer is well mixed and concentrations are uniform. We can clearly see that the concentration does not change with downwind distance in the near wake during day 1. We see a

smaller region affected by the near wake during day 3 and day 5, and a less clearly defined near wake region during day 2. Still, the model overestimates within a distance of about 5H of the barrier during days 2 and 3.



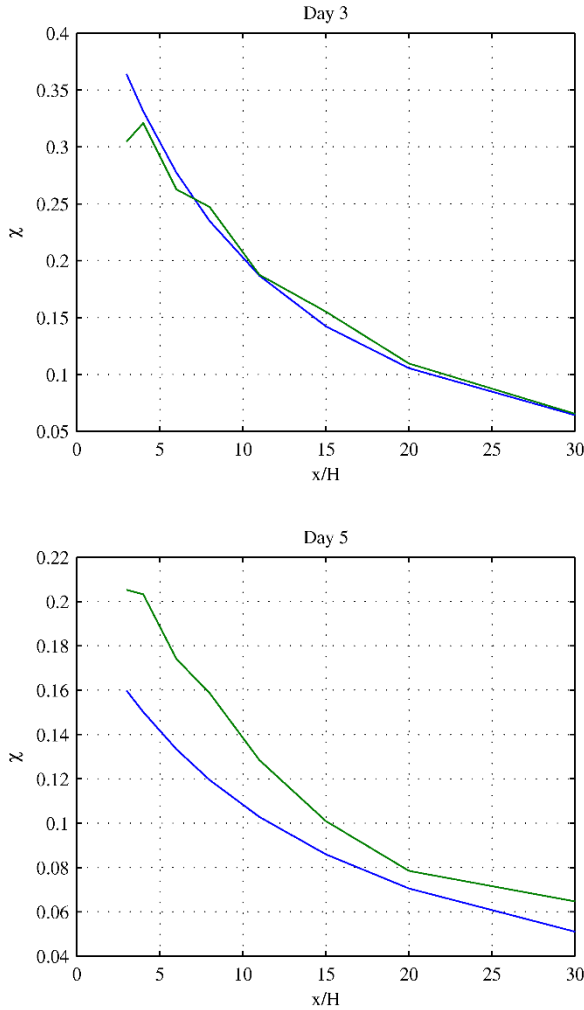


**Figure 27: Comparisons of the mean centerline concentration predicted by the source-shift with NRTS08. The model predicts mean centerline concentrations very well during neutral and slightly stable conditions. The model overestimates concentrations within the near wake of the barrier, which extends from the barrier to about  $5H$  downwind.**

### Comparison with Wind Tunnel Measurements

Figure 28 shows a comparison of the source-shift model with the infinite source concentrations measured in the wind tunnel for receptors located below a height of  $2H$ . In the wind tunnel the emission source was 48 cm long (72 m full scale), but the measured concentrations can be adjusted to represent the concentrations that would be measured if the source was infinitely long (Heist et al. 2009). The infinite source concentration refers to the concentration that is adjusted in this way.

Two wind tunnel simulations were conducted with a barrier downwind of the road, one with a smooth approach flow and one with a rough approach flow. The smooth approach flow

has a boundary layer with parameters  $z_0 = 0.27 \text{ m}$  and  $u_* = 0.25 \text{ m/s}$ , while the rough approach flow has a boundary layer with a displacement height of  $8.1 \text{ m}$  and  $z_0 = 0.78 \text{ m}$  and  $u_* = 0.3 \text{ m/s}$ . We used the 5 m wind speed of  $2.46 \text{ m/s}$  and  $2.98 \text{ m/s}$  for the smooth and rough cases, respectively. The comparisons for the smooth and rough cases are on the left and right, respectively.

There are some distinct features in the comparison which we can attribute to the effects of recirculation and vertical lofting, which are not modeled by the source-shift. We can group the data into groups where: 1) the model estimates and observations are correlated, 2) the model overestimates high concentrations and the observations are constant (data grouped along a horizontal line extending to the right on the figure), 3) the model underestimates for a scattered collection of receptors. The group where the model overestimates corresponds to the near wake of the barrier, where the observed concentration in the near wake is constant, similar to the concentration in Figure 27. The source-shift overestimates concentrations within the recirculation zone downwind of the barrier by up to a factor of two. This is consistent with the results of the comparison with NRTS08 data and is expected because the source-shift does not account for the physical effects of recirculation within the cavity downwind of the barrier. The group of data where the model underestimates corresponds to elevated receptors (above a height of about  $1H$ ).

The model tends to overestimate concentrations for the rough case. This is probably due to the choice of the wind speed used in the model. It is possible that the 5 m wind speed for the rough case was too small because of the large displacement height in the upstream boundary layer velocity profile.

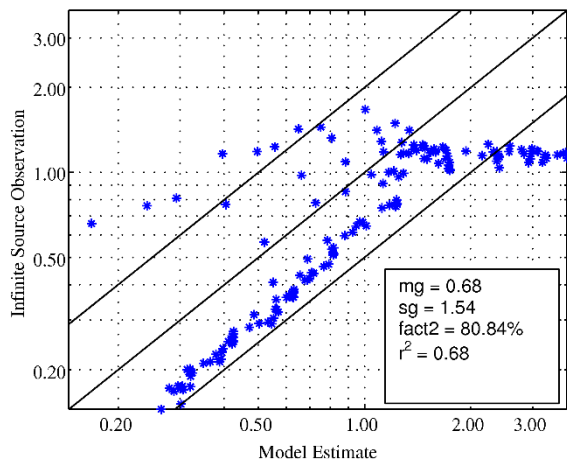
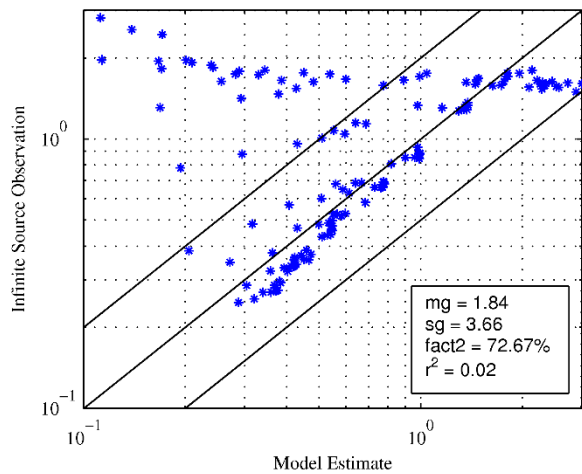


**Figure 28:** Comparison of source-shift model concentration with wind tunnel infinite source concentration for receptors below a height of  $2H$ . The smooth approach flow wind tunnel case ( $z_0 = 0.27 \text{ m}$ ,  $u_* = 0.25 \text{ m/s}$ ) is on the left and the rough approach flow wind tunnel case ( $z_0 = 0.78 \text{ m}$ ,  $u_* = 0.3 \text{ m/s}$ , displacement height =  $8.1 \text{ m}$ ) is on the right. The model was run with  $f_t=0.5$ . The model overestimates for receptors in the barrier's near wake and underestimates for elevated receptors above a height of about  $1H$ .

#### 4.4. Mixed-wake Model

The mixed-wake model is based on the Gaussian plume formulation, but the vertical concentration distribution,  $F_z$ , is modified to account for the effect of the barrier. Figure 29 is a schematic describing the physical basis of the mixed wake model. The vertical concentration profile that exists at some downwind location without a barrier, given by equation 3b, is indicated in Figure 29 by the red “No Barrier” curve, and the vertical concentration profile that we assume exists in the presence of a barrier is indicated by the black “With Barrier” curve.

When there is a barrier, the concentration is well mixed between the surface and the barrier height and then decreases to zero for receptors above the barrier height. The value of the concentration below the barrier height,  $C_s$ , is smaller than the ground level concentration without a barrier because more of the pollutant mass is elevated when the concentration is well mixed. So to conserve mass, the concentration near the surface must be smaller.

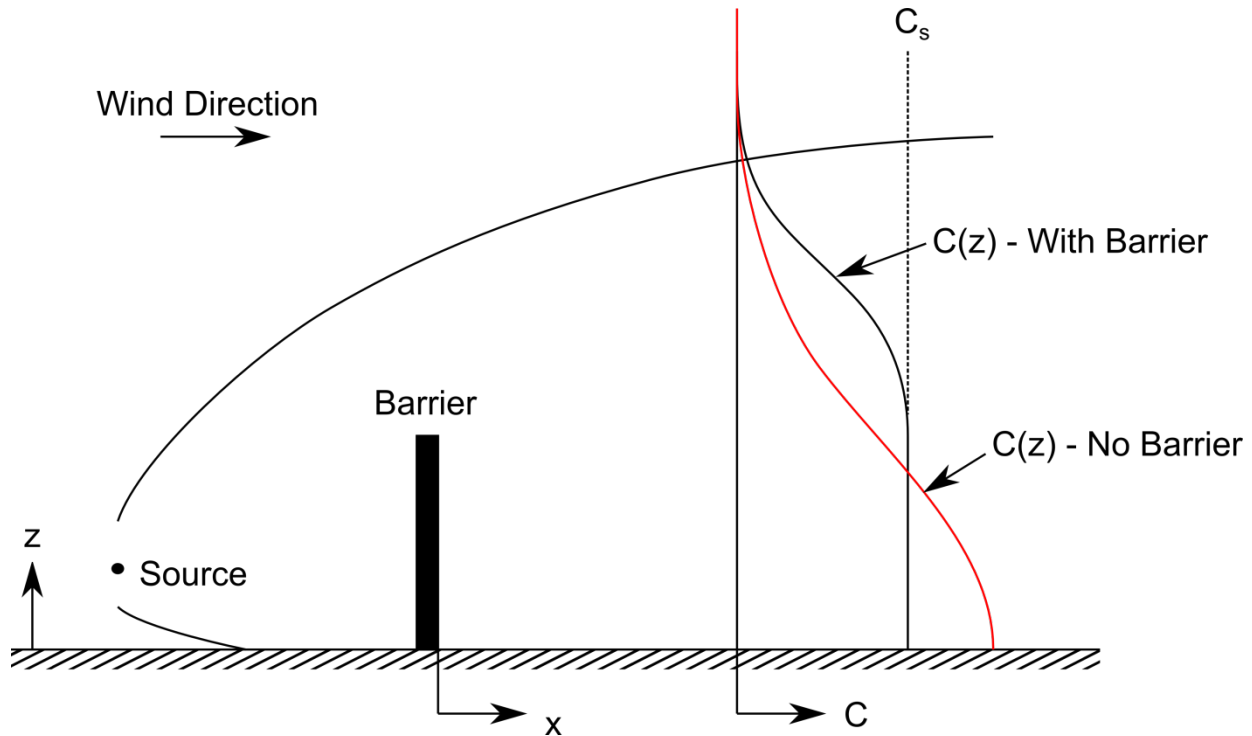


**Figure 29: Schematic of the mixed-wake model. The “No Barrier” vertical concentration profile represents the profile that the Gaussian plume formulation predicts and the “With Barrier” profile is used in the mixed-wake model. The pollutant mass is well-mixed below the barrier height in the mixed-wake model.**

With the ideas underlying the mixed-wake model in mind we can write an equation for the vertical concentration profile. Equation 13 describes a well-mixed wake zone below the barrier height, and a Gaussian profile above the barrier height:

$$\frac{F_z}{U} = C_s, z < H \quad (13a)$$

$$\frac{F_z}{U} = C_s \exp\left(-\frac{(z-H)^2}{2\sigma_z(x)^2}\right), z > H \quad (13b)$$

where the surface concentration  $C_s$  is given by equation 14:

$$C_s = \frac{1}{U\left(\frac{H}{2}\right)H + U(\bar{z})\sqrt{\frac{\pi}{2}}\sigma_z(x)} \quad (14)$$

and where the effective plume centerline height,  $\bar{z}$ , is given by:

$$\bar{z} = \frac{\frac{1}{2}H^2 + \sigma_z^2 + \sqrt{\frac{\pi}{2}}\sigma_z H}{H + \sqrt{\frac{\pi}{2}}\sigma_z} \quad (15)$$

which describes the center of mass of the plume when the wind speed is uniform with height.

The physical source height does not enter into the mixed-wake model equations; this makes intuitive sense because the barrier mixes the concentration downwind so the height of the source should not affect the concentration. Of course, if the source were elevated far above the barrier height, this would be incorrect. In this situation, the barrier would have little effect on the concentration.

Note that equation 13 describes  $F_z/U$ , and the wind speed is included in the surface concentration (equation 14). There are two important wind speeds in this formulation (which are included in equation 14): the wind speed at half the barrier height and the wind speed at the effective plume centerline height. The pollutant mass that is mixed below the barrier height is advected with the wind speed at half the barrier height, and the rest of the plume is advected with the wind speed at the effective plume centerline height.

The plume spread formulation used in the mixed wake model is the same as that used to predict concentrations over flat terrain with no barrier (equation 5). The concentration is given by equation 4 with the vertical concentration profile of equation 13 and 14.

The mixed-wake model should accurately represent both ground level and elevated receptors because the vertical concentration distribution incorporates the physical effects of vertical lofting.

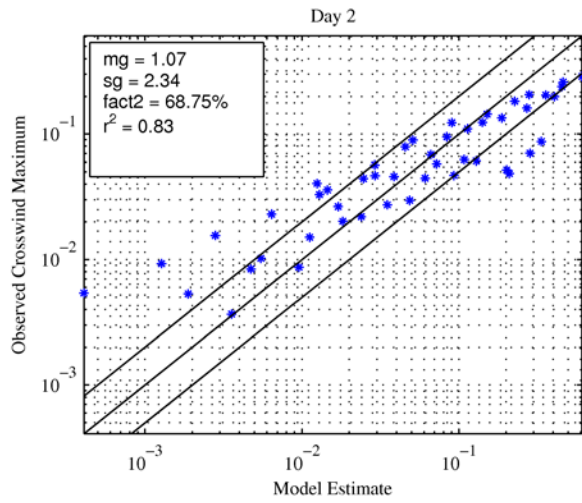
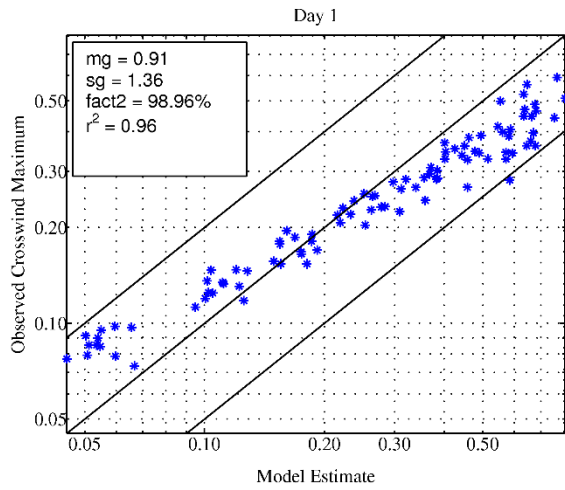
### **Comparison with NRTS08**

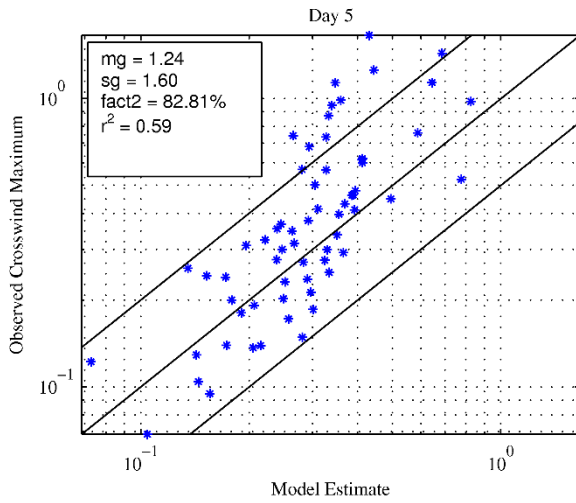
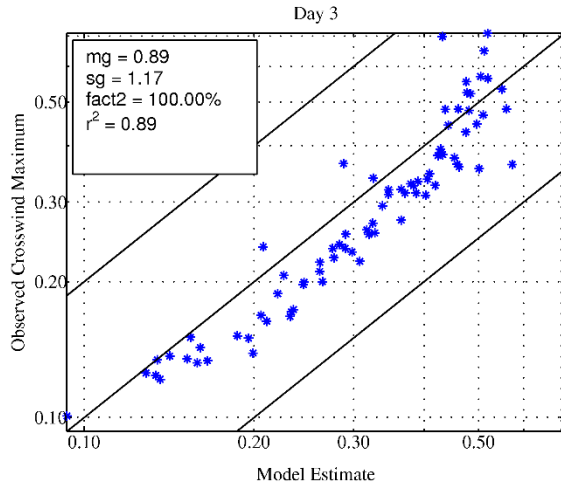
Figure 30 shows scatterplots comparing the mixed-wake model with NRTS08 crosswind maximum concentrations. For the comparison with NRTS08 we modified the turbulence used in the mixed-wake model formulation by calculating the surface friction velocity as follows:

$$u_* = u_{*flat} \frac{\sigma_w(barrier)}{\sigma_w(flat)} \quad (16)$$

where “flat” corresponds to the measured values on the non-barrier grid and “barrier” corresponds to the value measured by the sonic anemometer placed downwind of the barrier.

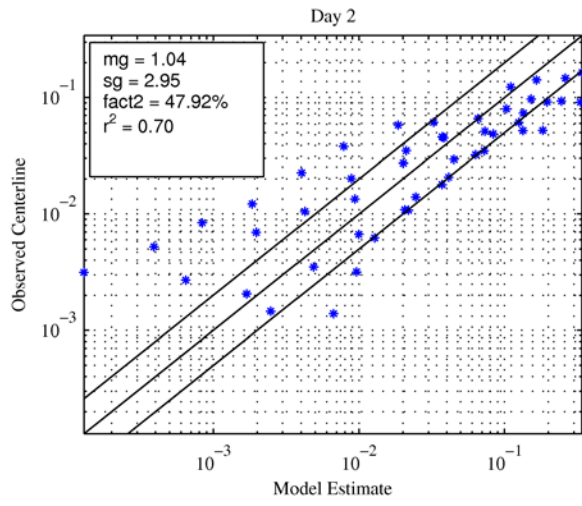
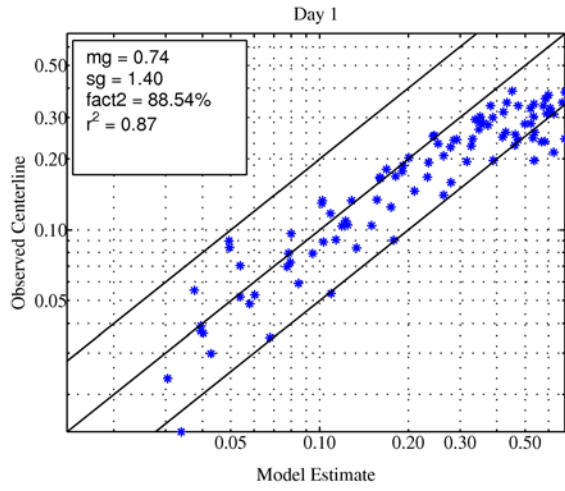
The mixed-wake model performs best during neutral and slightly stable atmospheric conditions. The mixed-wake model also does not underestimate concentrations during the very stable conditions of day 5 as the source-shift model does. The model tends to underestimate concentrations far from the barrier during days 1 and 2, and the cause is the same as that for the source-shift: the meandering algorithm is overestimating the amount of meandering. Overall the performance is similar to the source-shift, except during day 5, where the comparison with data is much better for the mixed-wake model than the source-shift.





**Figure 30: Comparison of mixed-wake model crosswind maximum concentrations with NRTS08 crosswind maximum concentrations. The model performance is similar to the source-shift, except during day 5. The model performs better than the source shift during day 5.**

Figure 31 shows a comparison of the mixed-wake model with centerline concentrations measured during NRTS08. The results are similar to the source-shift during days 1 and 2. One major difference between the models is that during day 3 the source-shift underestimates for several receptors, while the mixed-wake model does not underestimate.



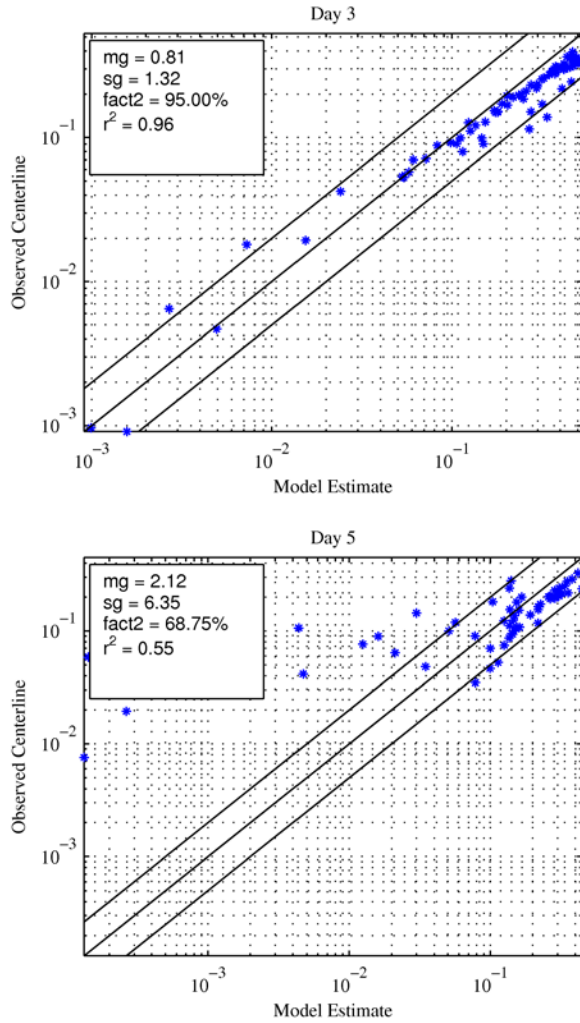
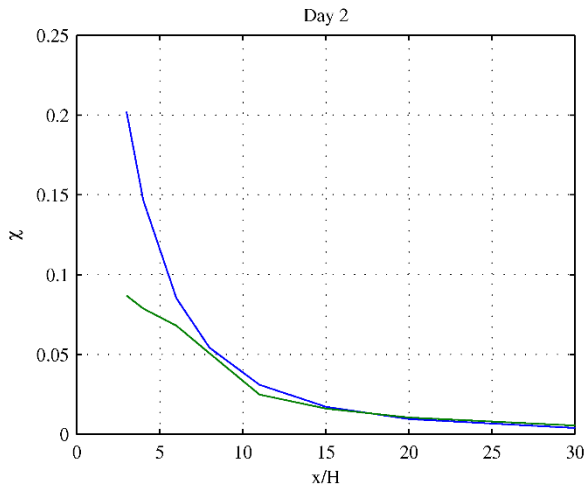
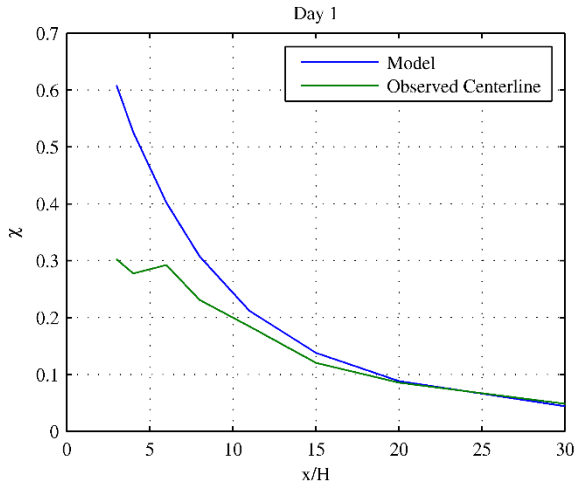


**Figure 31: Comparison of mixed-wake model centerline concentrations with NRTS08 centerline concentrations. The correlation of the model estimates with centerline concentrations during the slightly stable and very stable conditions of days 3 and 5 is better than those of the source-shift. The model performance is similar to the source-shift during days 1 and 2.**

The correlation of mixed-wake model estimates with centerline concentrations is better than that of the source-shift during day 3 and day 5, and similar to the source-shift during days 1 and 2. The standard deviation of residuals during day 5 is also smaller for the mixed-wake model than for the source-shift. The mixed-wake model predicts the mean centerline concentration during unstable conditions very well ( $m_g$  is 1.04 compared with the source-shift  $m_g$  of 0.59).

Figure 32 compares the spatial variation of the mean centerline concentrations predicted by the mixed-wake model with that of the corresponding NRTS08 observations. The results are similar to the source-shift. The mixed-wake model describes the spatial variation of the mean

concentration better than the source-shift during unstable and very stable conditions. The source-shift is better at describing the spatial variation of the mean centerline concentrations during slightly stable conditions.



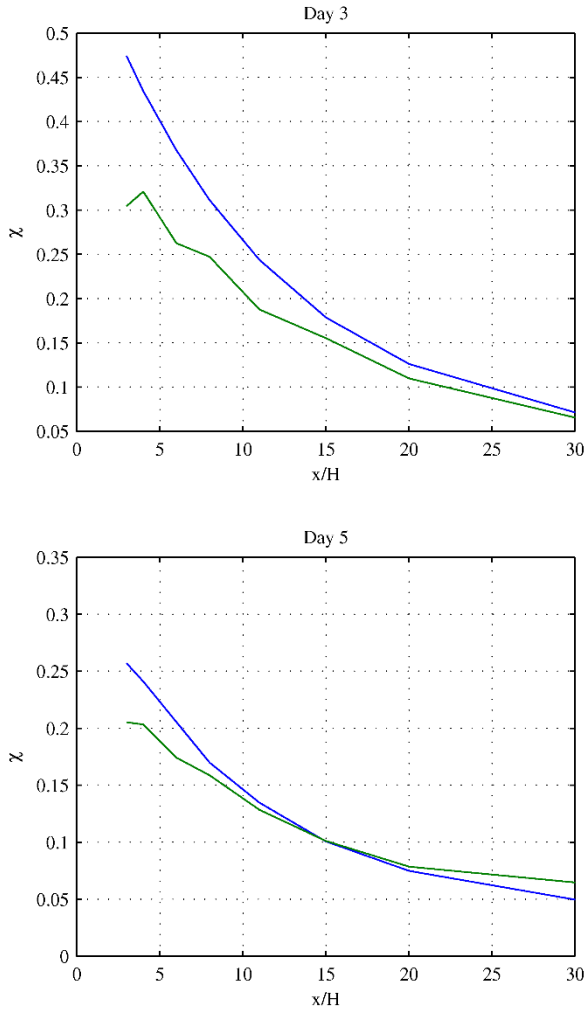


**Figure 32: Comparisons of the mean centerline concentration predicted by the mixed-wake model with NRTS08. The model predicts mean centerline concentrations very well during neutral, unstable, and very stable conditions. The model overestimates concentrations within the near wake of the barrier, which extends from the barrier to about 5H downwind. This is similar to the source-shift predictions.**

### Comparison with wind tunnel

Figure 33 shows a comparison of the mixed-wake model predictions with the wind tunnel infinite source concentrations. The comparisons for the smooth and rough wind tunnel cases are on the left and right, respectively. The model tends to overestimate concentrations in the near wake of the barrier, as we expect from the comparison with NRTS08. The correlation with the rough wind tunnel data is very good, but the model overestimates by about 50%. This is probably due to the choice of meteorological input to the model (see section 4.3 on the comparison of the source-shift with wind tunnel data). The model does not overestimate as much for the

comparison with the smooth data, but the correlation is not very good and there are some data points where the model underestimates. This is similar to the source-shift, but the mixed-wake model underestimates for fewer receptors than the source-shift, and the mixed-wake model has a better correlation. The data points where the mixed-wake model performs better than the source-shift correspond to elevated receptors. So we conclude that the mixed-wake model is better at predicting elevated concentrations (above a height of about 1H) than the source-shift.

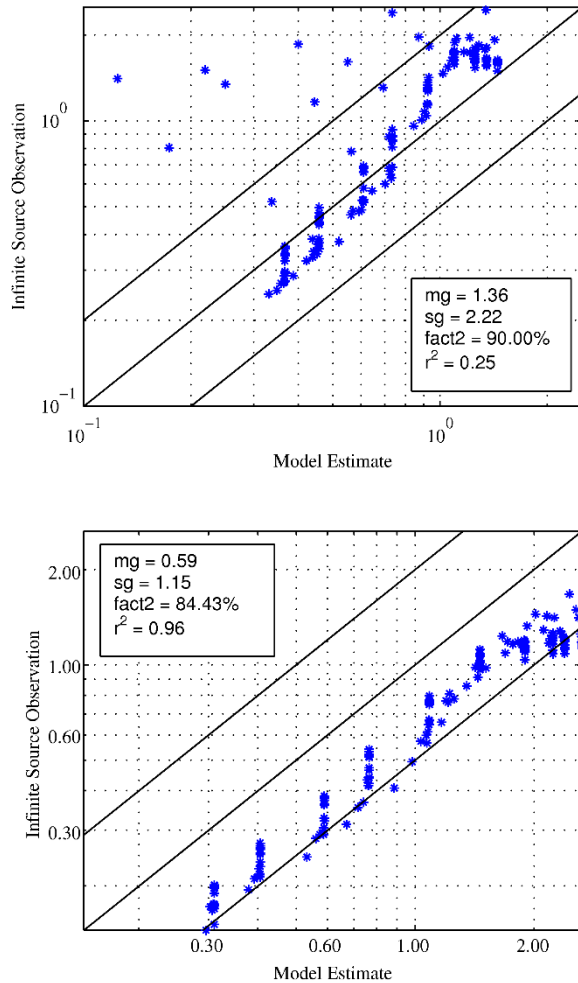


**Figure 33: Comparison of mixed-wake model concentration with wind tunnel infinite source concentration for receptors below a height of 2H. The smooth approach flow wind tunnel case ( $z_0 = 0.27\text{ m}$ ,  $u_* = 0.25\text{ m/s}$ ) is on the left and the rough approach flow wind tunnel case ( $z_0 = 0.78\text{ m}$ ,  $u_* = 0.3\text{ m/s}$ , displacement height = 8.1 m) is on the right. The model overestimates for receptors in the barrier's near wake. The model does not underestimate concentrations for elevated receptors like the source-shift does.**

We have compared the source-shift and mixed-wake models with NRTS08 and wind tunnel data. These models are based on the Gaussian plume formulation. We will now describe the Puttock-Hunt model, which is based on the eddy diffusivity based mass conservation equation.

#### 4.5. Puttock-Hunt

Puttock et al. (1979) developed a model that describes diffusion near objects with separated wakes. The model is a two-dimensional eddy diffusivity model with the following assumptions: 1) the concentration within the separated wake is constant 2) the net concentration flux across the separation streamline is zero 3) the mean flow outside the separated wake is potential flow 4) the eddy diffusivity is constant. They develop an analytical expression for the concentration and state that the solution is still a good approximation even if assumptions 3 and 4 are not satisfied. We solve the governing equation numerically and specify the Monin-Obukhov similarity profiles of wind speed and a form of the eddy diffusivity specific to flow over a sound wall instead of the constant wind speed and eddy diffusivity which are specified by assumptions 3 and 4.

Assumption 3 deserves some more explanation. Potential flow is by definition incompressible and irrotational. This type of flow can be expressed in terms of the scalar velocity potential,  $\phi$ , and stream function,  $\psi$ , which satisfy  $\nabla^2\phi = 0$  and  $\nabla^2\psi = 0$  and which are related to the velocity as follows:

$$(U, V) = \left( \frac{\partial\phi}{\partial x}, \frac{\partial\phi}{\partial y} \right) = \left( -\frac{\partial\psi}{\partial y}, \frac{\partial\psi}{\partial x} \right) \quad (17)$$

where  $U$  and  $V$  are the horizontal and vertical components of the wind speed. For two-dimensional flow, the potential and stream function are scalar fields. In the Puttock-Hunt model the velocity potential and stream function are model parameters that are specified to match the flow over a sound wall. We describe how these parameters are specified below.

The governing equation, modified for non-constant wind speed and eddy diffusivity, is:

$$U(\psi) \frac{\partial C}{\partial \phi} = \frac{\partial}{\partial \psi} \left( K_z(\psi) \frac{\partial C}{\partial \psi} \right) \quad (18)$$

where  $C$  is the concentration,  $K_z(\psi)$  is the vertical eddy diffusivity,

Equation 18 is derived by writing the advection diffusion equation in terms of the velocity potential and stream function assuming that the horizontal and vertical diffusivities are equal, and then neglecting the downwind diffusion term.

The boundary condition on the ground is:

$$\frac{\partial C}{\partial \psi} = 0 \quad (19a)$$

On the surface of the separated wake the concentration is equal to the constant wake concentration (by assumption 1):

$$C = C_w \quad (19b)$$

where  $C_w$  is the concentration within the wake. Far from the source the concentration goes to zero:

$$C \rightarrow 0 \text{ as } |\phi| \rightarrow \infty \quad (19c)$$

$$C \rightarrow 0 \text{ as } |\psi| \rightarrow \infty \quad (19d)$$

Equation 18 is solved using a finite difference method and then the resulting concentrations are transformed to the physical ( $x$ - $y$ ) domain using the specified stream function and velocity potential. A solution for the potential in the upper half plane (bounded by the  $x$ -axis and extending to infinity) is  $\phi = U_0 x$  and the stream function is  $\psi = -U_0 y$  where  $U_0$  is the approach flow velocity. The potential and stream function satisfy the Laplace equation (which is invariant under a conformal transformation) and equation 17, so we can determine the potential and stream function in the physical domain using a conformal transformation from the upper half plane to the physical domain. The conformal transformation is defined by the shape of the boundary in the physical domain. With this in mind, it is convenient to define the boundary of the sound wall recirculation zone by a polygon because any polygon can be mapped conformally to the upper half plane using the Schwarz-Christoffel transformation (Walker 1964). We define the approach flow velocity,  $U_0$ , as the velocity predicted by Monin-Obukhov similarity theory at the sound wall height.

The specific transformation we use is defined by Figure 34. The potential flow region extends to infinity in the  $y$ -direction and is bounded by the ground at  $y=0$  and by the hypotenuse

of two triangles which define the separated wake downwind of the wall and an upwind displacement zone where the flow is also separated. The barrier height is  $H$ , the downwind separation streamline touches the ground at  $x = w_d$ , and the displacement zone begins at  $x = -w_u$ . With these parameters specified the velocity potential and stream function are fully defined. The shape of the separated wake is somewhat arbitrary—we chose the simplest shape possible—but it turns out that the predicted concentrations are not very sensitive to the shape of the separation streamline, and are effected much more by the wall height and downwind extent of the wake.

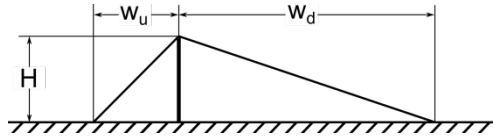


**Figure 34:** Schematic defining the boundary of the potential flow region. The variables are:  $H$ , the barrier height,  $w_d$ , the distance from the wall where the separation streamline touches the ground, and  $w_u$ , the upwind distance where the displacement zone begins.

The eddy diffusivity is calculated using an empirically determined expression for the standard deviation of vertical velocity fluctuations developed by Weil (1996). This formulation is the same as that used in the PRIME model (Schulman et al. 2000). We assume that the vertical eddy diffusivity can be related with the standard deviation of vertical velocity fluctuations by:

$$K_z = \frac{\sigma_w^2 l}{U} \quad (20)$$

where  $l$  is the turbulence length scale. The standard deviation of vertical velocity fluctuations is calculated using the following equation developed by Weil (1996):

$$\sigma_w = \sigma_{w0} + (1.7\sigma_{wN} - \sigma_{w0}) \left( \frac{x + R}{R} \right)^{-2/3} \quad (21)$$

where the subscript  $N$  refers to a value typical of neutrally stable atmospheric conditions and the subscript  $0$  refers to the ambient value. The diffusion length scale  $R$  is equal to  $2H$  for a long wall. Solving equation 20 for  $\sigma_w$ , plugging this into equation 21, and assuming the velocities and turbulence length scales are equal for the ambient, typical neutral, and behind-wall turbulence, results in the following expression for the eddy diffusivity downwind of the wall:

$$K_z^{0.5} = K_{z0}^{0.5} + (1.7K_{zN}^{0.5} - K_{z0}^{0.5}) \left( \frac{x+R}{R} \right)^{-2/3} \quad (22)$$

We substitute the Monin-Obukhov similarity profile of eddy diffusivity for the ambient and neutral diffusivities. The expressions for the similarity profiles of wind speed and eddy diffusivity are:

$$U(z) = \frac{u_*}{\kappa} \left[ \ln \left( \frac{z}{z_0} \right) + \psi_M \left( \frac{z_0}{L} \right) - \psi_M \left( \frac{z}{L} \right) \right] \quad (23)$$

$$K_z(z) = \frac{\kappa u_* z}{\phi_H(z/L)} \quad (24)$$

where  $\phi_H$  is the non-dimensional temperature profile,  $\psi_M$  is a similarity function related to the non-dimensional wind shear,  $\kappa$  is the Von-Karman constant, and  $z_0$  is the surface roughness length.

### Extension for Finite Source Length and Wind Direction

The Puttock-Hunt model assumes that the source and sound wall are infinitely long and that the wind direction is perpendicular to the roadway, but the model can be extended to account for finite sources and small angles between the wind direction and the normal to the roadway. We account for the angle between the wind direction and the normal to the roadway,  $\theta$ , by replacing the receptor's distance from the source with the effective downwind distance,  $x_{eff} = x/\cos(\theta)$  described in (Venkatram et al. 2006). We account for finite source length by multiplying model predictions by the factor:

$$f_t = 0.5[erf(t_1) - erf(t_2)] \quad (25)$$

where:

$$t_i = \frac{(y - y_i) \cos(\theta) + x_i \sin(\theta)}{\sqrt{2}\sigma_y(x \cos(\theta) + (y - y_i) \sin(\theta))} \quad (26)$$

and the subscript  $i=1,2$  refers to the beginning and end point of the source, respectively.

Equation 25 is a term which appears when the Gaussian plume equation is integrated in the crosswind direction (as in equation 4) to represent a line source. The term accounts for

horizontal concentration variation due to a finite length line source. If the source is infinitely long  $y - y_i$  becomes infinite and  $f_i$  becomes equal to 1.

### **Comparison with NRTS08**

Figure 35 compares the Puttock-Hunt model with NRTS08 centerline concentrations. The model was run with  $w_u = 1H$  and  $w_d = 5H$ . The model performs best during neutral and slightly stable atmospheric conditions, and worst during very stable conditions. The model overestimates concentrations within the recirculation zone downwind of the barrier during all days;  $m_g$  less than one during days 1 and 3 reflects this over-estimation near the barrier. During day 2 there is more spread in the data and the model overestimates more, even for receptors outside of the recirculation zone.

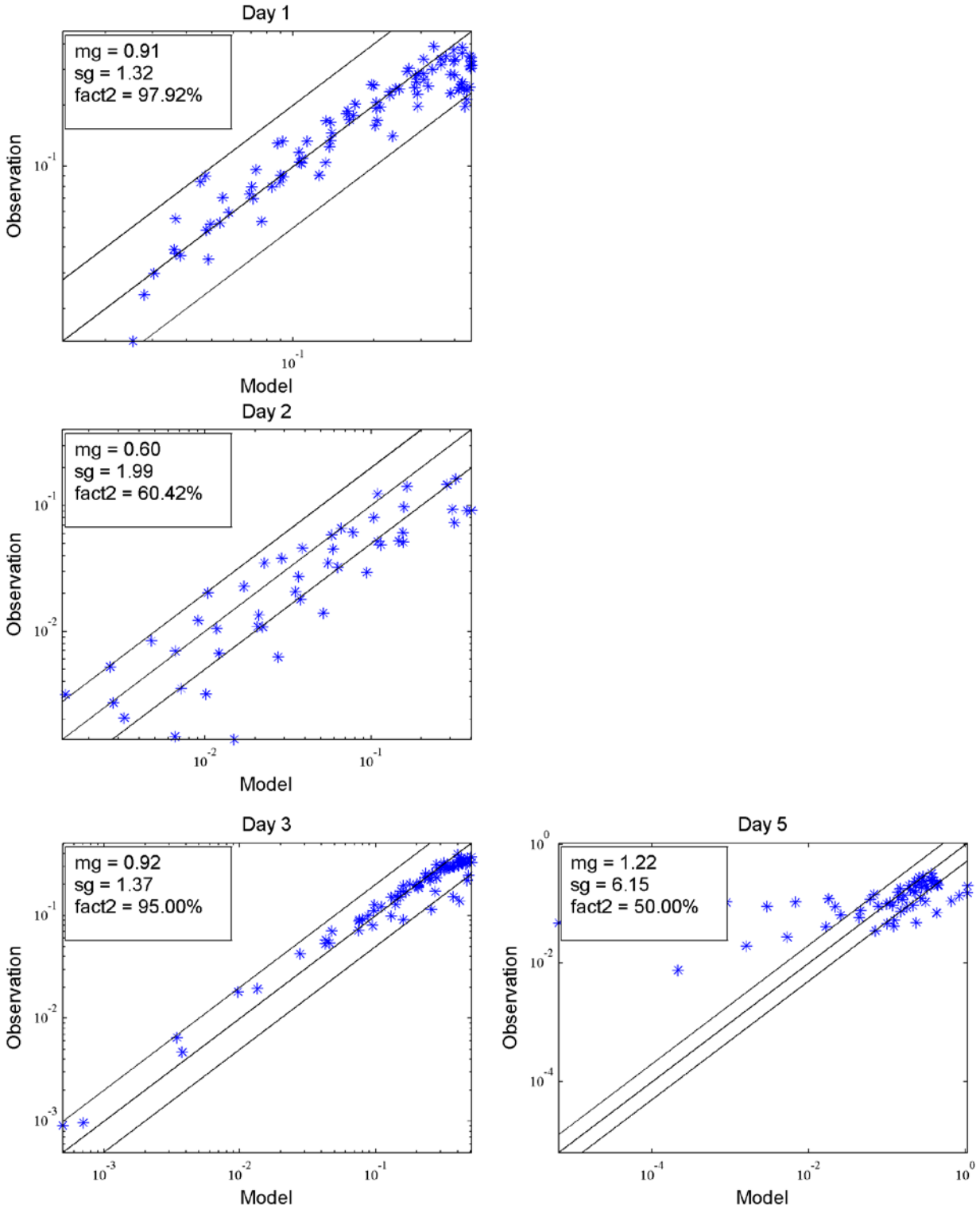


Figure 35: Comparison of Puttock-Hunt model centerline concentration with NRTS08 centerline concentrations. The model was run with  $w_u = 1H$  and  $w_d = 5H$ .

During day 5, some concentrations are under-estimated by several orders of magnitude, which is similar to the results of the source-shift. Again, the large observed concentrations may be due to tracer moving around the barrier edges and mixing into the center at large downwind distances. Overall the model performs well. The main issue with the model is that the concentration within the recirculation zone is over-estimated.

### **Comparison with wind tunnel**

Figure 36 shows a comparison of the Puttock-Hunt model predictions with the wind tunnel measurements made with the smooth and rough boundary layer approach flow and adjusted for an infinite source length. The model was run with  $w_u = 1H$  and  $w_d = 4H$ . All receptors below a height of  $2H$  are included in the plot. Figure 37 shows contours of the relative error between the Puttock-Hunt model predictions and the infinite source wind tunnel measurements for the rough boundary layer. The model overestimates by about a factor of two near the top of the barrier. The model does not overestimate within the recirculation zone as the source-shift model and mixed-wake model do, and the relative error is less than about 0.5 below a height of  $2H$ .

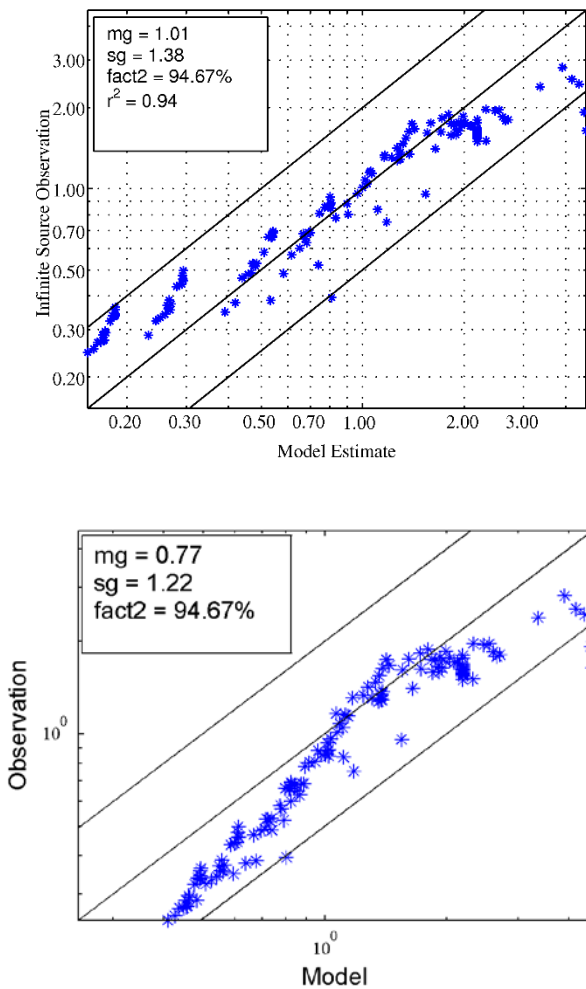


Figure 36: Comparison of Puttock-Hunt model concentration with wind tunnel infinite source concentration for receptors below a height of  $2H$ . The smooth approach flow wind tunnel case ( $z_0 = 0.27 \text{ m}$ ,  $u_* = 0.25 \text{ m/s}$ ) is on the left and the rough approach flow wind tunnel case ( $z_0 = 0.78 \text{ m}$ ,  $u_* = 0.3 \text{ m/s}$ , displacement height =  $8.1 \text{ m}$ ) is on the right. The model was run with  $w_u = 1H$  and  $w_d = 4H$ . The model does not overestimate concentrations in the barrier's near wake as much as the source-shift and mixed-wake models, and does not underestimate concentrations for elevated receptors as the source-shift does.

The overall comparison including elevated and ground level receptors is better for the Puttock-Hunt model than the source-shift model. The comparison is similar to the mixed-wake model, although the mixed-wake model has a smaller residual standard deviation. The Puttock-Hunt model has a smaller bias than the mixed-wake model ( $m_g = 0.59$  for the mixed-wake model), but this could be due to the meteorology that was input to the mixed-wake model.

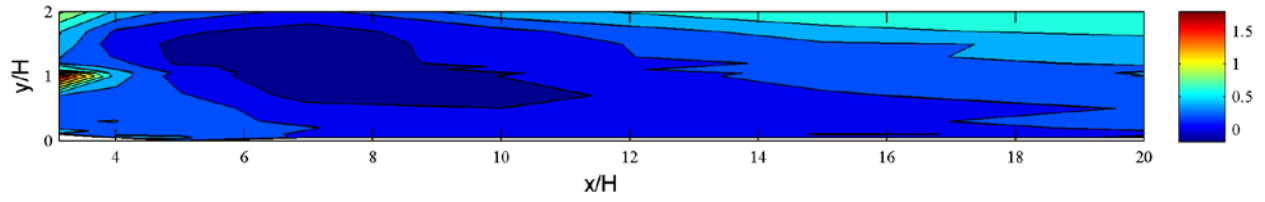


Figure 37: Contour plot of relative error between Puttock-Hunt model predictions and wind tunnel infinite source concentrations for the rough boundary layer. The model was run with  $w_u = 1H$  and  $w_d = 4H$ .

## 5. Conclusions of the Model Comparison with Observations

Table 2 summarizes the statistics of the source-shift, mixed-wake, and Puttock-Hunt models when compared with NRTS08 centerline concentrations. Table 3 summarizes the source-shift and mixed-wake model statistics for the comparison with NRTS08 crosswind maximum concentrations. Table 4 summarizes the model statistics for the comparison with wind tunnel infinite source concentrations.

Table 2: Summary of model statistics for comparison with NRTS08 centerline concentrations.

<i>Day</i>	Source-Shift				Mixed-Wake				Puttock-Hunt			
	1	2	3	5	1	2	3	5	1	2	3	5
$m_g$	0.84	0.59	1.22	6.16	0.74	1.04	0.81	2.12	0.91	0.60	0.92	1.22
$s_g$	1.33	2.41	1.83	12.1	1.40	2.95	1.32	6.35	1.32	1.99	1.37	6.15
factor of 2	99	44	86	45	89	48	95	69	98	66	95	50
$r^2$	0.88	0.75	0.84	0.10	0.87	0.70	0.96	0.55	0.89	0.77	0.96	0.41

Table 3: Summary of model statistics for comparison with NRTS08 crosswind maximum concentration.

<i>Day</i>	Source-Shift				Mixed-Wake			
	1	2	3	5	1	2	3	5
$m_g$	1.11	1.16	0.91	4.95	0.91	1.07	0.89	1.24
$s_g$	1.31	2.27	1.23	12.6	1.36	2.34	1.17	1.60
factor of 2	99	71	100	55	99	69	100	83
$r^2$	0.94	0.82	0.81	0	0.96	0.83	0.89	0.59

**Table 4: Summary of model statistics for comparison with wind tunnel infinite source concentrations for the smooth and rough approach flow.**

<i>Case</i>	Source-Shift		Mixed-Wake		Puttock-Hunt	
	Smooth	Rough	Smooth	Rough	Smooth	Rough
$m_g$	1.84	0.68	1.36	0.59	1.01	0.77
$s_g$	3.66	1.54	2.22	1.15	1.38	1.22
factor of 2	73	81	90	84	95	95
$r^2$	0.02	0.68	0.25	0.96	0.94	0.93

The mixed-wake model has a performance similar to the source-shift, except it predicts concentrations better during unstable conditions and it predicts the elevated concentrations better. The Puttock-Hunt model can predict the concentration in the barrier's near wake better than the mixed-wake model and the source-shift, but the model requires more assumptions and there are more parameters to adjust in the model. It is not clear if the model will produce good predictions for different barrier heights with the same parameters that we used for a 6 m barrier. This conclusion highlights an important deficiency in our comparison with measurements: we only have data for one barrier height. To evaluate the models better we must compare them with data for different barrier heights. In the absence of data from field studies or wind tunnels, we use results from CFD simulations to get a better sense of the model performance with different barrier heights.

## 6. CFD Simulations to Examine the Effect of Barrier Height

The above comparisons with measurements are for a 6 meter barrier. We must compare the models with measurements for different barrier heights, but the available concentration data for barriers do not describe the effect of variation in barrier height. The EPA wind tunnel experiment is the only experiment where multiple barrier heights were examined. This experiment examined a 6 m and a 9 m barrier. To get a better sense of whether the models work for different barrier heights we ran CFD simulations with barriers of different heights and compared the results with the model predictions. We used the Quick Urban and Industrial Complex (QUIC) dispersion modeling system and the k- $\epsilon$  CFD code from the OpenFOAM package. We also compared the model predictions with CFD simulations by Hagler et al. (2010)

## 6.1. QUIC

The Quick Urban and Industrial Complex (QUIC) dispersion modeling system uses empirical expressions to determine the mean wind vectors around buildings within the surface layer and uses a Lagrangian particle model to estimate concentration distributions. The QUIC dispersion modeling system also includes the option to use a simple CFD model (QUIC-CFD) to generate the wind vectors. The empirical formulation (QUIC-URB) has been used to simulate barriers (Bowker et al. 2007). We used both QUIC-URB and QUIC-CFD to estimate the concentration distribution for barriers that are 3 m, 6 m, and 9 m tall.

The barrier was 200 m long in the crosswind direction and 1 m thick. The domain extended 100 m upwind of the barrier and 500 m downwind. The wind direction was perpendicular for all cases. We defined the inlet velocity profile as a log profile with the same  $u_*$  and  $z_0$  as the smooth approach flow wind tunnel case.

A 50 m long source was placed 6 m upwind of the barrier at 1 m AGL. The Lagrangian particle model counts particles entering a grid of collecting boxes to calculate concentrations. We created a grid of 2 m by 2 m by 0.5 m (x by y by z) boxes. Particles were released from the source for 1100 s. The first 200 s allow the concentrations to reach steady state, and particles were counted during the last 900 s to calculate 15 minute average concentrations. The particle release rate was 5000 particles/s and the Lagrangian time step was 0.5 s.

The results of the QUIC simulations were disappointing. Figure 38 shows the concentrations calculated by QUIC-URB for an empty domain and a 3 m barrier when the source is located at  $x = -6$  m. Right away we see the strange result that QUIC predicts larger concentrations for a 3 m barrier than for the case of no barrier. This is contrary to what we expect based on measurements in the wind tunnel and from the Idaho Falls study. Although this result is strange, it is consistent with the result obtained by Bowker et al. (see Figure 6) (2007).

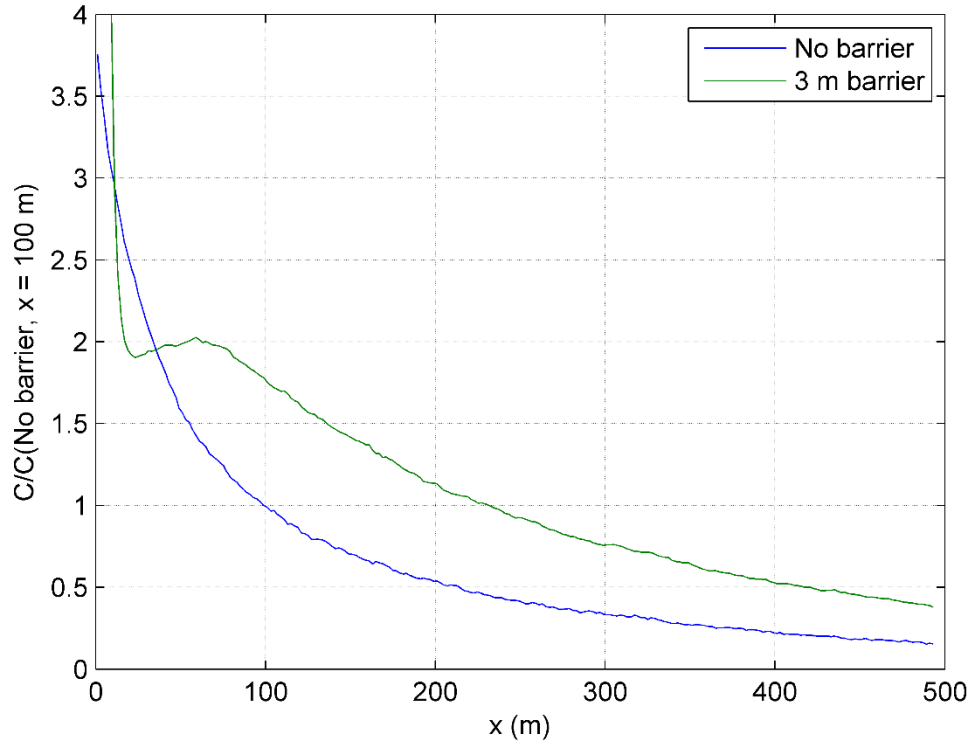


**Figure 38: QUIC-URB centerline concentration results for an empty domain and a 3 m barrier located at  $x = 0$ . The source is located at  $x = -6$  m. Concentrations are normalized by the QUIC simulated concentration in the empty domain at  $x = 100$  m.**

The QUIC-URB results for the 6 m and 9 m barriers are shown in Figure 39. The results are dominated by noise because the predicted concentrations are small. QUIC predicts that a 6 m barrier reduces concentrations by about a factor of 1000 relative to the open domain case, but based on measurements the reduction should be only about 50%. We conclude that QUIC has not accurately captured the essential physics governing dispersion over a barrier. It seems that in the 6 m and 9 m simulations the emissions did not travel over the top of the barrier, creating very small concentrations.

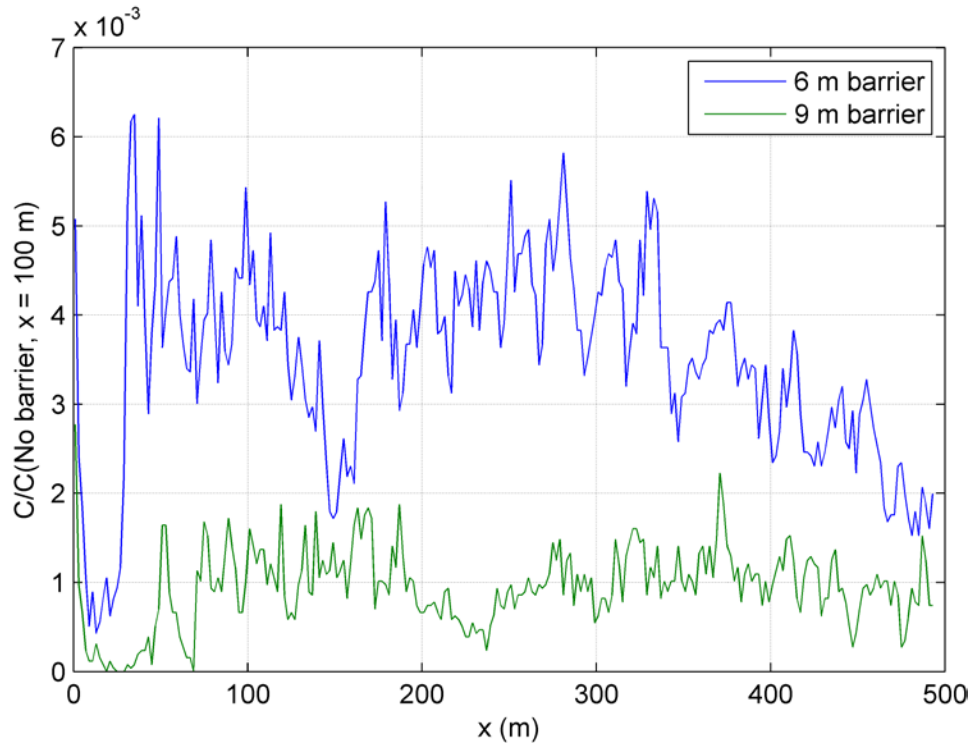


**Figure 39: QUIC-URB centerline concentration results for a 6 m and a 9 m barrier located at  $x = 0$ . The source is located at  $x = -6$  m. Concentrations are normalized by the QUIC simulated concentration in the empty domain at  $x = 100$  m.**

Figure 40 shows the QUIC-CFD results for the empty domain and the 3 m, 6 m, and 9 m barriers. The results for the 3 m barrier are similar to those predicted by QUIC-URB. The 6 m and 9 m barrier concentrations are not near zero as the QUIC-URB predictions are. Still, QUIC-CFD predicts that the 6 m barrier concentration is larger than the open domain concentration, while we expect the 6 m concentration to be about 50% less than the open domain concentration based on measurements.

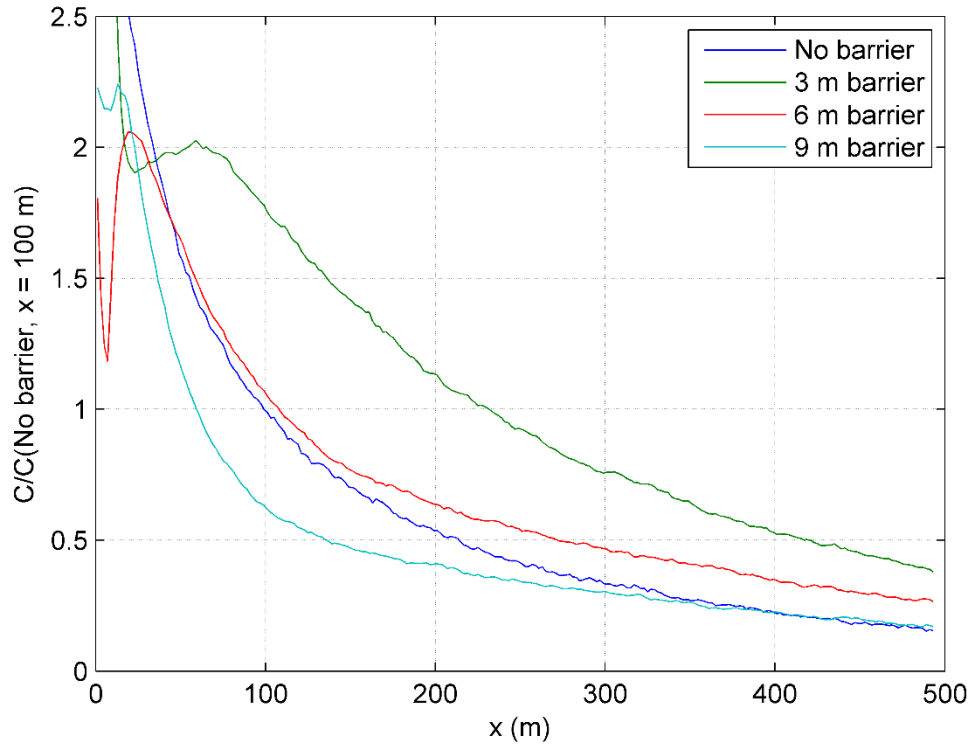


**Figure 40: QUIC-CFD centerline concentration results for no barrier, and a 3 m 6 m and 9 m barrier located at  $x = 0$ . The source is located at  $x = -6$  m. Concentrations are normalized by the QUIC simulated concentration in the empty domain at  $x = 100$  m.**

Based on our results and those of Bowker et al. (2007) we conclude that QUIC-URB cannot predict concentrations downwind of a barrier. The predicted concentration for a 3 m barrier should not be larger than the open domain concentration, and the predicted concentration should decrease as barrier height increases. Also, our QUIC-URB simulations for a 6 m and a 9 m barrier did not give us any significant results, indicating that there are possible numerical problems associated with using QUIC-URB to simulate dispersion over a barrier.

## 6.2. OpenFOAM CFD Model

OpenFOAM (OpenCFD Ltd 2012) is a freely available CFD code that includes the same features as other commonly used CFD packages such as FLUENT. We used the  $k-\epsilon$  turbulence model included in OpenFOAM to check the results of Hagler et al. (2011). We set up the model boundary conditions and source configuration in the same way as Hagler et al. (2011) and ran the model for four barrier heights: 3 m, 6 m, 9 m, and 18 m. The main difference between our run

and Hagler et al. is that our model was run in two dimensions (x-z plane), but Hagler et al. (2011) was run in three dimensions.

The computational domain is 200 m tall and extends from  $x = -200$  m to  $x = 4000$  m. The upstream face of the 0.5 m thick barrier is located at  $x = 0$  m. The mesh was generated by creating a coarse base mesh and refining the mesh in several stages. We used the OpenFOAM blockMesh utility to generate the base mesh with cells 8 m by 8 m. We then used the refineMesh utility to refine the mesh near the barrier and the ground. We refined the mesh in eight stages, resulting in a minimum cell size of 0.0313 m near the barrier and ground. The resulting mesh has 269000 cells.

The upstream boundary is a velocity inlet with the logarithmic wind speed profile for neutral atmospheric stability. The surface friction velocity is 0.307 m/s and the surface roughness length is 0.643 m. The turbulent kinetic energy at the inlet is fixed at a constant value of 0.3142  $\text{m}^2\text{s}^{-2}$  and the turbulent dissipation rate at the inlet is given by equation 27:

$$\epsilon = \frac{u_*^3}{\kappa(z + z_0)} \quad (27)$$

The wall functions are the standard functions for the k- $\epsilon$  model, except for the wall function for the turbulent viscosity on the ground, which is given by equation 28:

$$v_t = \frac{\kappa u_* z}{\ln\left(\frac{z}{z_0} + 1\right)} \quad (28)$$

The wall function for turbulent viscosity on the barrier surface is that used in fluent with  $C_s = 0.5$  and  $k_s = 0.006$  m.

Sources are placed 1 m AGL at  $x = -35.55$  m,  $-31.85$  m,  $-28.15$  m,  $-18.45$  m,  $-14.75$  m, and  $-11.05$  m to simulate a six lane highway.

The OpenFOAM framework does not include the option to solve an equation for a passive scalar. To solve for the concentration, we modified simpleFOAM to solve equation 4:

$$u \frac{\partial C}{\partial x} + w \frac{\partial C}{\partial z} = \frac{\partial}{\partial z} \left( v_t \frac{\partial C}{\partial z} \right) \quad (29)$$

The boundary conditions for equation 4 are zero inlet concentration and zero concentration gradient at the outlet. We made sure that the inlet velocity profile and boundary conditions were in equilibrium to produce a horizontally homogeneous flow upstream of the barrier. This means that the shear stress from the ground wall functions matches the shear stress that creates the specified inlet velocity profile, and the velocity profile does not change as the flow passes through an empty domain. Figure 41 shows the relative error in the velocity for different downwind locations in an empty simulation domain. The relative error is defined as  $err = \frac{U(x)-U(0)}{U(0)}$ , where  $U(0)$  is the velocity at the inlet and  $U(x)$  is the velocity at  $x$ . There is only one point at  $x = 400$  m where the error is larger than 0.05, and this only happens below a height of 1 m. The simulated flow can be considered horizontally homogeneous because the velocity does not change significantly throughout the domain.

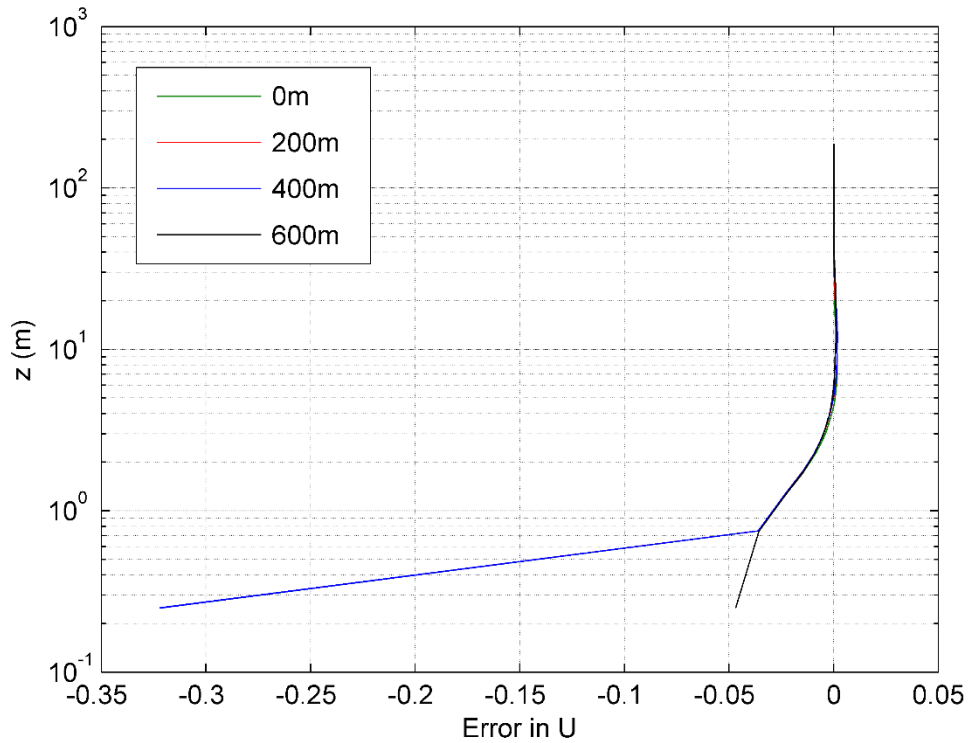


**Figure 41: Relative error in U at 200 m, 400 m, 600 m, and 800 m downwind of the inlet in the empty domain. The error is small and the flow is horizontally homogeneous.**

Figure 42 shows the results of the OpenFOAM simulations. In the figure we plot the ratio of the simulated concentration for a 3 m, 9 m, and 18 m barrier to the simulated concentration for

a 6 m barrier. We also include the results of Hagler et al.(2011) for comparison. The concentration ratio for the 9 m and 18 m barriers are similar to those predicted by Hagler et al. The OpenFOAM predictions of the ratio for the 3 m barrier are larger than those of Hagler et al. The predicted concentration ratio of Hagler et al. for the 3 m and 9 m barriers does not appear to approach 1 for large  $x$ , while the OpenFOAM predictions all appear to approach 1. Because the effect of barrier height should diminish with downwind distance we expect the concentration ratio to approach 1 far from the barrier.

The OpenFOAM results for the 9 m and 18 m barrier should at least qualitatively represent the concentration ratio that would be observed experimentally. We have less confidence in the result for the 3 m barrier because it does not match the result of Hagler et al.

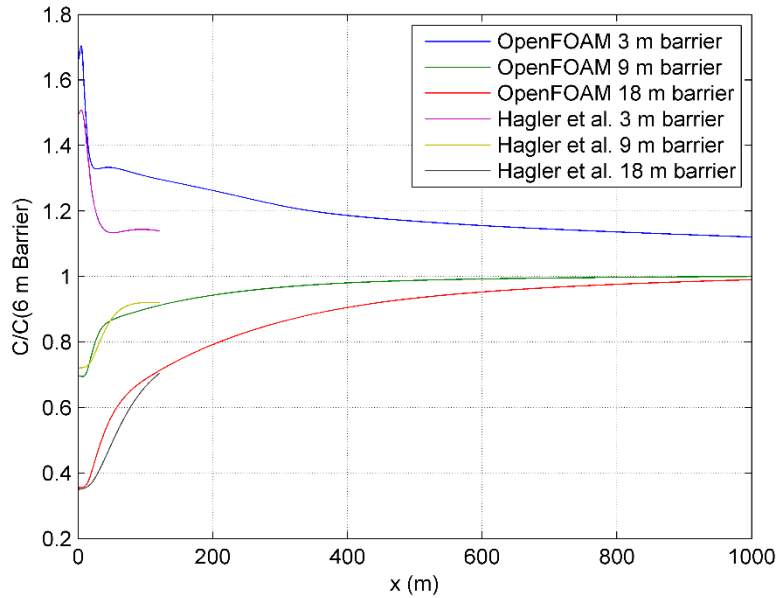


**Figure 42: Ratio of OpenFOAM simulated concentration for a 3 m, 9 m, and 18 m barrier to the simulated concentration for a 6 m barrier. The results of Hagler et al. are also included.**

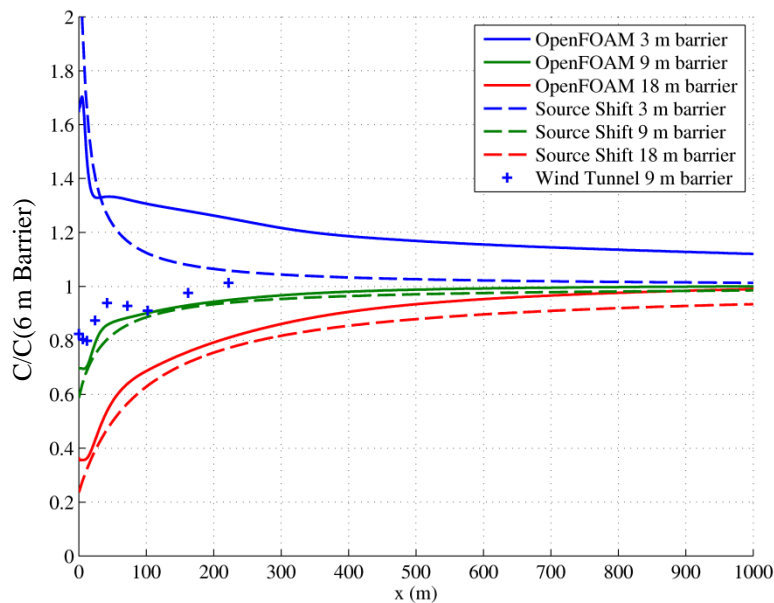
## 7. Barrier height Sensitivity

We now use the source shift, mixed wake, and Puttock Hunt models to examine the sensitivity of the concentration downwind of a barrier to the barrier height. First we compare the models with the results of the OpenFOAM simulations and the wind tunnel measurements. Next we run the models while varying meteorological conditions to see how these factors influence the sensitivity of the concentrations to barrier height. The results of the comparison with OpenFOAM are presented as plots of the ratio  $C(H)/C(6)$ , where  $C(H)$  is the concentration for

a specific model run with barrier height  $H$ , and  $C(6)$  is the concentration for the same model where the barrier height is 6 m.

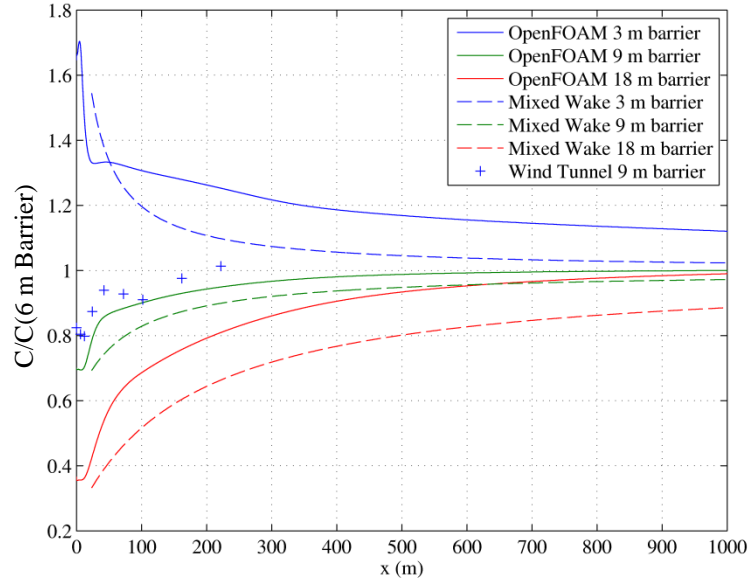
The meteorology that matches the upwind boundary layer of the OpenFOAM simulations and was supplied to the models for the comparison with OpenFOAM is:  $u_* = 0.307 \text{ m/s}$ ,  $z_0 = 0.643 \text{ m}$ .

Figure 43 shows the comparison of the source shift model with OpenFOAM and wind tunnel measurements. The source shift matches OpenFOAM well for a 9 m and 18 m barrier, but predicts a smaller concentration ratio than OpenFOAM for a 3 m barrier. The source shift prediction for a 3 m barrier is more consistent with the result of Hagler et al. than with those of OpenFOAM (see Figure 42). We believe that the OpenFOAM results are qualitatively correct, so we are confident that the source shift model can be used to analyze the sensitivity of concentrations to barrier height.



**Figure 43: Sensitivity of the source shift model to barrier height. The concentration ratio is the ratio of the simulated (and for the wind tunnel measured) concentration for 3 m, 9 m, and 18 m tall barriers to that of a 6 m tall barrier. The results of the OpenFOAM simulations and the wind tunnel measurements are also included for comparison.**

Figure 44 shows the comparison of the mixed wake model with OpenFOAM and wind tunnel measurements. The mixed wake model predicted concentration ratio is smaller than the OpenFOAM predictions for the 9 m and 18 m. The model predicts that the concentration ratio approaches 1 at a smaller rate than the source shift model and OpenFOAM do.



**Figure 44: Sensitivity of the mixed wake model to barrier height. The concentration ratio is the ratio of the simulated (and for the wind tunnel measured) concentration for 3 m, 9 m, and 18 m tall barriers to that of a 6 m tall barrier. The results of the OpenFOAM simulations and the wind tunnel measurements are also included for comparison.**

Figure 45 shows the comparison of the Puttock-Hunt model with OpenFOAM and wind tunnel measurements. The concentration ratio predicted by the Puttock-Hunt model shows a sharp increase with downwind distance for  $x < 100$  m. This is because we assume that the concentration within the separated wake is constant, but the concentration is not smooth at the end of the wake. This is illustrated by Figure 46, which shows the concentration predicted by the Puttock-Hunt model vs. downwind distance. The Puttock-Hunt model prediction for the 9 m barrier is similar to that of OpenFOAM for  $x > 100$  m, and the initial concentration ratio just downwind of the barrier is very close to the OpenFOAM prediction. It is difficult to say if the model produces acceptable results for the 3 m barrier because we do not have any experimental data to compare with.

The Puttock-Hunt model prediction for the 18 m barrier is much smaller than the OpenFOAM prediction. The uniform concentration within the separated wake decreases exponentially as the barrier height increases, so the predicted concentration for the 18 m barrier is very small. The dependence of the wake concentration on barrier height is determined by our assumption about the size of the separated wake. We assume the size of the wake scales with the barrier height, but this may not be true for a very tall barrier, or the concentration may not be

uniform throughout such a large wake (the wake is 72 m long for the 18 m barrier). For these reasons the Puttock-Hunt model may not be applicable to very tall barriers. Based on the comparison with OpenFOAM we limit the range of applicability of the Puttock-Hunt model to barriers less than 9 m tall.

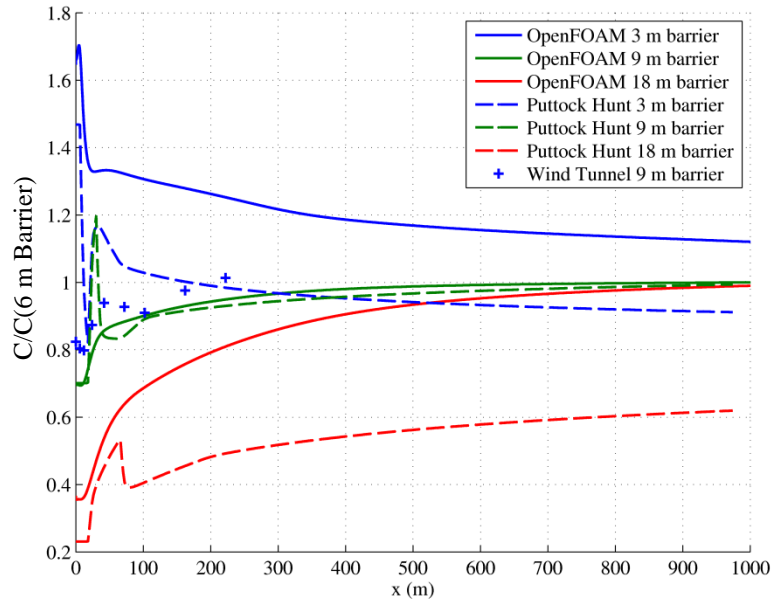


**Figure 45: Sensitivity of the Puttock-Hunt model to barrier height. The concentration ratio is the ratio of the simulated (and for the wind tunnel measured) concentration for 3 m, 9 m, and 18 m tall barriers to that of a 6 m tall barrier. The results of the OpenFOAM simulations and the wind tunnel measurements are also included for comparison.**

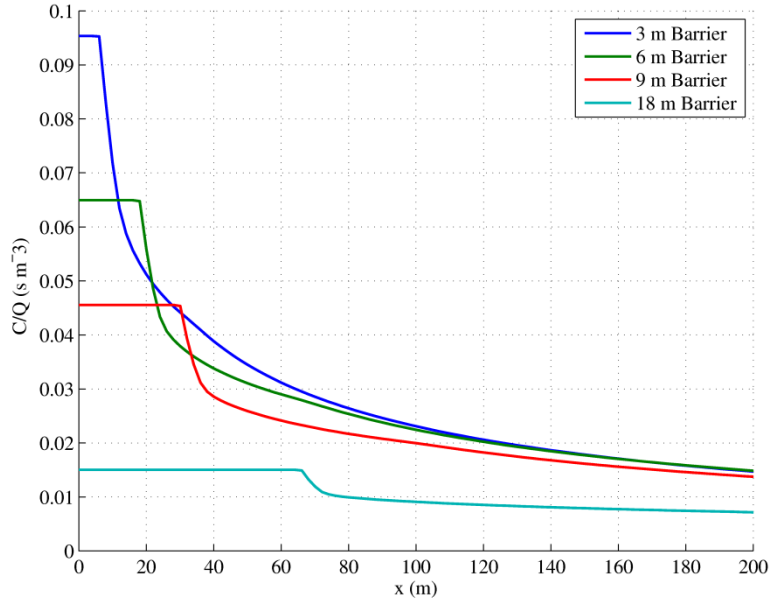


**Figure 46: Concentration predicted by the Puttock-Hunt model. The concentration is constant within the separated wake downwind of the barrier. Because the concentration is not smooth the concentration ratio is also not smooth and shows sharp changes near the end of the separated wake.**

### 7.1. Impact of Meteorology on Barrier height Sensitivity

We have compared the source-shift, mixed-wake, and Puttock-Hunt models with OpenFOAM to get a sense of the qualitative behavior of the models. We now present plots of the concentration predictions of the source-shift, mixed-wake, and Puttock-Hunt models with varying meteorological conditions to see how meteorological factors influence the sensitivity of the concentrations to barrier height. The models were run with a single source placed 6 m upwind of barrier at ground level. Concentrations were calculated at ground level. We use average meteorology determined from the meteorology measured during NRTS08 as the meteorological input to the models because the measurements span a wide range of atmospheric stabilities and are representative of real meteorological conditions.

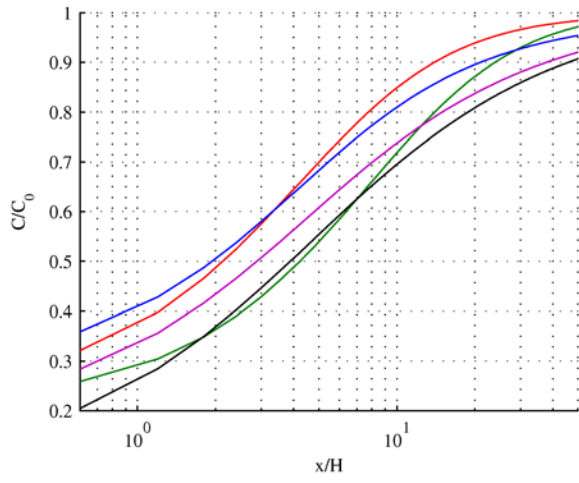
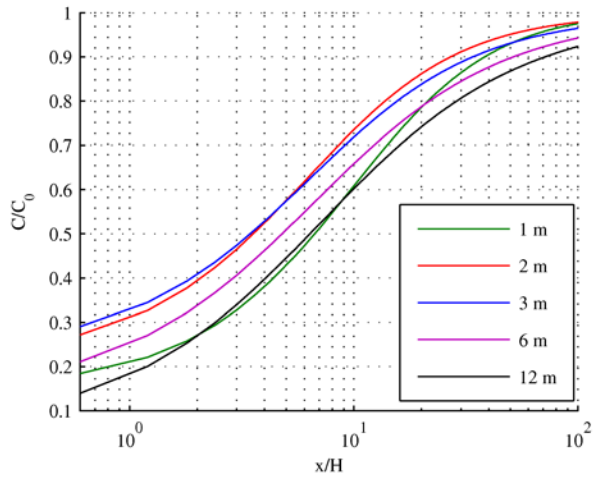
For each model we plot the ratio of the concentration with a barrier to that with no barrier vs. downwind distance for 5 barrier heights: *1 m, 2 m, 3 m, 6 m, and 12 m*. The model predictions for the meteorological conditions measured during each of the four days of NRTS08 are shown on separate plots, with near neutral stability on the upper left, very unstable on the upper right, slightly stable on the lower left, and very stable on the lower right. Table 5 is a summary of the meteorology input to the models.

**Table 5: Meteorology used in the barrier height sensitivity model runs. This meteorology is derived from measurements made during NRTS08.**

Modeled Stability	$U$ (m/s)	$u_*$ (m/s)	$L$ (m)
Neutral	6.7	0.66	-260
Unstable	1.4	0.3	-20
Stable	3.1	0.3	40
Very stable	1.8	0.1	13

Figure 47 shows the sensitivity of the source-shift model predictions to variations in the barrier height, plotted as a function of non-dimensional distance  $x/H$ , where  $H$  is the barrier height and  $x$  is the distance from the barrier. As expected, the largest impact of the change in barrier height occurs close to the barrier, and this impact decreases with distance as vertical mixing by atmospheric turbulence becomes more dominant relative to that induced by the barrier.

Atmospheric stability affects how far downwind the effects of the barrier persist. During unstable conditions (upper right) the concentration for all the barrier heights are within 20% of the flat terrain concentration at a downwind distance of about  $10H$ , while during very stable conditions (bottom right) the concentrations for the  $3\text{ m}$ ,  $6\text{ m}$ , and  $12\text{ m}$  barriers are still significantly different from the flat terrain concentration beyond  $x = 100H$ .



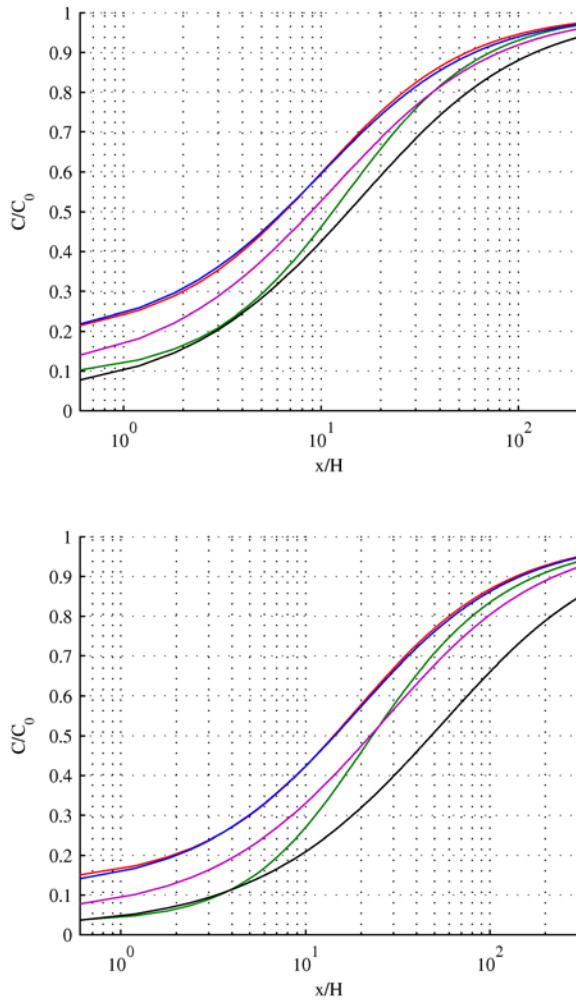


**Figure 47: Sensitivity of source-shift model predicted concentrations to changes in barrier height vs. downwind distance for meteorology representing neutral (top left), unstable (top right), slightly stable (bottom left), and strongly stable (bottom right) atmospheric conditions. The barrier height, H, takes values of 1 m, 2 m , 3 m, 6 m, and 12 m. Note the different horizontal scale.  $C_0$  is the flat terrain concentration (no barrier).**

Figure 48 shows the sensitivity of the mixed-wake model predictions to variations in the barrier height, versus downwind distance. The plots are similar to those for the source-shift model, except the mixed-wake model predicts a different concentration ratio near the barrier for different barrier heights, while the source-shift predicts a concentration ratio near the barrier that does not depend strongly on barrier height. The mixed-wake model also predicts a greater change in concentration when the barrier height is changed than the source-shift model does.

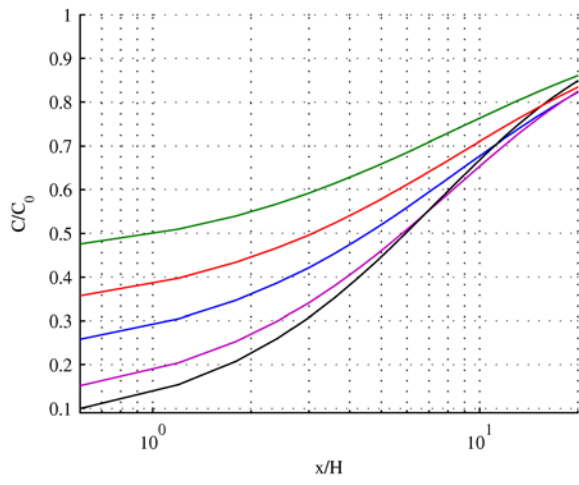
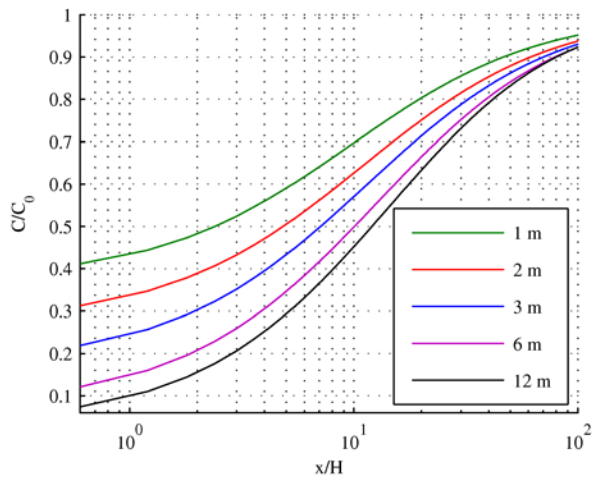
The concentration ratio near the barrier ranges from 0.5 to nearly 0, depending on atmospheric stability and barrier height. Each time the barrier height is doubled the concentration

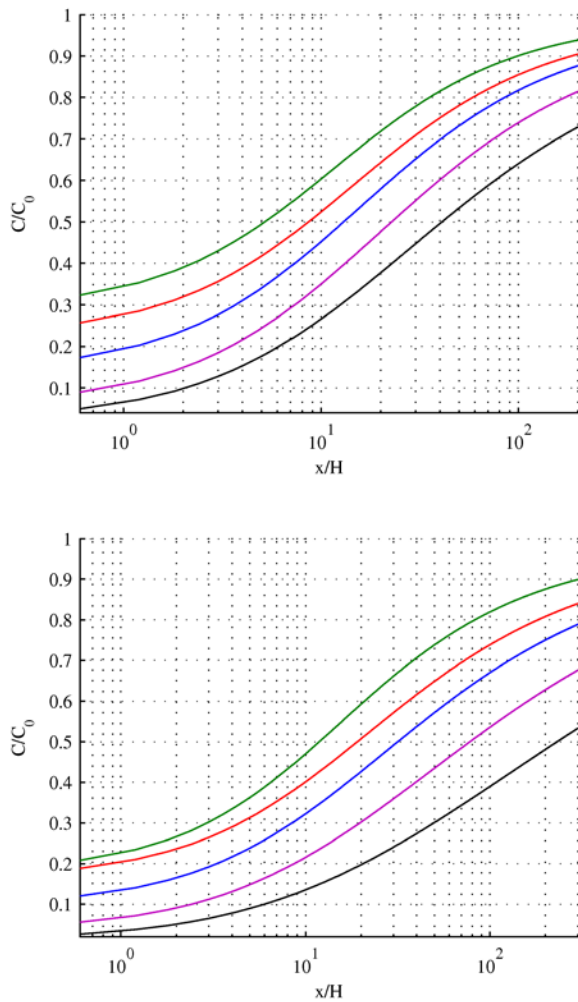
ratio is reduced by about 0.1 at receptors near the barrier during neutral and unstable atmospheric stability. During stable conditions the concentration ratio near the barrier is smaller. So it does not change as much when the barrier height is changed.

The change in barrier height has its greatest impact during stable conditions. This is significant because the largest concentrations occur during stable conditions corresponding to early morning, late evening, and nighttime periods.

During unstable conditions (upper right) the concentration for all the barrier heights is within 20% of the flat terrain concentration at a downwind distance of  $30H$ , while during very stable conditions (bottom right) the concentrations for the  $3\text{ m}$ ,  $6\text{ m}$ , and  $12\text{ m}$  barriers are still significantly different from the flat terrain concentration beyond  $x = 300H$ . Note that for a  $3\text{ m}$  barrier,  $300H$  is almost  $1\text{ km}$ .

The biggest difference between the source-shift and mixed-wake models occurs during very stable atmospheric conditions (bottom right). During these conditions, at a distance of  $300H$  from the wall for a  $12\text{ m}$  barrier, the concentration ratio predicted by the mixed-wake model is 0.5, and the ratio predicted by the source-shift model is only 0.8. The mixed-wake model tends to predict smaller concentration ratios than the source-shift during stable conditions.

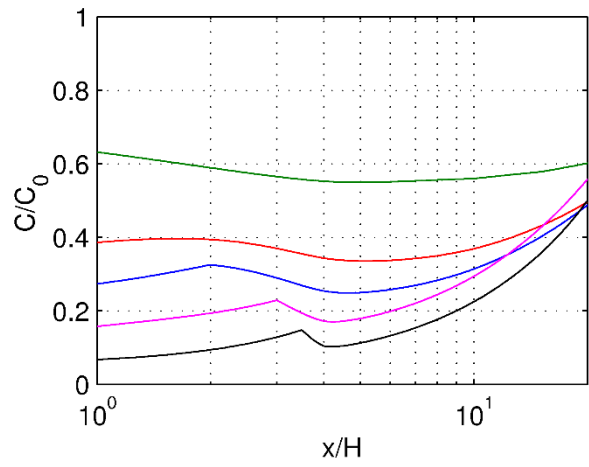
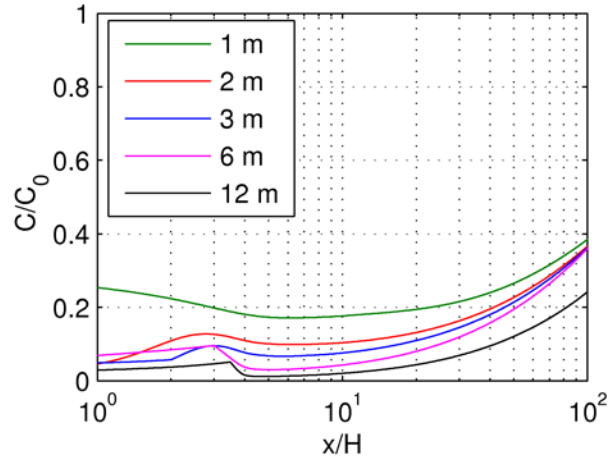




**Figure 48: Sensitivity of mixed-wake model predicted concentrations to changes in barrier height vs. downwind distance for meteorology representing neutral (top left), unstable (top right), slightly stable (bottom left), and strongly stable (bottom right) atmospheric conditions. The barrier height,  $H$ , takes values of 1 m, 2 m, 3 m, 6 m, and 12 m. Note the different horizontal scale.  $C_0$  is the flat terrain concentration (no barrier).**

Figure 49 shows the sensitivity of the Puttock-Hunt model predictions to variations in the barrier height versus downwind distance. The Puttock-Hunt model predicts diminishing changes in concentrations as the barrier height is changed, so a 6 m and a 12 m barrier have a very similar effect on concentrations. Changing the barrier height has the largest effect during stable atmospheric conditions (bottom), and the smallest effect during neutral and unstable conditions (top). This is similar to the other model predictions, but the source-shift and mixed-wake models show greater variation in concentrations for different atmospheric stabilities. The source-shift and mixed-wake models show significantly different concentration ratio between the slightly

stable and very stable conditions (bottom left and right), but the Puttock-Hunt model does not predict a large variation between these cases, except very close to the barrier. Also, the Puttock-Hunt model predicts that the concentration ratio does not approach 1 at large downwind distances, which is not realistic.



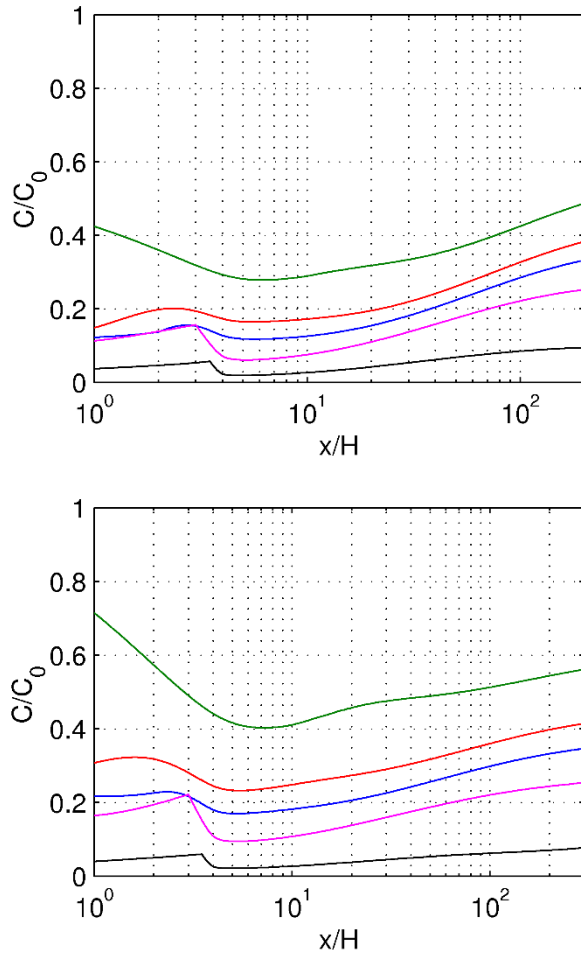


**Figure 49: Sensitivity of Puttock-Hunt model concentration estimates to changes in barrier height versus downwind distance for meteorology representing neutral (top left), unstable (top right), slightly stable (bottom left), and strongly stable (bottom right) atmospheric conditions. The barrier height,  $H$ , takes values of 1 m, 2 m, 3 m, 6 m, and 12 m. Note the different horizontal scale.  $C_0$  is the flat terrain concentration (no barrier).**

Some of the difference between the source-shift and mixed-wake models and the Puttock-Hunt models may be due to the effect of source location. These models were run with the source placed 6 meters from the barrier. Relative to a  $2H$  barrier (12 m), this is a small distance. The source is within the displacement zone upwind of the  $9\text{ m}$  and  $12\text{ m}$  barriers (see Figure 34), which may explain the similarity of the concentration ratios for these two cases. These concentrations are also likely affected by the assumption about the shape of the recirculation zone around the barrier. Because of these issues, we do not recommend using the Puttock-Hunt model to examine the effect of barrier height without more model evaluation.

## 8. Conclusions

Infinitely long roadside barriers affect dispersion of vehicle related emissions in three ways: 1) increase vertical dispersion through additional turbulence generated in the wake of the barrier, 2) induce vertical mixing behind the barrier in the cavity region, and 3) loft the emissions above the barrier. We have presented three models that account for these physical effects of barriers in different ways. Table 6 summarizes the three models and some basic conclusions about the benefits of each model.

The source-shift model shifts the source upwind to account for increased vertical turbulent mixing at a given distance but it does not account for vertical lofting or recirculation. This model tends to overestimate concentrations within the recirculation zone and underestimate concentrations at the elevated receptors. Model estimates of ground-level concentrations compare well with those from the CFD simulations.

The mixed-wake model simulates increased turbulent mixing below the height of the barrier and effectively lofts the plume above the barrier. The model thus does not underestimate elevated concentrations.

The Puttock-Hunt model is based on the two-dimensional eddy diffusivity formulation of the mass conservation equation. It treats the cavity as a well-mixed zone above which the flow follows potential flow. Among the three models, it is the best predictor of the elevated concentrations. However, the model requires specifying the shape of the wake and the mean flow and turbulence above it. Because of the uncertainty in describing these aspects of the flow, we recommend using the much simpler mixed-wake model because it captures the essentials of the effects of barriers, and its predictions compare well with data from Idaho Falls, the wind tunnel and CFD simulations.

**Table 6: Summary of the three models and the benefits of each model.**

Model	Physical Description	Pros	Cons
Source Shift	The source is shifted upwind to account for increased vertical turbulent mixing at a given distance. The model does not account for vertical lofting or recirculation	<ul style="list-style-type: none"> <li>• Predictions compare well with data from Idaho Falls, the wind tunnel, and CFD simulations</li> <li>• Simple</li> </ul>	<ul style="list-style-type: none"> <li>• Tends to overestimate concentrations within the recirculation zone</li> <li>• Underestimates concentrations at elevated receptors</li> <li>• Does not capture the nearly constant concentration within</li> </ul>

			the barrier's wake (due to recirculation)
Mixed Wake	Simulates increased turbulent mixing below the height of the barrier and vertical lofting over the top of the barrier	<ul style="list-style-type: none"> <li>• Predictions compare well with data from Idaho Falls, the wind tunnel, and CFD simulations</li> <li>• Captures the essentials of the effects of barriers</li> <li>• Does not underestimate elevated concentrations</li> <li>• Simple</li> </ul>	<ul style="list-style-type: none"> <li>• Does not capture the nearly constant concentration within the barrier's wake (due to recirculation)</li> </ul>
Puttock Hunt	Based on the two-dimensional eddy diffusivity formulation of the mass conservation equation. It treats the cavity as a well-mixed zone above which the flow follows potential flow	<ul style="list-style-type: none"> <li>• The best predictor of elevated concentrations</li> <li>• Accounts for recirculation within the barrier's wake</li> </ul>	<ul style="list-style-type: none"> <li>• Complex - Requires specifying the shape of the wake and the mean flow and turbulence above it.</li> <li>• Sensitivity to barrier height indicates more model validation is necessary before the model can be recommended</li> </ul>

A sensitivity study of the effect of barrier height indicates that the effect of changes in barrier height have the greatest influence on concentrations at receptors near the barrier. Atmospheric stability influences how far downwind the concentrations are affected by a barrier. During very stable conditions the barrier effect persists to larger downwind distances than during unstable or neutral conditions.

There are differences between the sensitivity to barrier height predicted by the three models. The source-shift model and mixed-wake models show similar sensitivities, but the mixed-wake model shows a larger impact of barrier height close to the barrier than the source-shift model during near neutral and very unstable conditions. During stable conditions, the larger impact associated with the mixed wake model persists for distances up to 300H.

The variation of the impact of barrier height predicted by the Puttock-Hunt model differs from those of the other two models. The model predicts much less variation of the concentration ratio with downwind distance than the other models, and also shows less variation due to the effect of atmospheric stability.

The mixed-wake and source-shift models perform well, but they do not capture the concentration within the barrier's near wake. The recirculating flow that exists within the near wake mixes the pollutant and creates a region that extends about 5H downwind of the barrier where the ground level concentration does not change with downwind distance.

The modeling results from this study show that the primary effect of the roadside is to enhance the initial spread of the plume by an amount that depends on the height of the barrier. The impact of the barrier as a function of distance from the barrier also depends on atmospheric turbulence and distance of the line source from the barrier. The interaction of these factors can be illustrated by formulating a simple model (Venkatram et al. 2007) for dispersion of emissions from a road with an emission rate of  $Q$  per unit length of a road that has a width  $w$ . Equation 14 for the mixed-wake model suggests the following expression for the vertical spread of the plume:

$$\sigma_z(x) = h_0 + \frac{\sigma_w x}{U} \quad (30)$$

where  $\sigma_w$  includes the effects of the barrier on atmospheric turbulence, and  $h_0 = \sqrt{\frac{2}{\pi}} H$ . Then, the concentration  $C(x)$ , at a distance  $x$  from the barrier, when the wind direction is perpendicular to the road, is given by (Venkatram et al. 2007),

$$C(x) = \sqrt{\frac{2}{\pi}} \frac{Q}{\sigma_w w} \ln \left( 1 + \frac{w}{\frac{h_0 U}{\sigma_w} + x} \right) \quad (31)$$

We see that the presence of the barrier is equivalent to shifting the road upwind by the distance  $\sqrt{\frac{2}{\pi}} \frac{HU}{\sigma_w}$ . The expression for the sensitivity of the concentration to  $h_0$  is,

$$\frac{dC(x)}{dh_0} = -\sqrt{\frac{2}{\pi}} \frac{Q}{\left( h_0 + \frac{\sigma_w}{U} (x + w) \right)} \frac{1}{(h_0 U + \sigma_w x)} \quad (32)$$

Near the barrier,  $x=0$ , the sensitivity is proportional to  $1/h_0^2$ . The expression also tells us that the impact of the barrier height,  $h_0$ , becomes less important as the width of the road,  $w$ , increases.

Although the mixed-wake and source-shift models are highly simplified depictions of dispersion of road emissions in the presence of barriers, they capture the dominant physics as indicated by the agreement between model estimates and data from the Idaho Falls field study and the EPA wind tunnel. So it is instructive to apply the model to estimate the impact of a barrier on concentrations measured next to a freeway in Los Angeles.

### 8.1. Hypothetical Scenario where a Barrier is used to Reduce Near-Road Concentrations of Roadway Emissions

During March of 2008, Hu et al.(2009) measured concentrations during early morning hours near the I-10 freeway in Santa Monica(Hu et al. 2009)(Hu et al. 2009)(Hu et al. 2009). They found that the concentrations were much larger than during daytime hours due to the stable atmospheric conditions that exist during early morning. The NO concentration was about 160 ppb near the freeway and about 100 ppb at a distance of 500 m from the freeway. There is already a noise barrier next to the freeway which influences the observed NO concentrations, but it is only about 3 m tall. We now describe a hypothetical scenario where we increase the barrier height to reduce early morning NO concentrations.

We simulated the concentration next to the freeway using the mixed-wake model. The freeway was modeled as 8 parallel line sources, each with an emission rate of  $1.1 * 10^{-4} \frac{g}{ms}$ . The emission rate was determined by first choosing an emission rate based on the traffic count measured by Hu et al.(2009) and an emission factor of  $3.11 * 10^{-4} \frac{g}{m}$  for NO<sub>x</sub>. The emission rate was then adjusted to match observations, resulting in the emission rate of  $1.1 * 10^{-4} \frac{g}{ms}$  for each of the 8 line sources. The sources were placed 1 m AGL and given an initial vertical spread of 1 m. The wind speed was taken to be  $1 m/s$  based on measurements, and  $u_*$  was estimated to about  $0.1 m/s$ . The Monin-Obukhov length was taken to be 5 m, representing very stable conditions.

Figure 50 shows the predicted concentration for a barrier height of 3 m and the effect of increasing the barrier height from 3 m to 4 m and to 6 m. We see that increasing the height to 4 m reduces the concentration at 500 m from the freeway from 100 ppb to 80 ppb, and increasing the height to 6 m reduces the concentration at 500 m to 60 ppb. The maximum concentration near the freeway is reduced from 300 ppb to 200 ppb and 100 ppb for the 4 m and 6 m barrier, respectively.

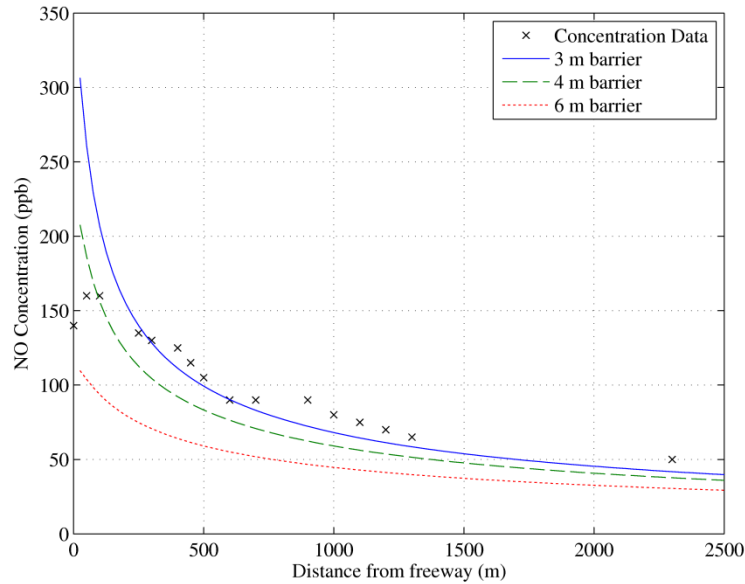


**Figure 50:** The predicted NO concentration for a barrier height of 3 m and the effect on concentrations of increasing the barrier height from 3 m to 4 m and 6 m. Increasing the barrier height to 4 and 6 m reduced the concentration at 500 m from 100 ppb to 80 ppb and 60 ppb, respectively. The downwind distance is measured from the center of the freeway.

This example shows that a barrier has the potential to reduce near-road concentrations of roadway emissions.

## 9. Recommendations

The models developed in this project provide an adequate description of data related to the impact of infinitely long roadside barriers on dispersion of emissions from vehicles on roads. These models can provide guidance on the design of roadside barriers. However, the predicted sensitivity of roadside concentrations to barrier dimensions requires further evaluation with observations from field studies designed to examine this issue; the Idaho Falls study (Finn et al., 2010) used a barrier with a single height, 6 m.

We can gain more confidence in the models for dispersion in the presence of barriers through experiments to study:

1. The effects of barrier height on concentrations as a function of distance from the road;
2. The effects of barriers on turbulence and mean flow
3. The relationship between the width of the road and the effectiveness of the barrier
4. The vertical distribution of concentration

## 5. The role of vehicle induced turbulence

It is especially important to evaluate these models with data from controlled wind tunnel (Heist et al. 2009) and tracer studies (Finn et al. 2010) where uncertainties associated with emissions and governing micrometeorology are small.

Most of the studies conducted thus far have focused on the effects of a single downwind barrier on reducing concentrations. Heist et al. (2009) have examined barrier pairs in their wind tunnel study, but have not drawn any conclusions from their observations. Because most barriers come in pairs, it is necessary to pay much more attention to their effects on flow and dispersion. Barriers on both sides of the road form a street canyon, which is depicted in Figure 51. The near surface flow in a street canyon can be towards the upwind barrier, so that emissions can be drawn towards the upwind barrier before being captured by the mean flow. In this situation, the effect of the downwind barrier might be substantially smaller than that indicated by single barrier studies. There is a need for laboratory and field studies on the effects of twin barriers on the impact of vehicle emissions.

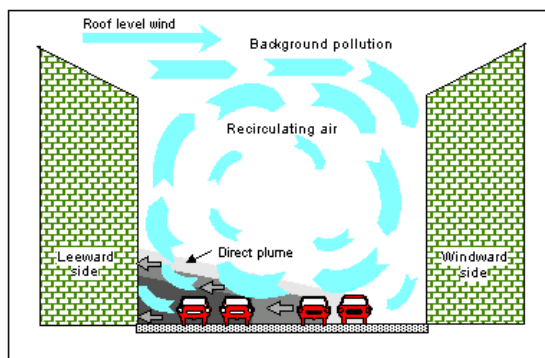


**Figure 51: Flow and dispersion in a street canyon.**

## 10. Acknowledgements

We are grateful to Steven Perry, David Heist, Michelle Snyder, and Vlad Isakov of the United States Environmental Protection Agency (USEPA) for sharing the data from the Idaho Falls field study (Finn et al. 2010) and the Wind Tunnel study (Heist et al., 2009). These data were vital in developing the dispersion models described in this report. We also thank these USEPA scientists for their advice in formulating the models.

## 11. References

- Baldauf, R., Thoma, E., Khlystov, A., Isakov, V., Bowker, G., Long, T., and Snow, R. 2008. Impacts of noise barriers on near-road air quality. *Atmospheric Environment* 42 (October), 7502–7507. doi:10.1016/j.atmosenv.2008.05.051.
- Bowker, G., Baldauf, R., Isakov, V., Khlystov, A., and Petersen, W. 2007. The effects of roadside structures on the transport and dispersion of ultrafine particles from highways. *Atmospheric Environment* 41 (December), 8128–8139. doi:10.1016/j.atmosenv.2007.06.064.
- Brauer, M. 2002. Air Pollution from Traffic and the Development of Respiratory Infections and Asthmatic and Allergic Symptoms in Children. *American Journal of Respiratory and Critical Care Medicine* 166 (October 15), 1092–1098. doi:10.1164/rccm.200108-007OC.
- Cimorelli, A. J., Perry, S. G., Venkatram, A., Weil, J. C., Paine, R. J., Wilson, R. B., Lee, R. F., Peters, W. D., and Brode, R. W. 2005. AERMOD: A Dispersion Model for Industrial Source Applications. Part I: General Model Formulation and Boundary Layer Characterization. *Journal of Applied Meteorology* 44, 682–693. doi:10.1175/JAM2227.1.
- Finkelstein, M. M., Jerrett, M., and Sears, M. R. 2004. Traffic air pollution and mortality rate advancement periods. *American journal of epidemiology* 160 (July 15), 173–177. doi:10.1093/aje/kwh181.
- Finn, D., Clawson, K. L., Carter, R. G., Rich, J. D., Eckman, R. M., Perry, S. G., Isakov, V., and Heist, D. K. 2010. Tracer studies to characterize the effects of roadside noise barriers on near-road pollutant dispersion under varying atmospheric stability conditions. *Atmospheric Environment* 44, 204–214. doi:10.1016/j.atmosenv.2009.10.012.
- Hagler, G. S. W., Tang, W., Freeman, M. J., Heist, D. K., Perry, S. G., and Vette, A. F. 2011. Model evaluation of roadside barrier impact on near-road air pollution. *Atmospheric Environment* 45 (May), 2522–2530. doi:10.1016/j.atmosenv.2011.02.030.

- Harrison, R. M., Leung, P. L., Somervaille, L., Smith, R., and Gilman, E. 1999. Analysis of incidence of childhood cancer in the West Midlands of the United Kingdom in relation to proximity to main roads and petrol stations. *Occupational and environmental medicine* 56 (December), 774–780.
- Heist, D. K., Perry, S. G., and Brixey, L. A. 2009. A wind tunnel study of the effect of roadway configurations on the dispersion of traffic-related pollution. *Atmospheric Environment* 43 (October), 5101–5111. doi:10.1016/j.atmosenv.2009.06.034.
- Hitchins, J., Morawska, L., Wol, R., and Gilbert, D. 2000. Concentrations of submicrometre particles from vehicle emissions near a major road. *Atmospheric Environment* 34, 51–59.
- Hoek, G., Brunekreef, B., Goldbohm, S., Fischer, P., and Van den Brandt, P. a. 2002. Association between mortality and indicators of traffic-related air pollution in the Netherlands: a cohort study. *Lancet* 360 (October 19), 1203–1209. doi:10.1016/S0140-6736(02)11280-3.
- Hooghwerff, J., Tollenaar, C. C., and Van der Heijden, W. J. 2010. In-situ air quality measurements on existing and innovative noise barriers. In *International Conference on Modelling, Monitoring and Management of Air Pollution*, ed. C. A. Brebbia and J. W. S. Longhurst, 129–139. Kos, Greece: WIT Press.
- Hu, S., Fruin, S., Kozawa, K., Mara, S., Paulson, S. E., and Winer, A. M. 2009. A wide area of air pollutant impact downwind of a freeway during pre-sunrise hours. *Atmospheric Environment* 43 (May), 2541–2549. doi:10.1016/j.atmosenv.2009.02.033.
- Huber, A. H. 1984. Evaluation of a method for estimating pollution concentrations downwind of influencing buildings. *Atmospheric Environment* 18 (January), 2313–2338. doi:10.1016/0004-6981(84)90003-9.
- Huber, A. H. 1988. Performance of a Gaussian model for centerline concentrations in the wake of buildings. *Atmospheric Environment* 22 (January), 1039–1050. doi:10.1016/0004-6981(88)90334-4.

- Huber, A. H., and Snyder, W. H. 1982. Wind tunnel investigation of the effects of a rectangular-shaped building on dispersion of effluents from short adjacent stacks. *Atmospheric Environment* 16 (January), 2837–2848. doi:10.1016/0004-6981(82)90034-8.
- Iser, F., and Scharl, C. 2009. EU-LIFE Projekt SPAS Task 3: Simulationen Abschlussbericht. *Life Spas Klagenfurt | Feinstaub EU Feinstaubfilter Feinstaub Feinstaubbelastung Lärmschutz*. [http://www.life-spas.at/deutsch/includes/Iser\\_SPAS\\_Endbericht\\_-\\_Final\(1\).pdf](http://www.life-spas.at/deutsch/includes/Iser_SPAS_Endbericht_-_Final(1).pdf).
- Kim, J. J., Smorodinsky, S., Ostro, B., Lipsett, M., Singer, B. C., and Hogdson, A. T. 2002. Traffic-related Air Pollution and Respiratory Health: the East Bay Children’s Respiratory Health Study. *Epidemiology* 13, S100.
- Kittelson, D. B., Watts, W. F., and Johnson, J. P. 2004. Nanoparticle emissions on Minnesota highways. *Atmospheric Environment* 38 (January), 9–19. doi:10.1016/j.atmosenv.2003.09.037.
- Magistrat Klagenfurt. 2011. EU-LIFE project SPAS. *Life Spas Klagenfurt | Feinstaub EU Feinstaubfilter Feinstaub Feinstaubbelastung Lärmschutz*. <http://www.life-spas.at>.
- McCrae, I. 2010. Scientific Board Review: International review of the Air Quality Innovation Programme (IPL). *Innovation Program Air Quality*. <http://www.ipl-airquality.nl/data/Eindrapport SB definitief.pdf>.
- Ning, Z., Hudda, N., Daher, N., Kam, W., Herner, J., Kozawa, K., Mara, S., and Sioutas, C. 2010. Impact of roadside noise barriers on particle size distributions and pollutants concentrations near freeways. *Atmospheric Environment* 44 (August), 3118–3127. doi:10.1016/j.atmosenv.2010.05.033.
- OpenCFD Ltd. 2012. OpenFOAM - The Open Source Computational Fluid Dynamics (CFD) Toolbox. <http://www.openfoam.com/>.

- Puttock, J. S., and Hunt, J. C. R. 1979. Turbulent Diffusion From Sources Near Obstacles with Separated Wakes - Part I. An Eddy Diffusivity Model. *Atmospheric Environment* 13, 1–13.
- Rodler, J., and Henn, M. 2009. Filter Effect of SPAS and Impact on Air Quality. *Life Spas Klagenfurt | Feinstaub EU Feinstaubfilter Feinstaub Feinstaubbelastung Lärmschutz*. [www.life-spas.at/deutsch/includes/19\\_SPAS\\_Rodler\\_eng.pdf](http://www.life-spas.at/deutsch/includes/19_SPAS_Rodler_eng.pdf).
- Schulman, L. L., Strimaitis, D. G., and Scire, J. S. 2000. Development and Evaluation of the PRIME Plume Rise and Building Downwash Model. *Journal of the Air & Waste Management Association* 50, 378–390.
- Venkatram, A., and Horst, T. W. 2006. Approximating dispersion from a finite line source. *Atmospheric Environment* 40 (April), 2401–2408. doi:10.1016/j.atmosenv.2005.12.014.
- Venkatram, A., Isakov, V., Thoma, E., and Baldauf, R. 2007. Analysis of air quality data near roadways using a dispersion model. *Atmospheric Environment* 41 (December), 9481–9497. doi:10.1016/j.atmosenv.2007.08.045.
- Venkatram, A., Snyder, M. G., Heist, D. K., Perry, S. G., Petersen, W. B., and Isakov, V. 2013. Re-formulation of Plume Spread for Near-Surface Dispersion. *Atmospheric Environment* (June). doi:10.1016/j.atmosenv.2013.05.073.
- Walker, M. 1964. *The Schwarz-Christoffel transformation and its applications; a simple exposition*. New York: Dover Publications.
- Weil, J. C. 1996. *Ninth Joint Conference on Applications of Air Pollution Meteorology with the Air & Waste Management Association*. Boston, MA: American Meteorological Society.
- Wilson, D. J., and Britter, R. E. 1982. Estimates of building surface concentrations from nearby point sources. *Atmospheric Environment* 16, 2631–2646.
- Zhu, Y., Hinds, W. C., Kim, S., Shen, S., and Sioutas, C. 2002a. Study of ultrafine particles near a major highway with heavy-duty diesel traffic. *Atmospheric Environment* 36 (September), 4323–4335. doi:10.1016/S1352-2310(02)00354-0.

Zhu, Y., Hinds, W. C., Kim, S., and Sioutas, C. 2002b. Concentration and Size Distribution of Ultrafine Particles Near a Major Highway. *Journal of the Air & Waste Management Association* 52, 1032–1042.